INFORMATION TO USERS

This manuscript has been reproduced from the microfilm master. UMI films the text directly from the original or copy submitted. Thus, some thesis and dissertation copies are in typewriter face, while others may be from any type of computer printer.

The quality of this reproduction is dependent upon the quality of the copy submitted. Broken or indistinct print, colored or poor quality illustrations and photographs, print bleedthrough, substandard margins, and improper alignment can adversely affect reproduction.

In the unlikely event that the author did not send UMI a complete manuscript and there are missing pages, these will be noted. Also, if unauthorized copyright material had to be removed, a note will indicate the deletion.

Oversize materials (e.g., maps, drawings, charts) are reproduced by sectioning the original, beginning at the upper left-hand corner and continuing from left to right in equal sections with small overlaps. Each original is also photographed in one exposure and is included in reduced form at the back of the book.

Photographs included in the original manuscript have been reproduced xerographically in this copy. Higher quality 6" x 9" black and white photographic prints are available for any photographs or illustrations appearing in this copy for an additional charge. Contact UMI directly to order.

UMI

A Bell & Howell Information Company
300 North Zeeb Road, Ann Arbor MI 48106-1346 USA
313/761-4700 800/521-0600

Reproduced with permission of the copyright owner. Further reproduction prohibited without permission.

Reproduced with permission of the copyright owner. Further reproduction prohibited without permission.

TIME RESOLVED OPTICAL METHODS FOR THE STUDY OF PROTEIN FOLDING AND CONFORMATION

by

Anne Gershenson

A dissertation submitted in partial fulfillment
of the requirements for the degree of
Doctor of Philosophy
(Physics)
in The University of Michigan
1996

Doctoral Committee:

Professor Duncan G. Steel, Co-Chair
Professor Ari Gafni, Co-Chair
Professor Daniel Axelrod
Professor Samuel Krimm
Assistant Professor Frederick C. MacKintosh

Reproduced with permission of the copyright owner. Further reproduction prohibited without permission.

UMI Number: 9711968

Copyright 1996 by
Gershenson, Anne

All rights reserved.

UMI Microform 9711968
Copyright 1997, by UMI Company. All rights reserved.

This microform edition is protected against unauthorized
copying under Title 17, United States Code.

UMI
300 North Zeeb Road
Ann Arbor, MI 48103

Reproduced with permission of the copyright owner. Further reproduction prohibited without permission.

© Anne Gershenson
All Rights Reserved 1996

Reproduced with permission of the copyright owner. Further reproduction prohibited without permission.

For my sisters

Simma & Becca

Reproduced with permission of the copyright owner. Further reproduction prohibited without permission.

ACKNOWLEDGMENTS

None of this work would have been accomplished without the ideas, help, support and advice of my thesis advisors Professor Duncan G. Steel and Professor Ari Gafni.

Dr. Joe Schauerte answered a myriad (he never did keep count) of questions and was a good critic of ideas. Both he and Chris Fischer provided invaluable help in dealing with all the complications of the temperature jump experiments. Also, thanks to Chris for making sure that the ghost of Raman was appeased. Kathleen C. Wisser provided help with columns, gels and other biochemical stuff in addition to general friendship. Thanks to Joe Mersol for helping to get me started in the lab and showing me how to do phosphorescence experiments. Thanks are also due to all the members of the Gafni/Steel lab past and present in particular, Dr. Bruce Schlyer, Dr. Nils Bergenhem, Mike Lewis, Peter Wolanin, Vinod Subramaniam, Peter Tumino and Jeff Plomer.

Additional advice on temperature jump experiments came from Dr. Peggy Thompson at NIH. Various and sundry electronics advice and circuits were cheerfully provided by Robert Dennis. Thanks to Dr. Dave Ballou and Dr. Bruce Palfey for the use of their stopped flow setup and for stopped flow advice. I acknowledge financial support from the National Institutes of Health and the University of Michigan.

My years in Ann Arbor would not have been survivable or fun without the other members of the U of M graduate physics class of 1990. Also, Stephanie Miller, Peter MacPherson, Miriam Allersma, Elaine DiMasi, Joanne Wellman and Tator deserve special credit for helping to keep me relatively sane. Finally thanks to my parents and sisters for support and advice.

Reproduced with permission of the copyright owner. Further reproduction prohibited without permission.

TABLE OF CONTENTS

DEDICATION ii

ACKNOWLEDGMENTS iii

LIST OF FIGURES vi

LIST OF TABLES viii

LIST OF APPENDICES ix

CHAPTER

I. PROTEIN FOLDING 1

Experimental Methods 7
References 13

II. THE TRIPLET STATE AND PROTEIN CONFORMATION 15

Introduction 15
Singlet and Triplet States 15
Spin-Orbit Coupling 17
Non-radiative Decay of the Triplet State 19
Quenching Mechanisms 20
Quenching the Trp Triplet State 24
A Sample Application 25
Materials & Methods 28
Cytochrome c acetylation 28
Phosphorescence 30
Results 32
Discussion & Conclusions 34
References 36

III. PHOSPHORESCENCE AND TRANSIENT ABSORPTION 39

Introduction 39
Materials and Methods 41
Rate Equations 42
Instrumentation 43
Data Analysis 47
Discussion 54
Conclusions 56

Reproduced with permission of the copyright owner. Further reproduction prohibited without permission.

References 58

IV. EARLY EVENTS IN PROTEIN FOLDING 60

References 67

V. PH JUMPING 70

Introduction 70
Materials and Methods 71
Spectroscopy 72
Laser induced pH jump 73
pH jump data analysis 76
Results 78
HPTS experiments 78
PGA & AO 80
Adding HPTS 85
Discussion 87
Conclusions 90
References 91

VI. TEMPERATURE JUMPS 94

Introduction 94
Cold and Heat Denaturation 96
Myoglobin & Apomyoglobin 99
Ribonuclease T1 101
Materials & Methods 103
Preparation of ApoMb 104
Temperature Jump Instrumentation 105
Results 108
Discussion, Improvements & Conclusions 114
References 120

VII. CONCLUSION OR THE IMPORTANCE OF LASER PUMP-PROBE 125

References 130

APPENDICES 131

Reproduced with permission of the copyright owner. Further reproduction prohibited without permission.

LIST OF FIGURES

Figure

1.1. Amino acid & peptide bond structure 2

1.2. The hierarchy of protein structure 3

1.3. Energy landscape for protein folding 6

2.1. Energy level diagram showing some possible excitation and relaxation mechanisms for tryptophan 16

2.2. Acceptor and donor molecules with (a) on center dipoles and (b) off center dipoles 22

2.3. Optical density versus concentration of acetylated cytochrome c 29

2.4. Setup for monitoring phosphorescence lifetimes 31

2.5. Quenching of alkaline phosphatase phosphorescence by acetylated and unmodified cytochrome c 33

2.6. Alkaline phosphatase phosphorescence quenching rate versus concentration of cytochrome c for both acetylated and unmodified cytochrome c 34

3.1. Idealized transient absorption spectra of the tryptophan triplet state, neutral radical, cation radical and solvated electron 40

3.2. Decay processes which are important for transient absorption experiments aimed at measuring the lifetime of the lowest triplet state 42

3.3. Schematic of the phosphorescence and transient absorption apparatuses 44

3.4. Data and apparatus for RC circuit simulated data 46

3.5. Room temperature phosphorescence and transient absorption of deoxygenated alkaline phosphatase 49

3.6. Transient absorption of rabbit phosphoglycerate kinase at room temperature 53

5.1. The photoexcitation of HPTS leading to a pH jump 73

5.2. Absorbance of bromcresol green in sodium acetate 74

Reproduced with permission of the copyright owner. Further reproduction prohibited without permission.

5.3. Schematic of the apparatus used to initiate and monitor the pH jump.....75

5.4. (a) Change in transmission at 632.8 nm of a solution containing bromcresol green and HPTS. (b) Change in proton concentration as seen by the bromcresol green at various 355 nm laser intensities 79

5.5. (a) Absorption spectra of acridine orange with and without poly-glutamic acid. (b) Absorption spectra of HPTS with and without poly-glutamic acid and/or acridine orange.....81

5.6. Uncorrected fluorescence emission spectra of acridine orange with and without HPTS or poly-glutamic acid.....84

5.7. Circular dichroism of acridine orange with poly-glutamic acid and/or HPTS 86

6.1. Absorption of water in the near infrared as recorded by a Cary 2400 spectrophotometer (Varian) 95

6.2. Horse heart myoglobin structure, heme not shown, with tryptophan residues in black (Protein Databank 1myb) 100

6.3. Crystal structure of *Aspergillus oryzae* ribonuclease T_1 (Protein Databank 2rnt) 102

6.4. Block diagram of the temperature jump apparatus..... 106

6.5. Normalized, corrected fluorescence spectra of horse skeletal muscle apomyoglobin..... 109

6.6. Changes in fluorescence (a) and circular dichroism (b) due to cold and heat denaturation of horse apomyoglobin 110

6.7 The change in transmission at 290 nm due to the heat denaturation of ribonuclease T_1 112

6.8. Temperature jump as monitored by the absorption at 632.8 nm of the pH indicator methylthymol blue..... 113

Reproduced with permission of the copyright owner. Further reproduction prohibited without permission.

LIST OF TABLES

Table

3.1. Amplitude and lifetime determinations for room temperature phosphorescence and transient absorption data of alkaline phosphatase 50

3.2. Amplitudes and lifetimes for three exponential fits to the transient absorption experiments on deoxygenated rabbit muscle phosphoglycerate kinase 54

Reproduced with permission of the copyright owner. Further reproduction prohibited without permission.

LIST OF APPENDICES

Appendix

A. Abbreviations and Variables 132

B. Chemical Structures 134

C. Some Useful Equations 136

Reproduced with permission of the copyright owner. Further reproduction prohibited without permission.

CHAPTER I

PROTEIN FOLDING

In living organisms, proteins serve a variety of essential functions. Among these roles are catalysis, transport and regulation. In order to perform any of these tasks, a protein must have a compact, well defined three dimensional structure.

Proteins have a hierarchy of structures. They are synthesized as chains of amino acids connected by peptide bonds (Fig. 1.1), and this amino acid sequence is the primary structure (Fig. 1.2). The one dimensional polypeptide chains form helices, sheets and turns which are a protein's secondary structure. Secondary structure packs together into domains referred to as the tertiary structure, and the domains pack together into the quaternary structure. How a protein proceeds from primary structure to the final, compact form is known as protein folding.

In the 1950s, Anfinsen established that proteins are thermodynamically stable i.e. that the final conformation of a protein is determined by amino acid sequence and the environment (temperature, salt concentration, etc.), and not by the manner in which the protein was unfolded and refolded (Anfinsen 1973). This conclusion was based on *in vitro* experiments in which bovine pancreatic ribonuclease was denatured (unfolded) in 8 molar urea, and the protein was oxidized allowing the formation of a population of ribonuclease with a random distribution of disulfide bonds (called "scrambled" ribonuclease). The urea was diluted out, a small amount of reducing agent was added to reduce the scrambled disulfide bonds and the protein was allowed to refold. The refolded protein was homogenous and virtually indistinguishable from the native protein showing that the initial, unfolded conformation did not dictate the final, folded conformation (Anfinsen 1973).

Reproduced with permission of the copyright owner. Further reproduction prohibited without permission.

These experiments led to investigations into how protein folding occurs and how to translate a protein's primary structure into a three dimensional structure.

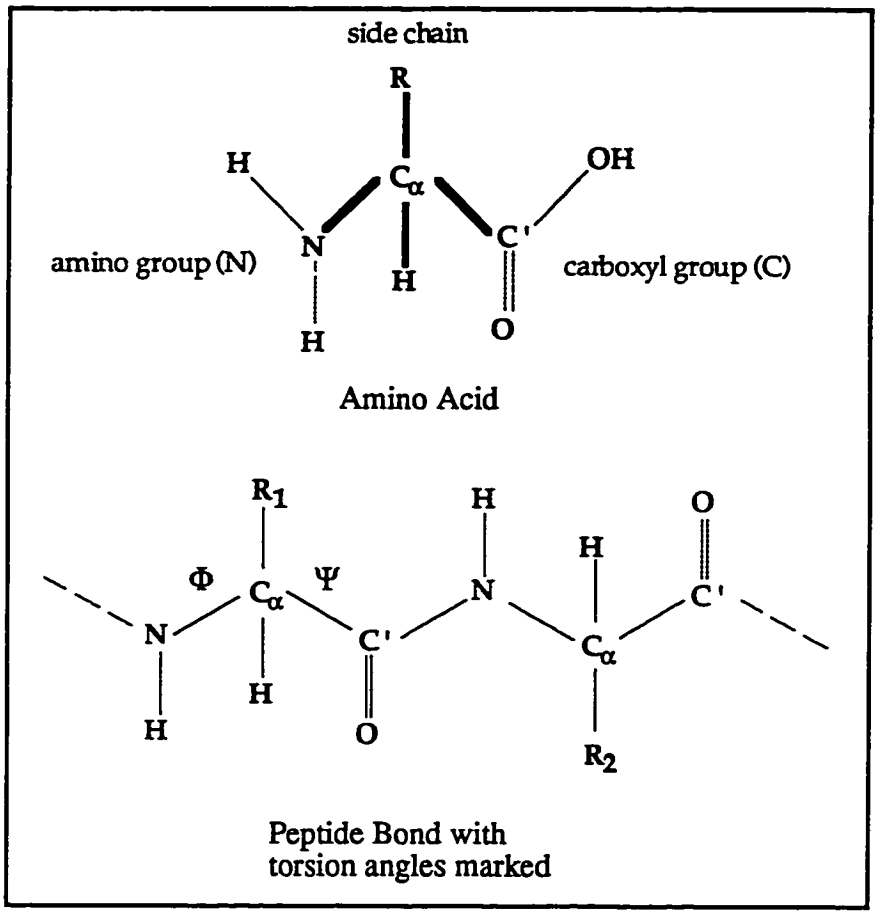

Figure 1.1. Chemical structure of amino acids and peptide bond. The side chain, R, is what distinguishes the various amino acids.

In addition to its intrinsic scientific interest, an understanding of protein folding would be relevant for a variety of applications. There are a number of diseases such as cystic fibrosis and Alzheimer's disease which are associated with misfolded proteins due to problems along the protein folding pathway (Thomas et al. 1995). Additionally, with the advent of the Human Genome Project and other gene sequencing efforts, the number of known protein amino acid sequences has increased dramatically. The ability to translate these sequences into three dimensional protein structures without time consuming experimental determinations of structure using either x-ray crystallography or nuclear

Reproduced with permission of the copyright owner. Further reproduction prohibited without permission.

magnetic resonance (NMR) would aid efforts to understand the functions of these newly sequenced proteins. Finally, an understanding of protein folding could lead to the ability to design new, more stable or efficient proteins for applications in medicine and industry.

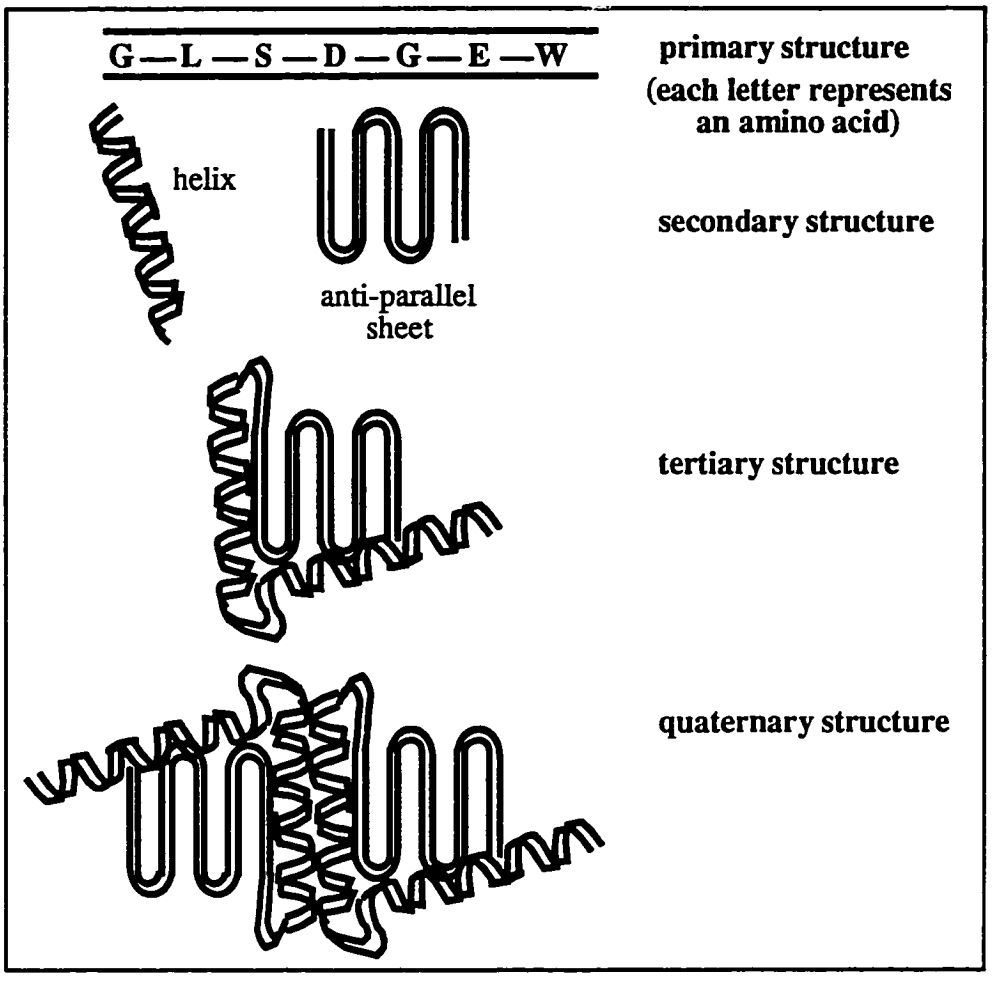

Figure 1.2. The hierarchy of protein structure.

Folded proteins are only marginally stable. The difference in Gibbs free energy between the folded and denatured state is on the order of 50 kJ/mol (Jaenicke 1996) meaning that proteins can be easily unfolded by changing solution parameters such as temperature, pH or salt concentrations. The free energy of stabilization of proteins is a small difference between large numbers since the attractive and repulsive contributions from all of the amino acids must be included (Jaenicke 1996)

Reproduced with permission of the copyright owner. Further reproduction prohibited without permission.

Van der Waals interactions, electrostatic interactions, hydrogen bonding and hydrophobic interactions all contribute to the free energy of proteins and thus to protein folding. These interactions occur not just between amino acids but also between the protein and the solvent molecules. Van der Waals interactions are dipolar forces between fixed or induced molecular dipoles. For distances less than the sum of the van der Waals radii of two polarizable atoms (the van der Waals radius is based on the smallest distance between adjacent, but non-bonded atoms in the crystalline state (Creighton 1993)), the van der Waals interaction is repulsive due to the Pauli exclusion principle while it is attractive for distances which are 0.3 to 0.5 Å greater than the sum of the van der Waals radii (Creighton 1993). Van der Waals forces are important only over short distances and only because amino acids are dipolar.

Electrostatic forces are due to interactions between charged groups, such as the amino acid lysine. Electrostatic repulsions are an important factor in the unfolding of proteins at extremes of pH (Dill 1990). Electrostatics can also contribute to protein stability due to the formation of salt bridges between oppositely charged ion pairs, this stabilization may be particularly important for proteins which remain active and folded under extreme conditions (Jaenicke 1996).

Hydrogen bonds are ionic bonds which arise when a hydrogen atom covalently bound to one atom is also ionically bonded to a second atom (Pauling 1960). In order for this to happen, the second atom must be electronegative. Hydrogen bonding occurs amongst amino acids and between amino acids and water. The various types of secondary structure are characterized by specific hydrogen bonding patterns of the peptide backbone (Branden and Tooze 1991), but the change in free energy due solely to hydrogen bonding does not explain protein folding (Dill 1990).

The hydrophobic interaction relates to the energy of transfer of nonpolar solutes into aqueous solutions (Creighton 1993; Dill 1990) The results of this transfer are extremely temperature dependent. Due to translational entropy, water and nonpolar solutes

Reproduced with permission of the copyright owner. Further reproduction prohibited without permission.

will mix at high temperatures (Dill 1990), and at low temperatures the ordering of water around nonpolar solutes will also allow mixing of water and solute (Creighton 1993; Dill 1990). However, at intermediate temperatures there will be partitioning of water and nonpolar solutes as is seen when water and oil are mixed at room temperature. This interaction is what leads to the burial of nonpolar, hydrophobic residues in the interior of proteins.

Protein folding or unfolding usually involves abrupt transitions indicating that it is a cooperative process, i.e. that the disruption of a single interaction can perturb surrounding interactions. For small proteins, this abrupt transition is often seen to occur under the same conditions no matter what method is used to monitor protein conformation leading to the modeling of protein folding as a two state transition between the native, N, and unfolded, U, state (Privalov 1992):

$$N \rightleftharpoons U \qquad (1.1)$$

The unfolded state consists of a set of interconverting conformations with little or no well-defined structure. The native structure has a compact form with few possible conformations.

For other proteins, folding intermediates, I, are seen in both equilibrium experiments and kinetic experiments leading to a different model:

$$N \rightleftharpoons I_1 \rightleftharpoons I_2 \rightleftharpoons \ldots\ldots \rightleftharpoons U \qquad (1.2)$$

As in the two state model, the native state need not be a single conformation it is rather a set of conformations with a narrow distribution. The same applies to the intermediate states, although the distribution is wider than that of the native state since the protein is no longer as compact. The unfolded state has a large distribution due to its many degrees of freedom (Creighton 1990). The intermediates seen in kinetic and equilibrium experiments may be different.

The total number of three dimensional conformations available to a protein is immense. Each peptide bond in a protein has 2 torsion angles ϕ and ψ about the α carbon

Reproduced with permission of the copyright owner. Further reproduction prohibited without permission.

(Fig.1.1). If a protein contains N amino acids and there are three stable conformations of each torsion angle, then 3^{2N} possible conformations are available to the protein (Voet and Voet 1990). This formulation also assumes no freedom of movement of the side chain and that all possible conformations are energetically equivalent. If the protein can sample 10^{13} conformations per second then it will take approximately $\frac{3^{2N}}{10^{13}}$ seconds for the protein to explore all possible conformations. For an 100 residue protein this corresponds to 10^{81} seconds or more than the age of the universe (Levinthal 1968; Voet and Voet 1990). Proteins fold in milliseconds to hours (Creighton 1993) and this contradiction between the actual time it takes for a protein to fold and the calculated time is called Levinthal's paradox (Levinthal 1968; Voet and Voet 1990).

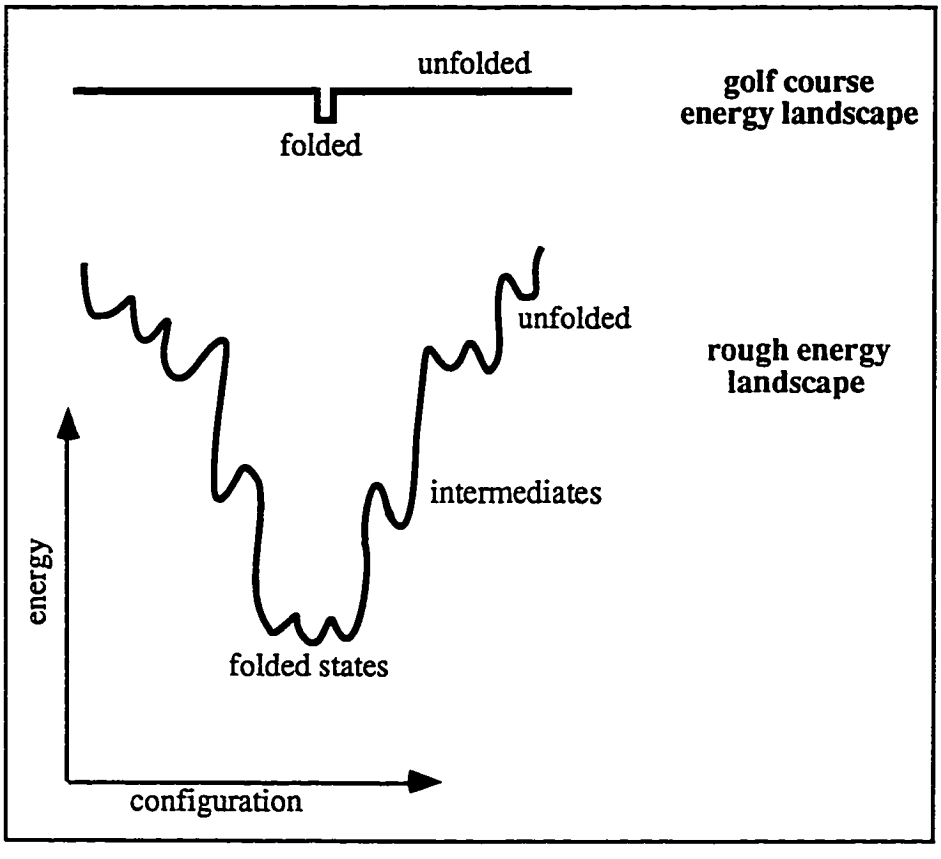

Figure 1.3. Energy landscapes for protein folding.

One way around Levinthal's paradox is to restrict the number of conformations available to the protein. Not all ϕ and ψ angles are possible due to steric hindrance, the fact

Reproduced with permission of the copyright owner. Further reproduction prohibited without permission.

that two amino acid residues cannot be in the same place, and this restricts the number of conformations. Additionally, the assumption of a flat (golf course) energy landscape, in which all conformations are isoenergetic except for the folded conformation, is not valid for a real protein. Depending on the protein's environment some conformations will be more energetically favorable than others.

One model of this energy surface, a one dimensional slice through a multidimensional plot of energy vs. number of configurations, is of a funnel at the bottom of which is the conformation or set of conformations with minimum energy (Fig. 1.3). In this case, protein folding is analogous to a ball rolling down a bumpy hill. This "rough" energy landscape has an overall funnel shape, but the walls of the funnel are not smooth so that a folding protein can get trapped in local energy minima. These energy minima are partly caused by "frustration", all the amino acids in the protein cannot be at their individual energy minima due to chain connectivity and interactions with the other amino acids in the protein (Frauenfelder and Wolynes 1994) . These barriers are generally easily overcome by thermal fluctuations of the protein (Bryngelson et al. 1995). There are also higher barriers in this landscape, places where rearranging contacts between amino acids to go from one conformation to another exacts a large energy price (Bryngelson et al. 1995). Such barriers can slow down protein folding (Dill et al. 1995). This model of protein folding helps to circumvent the Levinthal paradox as well as providing a model for the range of protein folding times.

Experimental Methods

Protein folding can be probed using a number of different methods. These include scanning calorimetry, NMR, mass spectrometry and optical techniques using wavelengths from the ultraviolet (UV) to the infrared (IR). Each of these techniques has its own set of advantages and disadvantages. Scanning calorimetry allows the direct measurement of the change in heat capacity due to protein denaturation and allows conclusions to be directly

Reproduced with permission of the copyright owner. Further reproduction prohibited without permission.

drawn about the cooperativity of a transition (Privalov 1992), but this method yields no information about the structure of the protein under investigation. NMR experiments can yield very detailed pictures of protein conformation but the size of proteins which can be studied by NMR is limited, experiments require high protein concentrations and experiments can take hours to complete so that protein folding cannot be followed in real time. Unlike any of the other techniques, mass spectrometry does not average over populations so that if there is a mass difference between slightly different protein conformations, due for instance to hydrogen-deuterium exchange experiments where solvent exposed hydrogen atoms can exchange with deuterium atoms, the presence of different conformations in a single solution can be detected (Miranker et al. 1996). However structural information is difficult to obtain from this technique alone. Finally, optical techniques allow folding experiments to be conducted in real time. The information obtained, for experiments in the UV and visible range, tends to be either extremely local (luminescence, near UV circular dichroism) or global (far UV circular dichroism).

Proteins absorb light both in the UV due to electronic transitions and in the IR due to the excitement of vibrational modes of the molecule. Additionally, prosthetic groups such as the heme in myoglobin can lead to electronic absorption in the visible range. All of the work in this dissertation involved using UV or visible light.

To first order, electronic absorption is due to the interaction of the induced or permanent molecular electric dipole moment, μ, with the incident electric field (Cantor and Schimmel 1980). The electric field is constant over the dimensions of the molecule so that only μ operates on the initial state of the molecule, ψ_a. The electric dipole transition moment, M_{ba}, between ψ_a and excited state ψ_b is (Cantor and Schimmel 1980):

$$M_{ba} = \langle \psi_b | \mu | \psi_a \rangle = e \langle \psi_b | \sum_i \vec{r}_i | \psi_a \rangle \qquad (1.3)$$

where $\mathbf{r}_i$ is the position vector of the ith electron. The transition rate, $\frac{dP_b}{dt}$, is proportional to the square of M_{ba} times the intensity of the light, I(v) (Cantor and Schimmel 1980):

Reproduced with permission of the copyright owner. Further reproduction prohibited without permission.

$$\frac{dP_b}{dt} \propto \left|\langle \psi_b | \mu | \psi_a \rangle\right|^2 I(\nu) \qquad (1.4)$$

The amount of light transmitted through an absorbing sample, I, is (Cantor and Schimmel 1980):

$$I = I_o 10^{-\epsilon C \ell} \qquad (1.5)$$

where I_0 is the intensity of the incident light, ϵ is the molar extinction coefficient in liter/(mole cm) and is dependent on the incident wavelength, C is the concentration of absorbing molecules in moles/liter and ℓ is the path length of the light. The exponent, $\epsilon C \ell$, is referred to as the absorbance or the optical density (OD). This formulation is known as the Beer-Lambert law (see appendix C).

A protein's peptide backbone absorbs at wavelengths below 230 nm in the far UV region. There is a particularly intense absorption band centered at 190 nm (Cantor and Schimmel 1980). At wavelengths between 230 and 300 nm, the near UV region, protein absorption is dominated by the aromatic amino acids phenylalanine (Phe), tyrosine (Tyr) and tryptophan (Trp). Absorption by phenylalanine is centered around 250 nm and is orders of magnitude weaker than that of tyrosine and tryptophan (Cantor and Schimmel 1980). Tyrosine absorption is centered around 274 nm while tryptophan absorption is comprised of three transitions between 240 and 290 nm.

Absorption measurements may be used to monitor protein conformation. In some proteins, conformational changes lead to a shift in the near UV absorption peak. For these proteins, such as ribonuclease T1 (see ch. VI) folding can be followed by monitoring the change in absorption at a specific wavelength. However, not all proteins show absorption changes upon folding or unfolding.

Even in proteins where conformational changes do not lead to absorption changes, the optical activity as measured by circular dichroism (CD) will change if the conformational change is large enough. Optical activity arises from the coupling between μ and the induced magnetic dipole moment, **m**. The magnetic dipole moment is proportional

Reproduced with permission of the copyright owner. Further reproduction prohibited without permission.

to the cross product between the position operator, **r** and the momentum operator, **p**, (Cantor and Schimmel 1980):

$$\mathbf{m} = \frac{e}{2mc}(\mathbf{r} \times \mathbf{p}) \qquad (1.6)$$

where e is the charge of the electron, m is the electron mass and c is the speed of light. If a component of **m** is parallel to μ then there is optical activity with a rotational strength, R_{ab}, of (Cantor and Schimmel 1980):

$$R_{ab} = \mathrm{Im}\left(\langle \psi_a | \mu | \psi_b \rangle \bullet \langle \psi_b | \mathbf{m} | \psi_a \rangle\right) \qquad (1.7)$$

In order for R_{ab} to be nonzero, a molecule must be asymmetric (Cantor and Schimmel 1980) as is the case for an α helix which has a large far UV CD signal. Alternately, there may be an interaction between **m** of the excited molecule and μ of a nearby molecule; for example, an indole ring (the side chain of Trp) is planar and has no optical activity, but when incorporated into a protein, there can be a large optical activity signal from Trp if there is a nearby electrical dipole.

In CD experiments, the difference in absorption between left and right circularly polarized light is measured as molar ellipticity [θ] in degrees:

$$\theta = 2.303\left(OD_L - OD_R\right)\frac{180}{4\pi} \quad \text{degrees} \qquad (1.8)$$

$$[\theta] = \frac{100\theta}{C\ell} \qquad (1.9)$$

where L and R refer to left and right circular polarization, θ is the measured ellipticity, [θ] is the ellipticity corrected for protein concentration, C, and path length, ℓ. The commonly used units for [θ] are degrees cm^2 per decimole. In the far UV region, θ is very dependent on the conformation of the peptide backbone (secondary structure) so that helices, sheets and random coil structures make distinct contributions to the CD signal. Changes in the far UV CD can be correlated to loss or gain of secondary structure although care must be taken since aromatic amino acids also can contribute to the CD signal in this wavelength range (Woody 1994).

Reproduced with permission of the copyright owner. Further reproduction prohibited without permission.

The aromatic amino acids also yield a CD signal in the near UV region. This signal is affected by side chain conformation and the rigidity of the region in which the aromatic amino acids reside. While the far UV CD signal yields a global measure of structure since it includes contributions from all regions of the protein, the near UV signal is limited to information about the environment surrounding the aromatic amino acids.

Measurement of luminescence spectra and lifetimes can yield information about protein conformation particularly for proteins which do not show changes in absorption. The rate of spontaneous emission is dependent on the square of M_{ba} analogously to absorption. However, since the luminescence techniques used in these studies involved only spontaneous and not stimulated emission, the rate of emission, $\frac{dn_b}{dt}$, is dependent on the number of excited molecules, n_b, and not the excitation light intensity (see equation 1.4) (Cantor and Schimmel 1980):

$$\frac{dn_b}{dt} \propto - |\langle \psi_b | \mu | \psi_a \rangle|^2 n_b \qquad (1.10)$$

Luminescence can be more sensitive to environmental changes due to the long lifetime of the excited state compared to the time scale of 10^{-15} seconds for absorption processes (Cantor and Schimmel 1980). Observed luminescence lifetimes are affected not only by the radiative lifetime of the chromophore but also by competing relaxation mechanisms. The observed lifetime, τ_L, is defined as (Cantor and Schimmel 1980):

$$\tau_L = \frac{1}{\sum_i k_i} \qquad (1.11)$$

The k_is are the rate constants of all processes that lead to loss of population from the excited state. Decay mechanisms include luminescence, collisional quenching, complex formation, energy transfer and excited state reactions. Rates of processes that compete with and thus quench luminescence are directly affected by the local environment of the chromophore; for instance, a chromophore in the interior of a molecule is less likely to be collisionally quenched than one on the surface. Analogously to near UV CD, luminescence

Reproduced with permission of the copyright owner. Further reproduction prohibited without permission.

measurements only yield information about changes in the environment around the emitting chromophore.

In proteins only the aromatic amino acids Phe, Tyr and Trp are luminescent. Phe and Tyr occur more frequently in proteins than does Trp (Voet and Voet 1990), but Phe has a fluorescence quantum yield of approximately 0.04 in solution at pH 7 (Cantor and Schimmel 1980) and is rarely observed to emit. Tyr has a significantly higher quantum yield but is easily quenched in proteins by processes such as energy transfer to Trp residues and proton transfer to charged carboxyl groups or uncharged amino groups (Permyakov 1993). Additionally, if the hydroxyl group of the Tyr residue is hydrogen bonded to peptide bonds the residue is nonfluorescent (Lakowicz 1983). Trp has the highest quantum yield (Cantor and Schimmel 1980) and the longest observed luminescence lifetimes of all three aromatic amino acids.

The work performed for this dissertation used the UV and visible techniques described above to investigate protein folding and/or protein conformation on two time scales. The first experiments employed triplet spectroscopy to look at protein conformation on long (seconds and longer) time scales. The rest of the dissertation explores ways to experimentally observe the earliest events in protein folding using optical techniques.

Reproduced with permission of the copyright owner. Further reproduction prohibited without permission.

References

Anfinsen, C. B. (1973). "Principles that Govern the Folding of Protein Chains." *Science*, 181, 223-230.

Branden, C., and Tooze, J. (1991). *Introduction to Protein Structure*, Garland Publishing, Inc, New York, New York.

Bryngelson, J. D., Onuchic, J. N., Socci, N. D., and Wolynes, P. G. (1995). "Funnels, Pathways and the Energy Landscape of Protein Folding: A Synthesis." *Proteins*, 21, 167-195.

Cantor, C. R., and Schimmel, P. R. (1980). *Biophysical Chemistry Part II: Techniques for the Study of Biological Structure and Function*, W. H. Freeman and Company, New York.

Creighton, T. E. (1990). "Protein Folding." *Biochemical Journal*, 270, 1-16.

Creighton, T. E. (1993). *Proteins: Structures and Molecular Properties*, W. H. Freeman and Company, New York.

Dill, K. A. (1990). "Dominant Forces in Protein Folding." *Biochemistry*, 29(31), 7133-7155.

Dill, K. A., Bromberg, S., Yue, K., Fiebig, K. M., Yee, D. P., Thomas, P. D., and Chan, H. S. (1995). "Principles of Protein Folding - A Perspective from Simple Exact Models." *Protein Science*, 4, 561-602.

Frauenfelder, H., and Wolynes, P. G. (1994). "Biomolecules: Where the Physics of Complexity and Simplicity Meet." *Physics Today*, 47, 58-64.

Jaenicke, R. (1996). "Stability and Folding of Ultrastable Proteins: Eye Lens Crystallins and Enzymes from Thermophiles." *FASEB Journal*, 10(1), 84-92.

Lakowicz, J. R. (1983). *Principles of Fluorescence Spectroscopy*, Plenum Press, New York.

Levinthal, C. (1968). "Are there Pathways for Protein Folding?" *J. Chim. Phys.*, 65, 44-45.

Miranker, A., Robinson, C. V., Radford, S. E., and Dobson, C. M. (1996). "Investigation of Protein Folding by Mass Spectrometry." *FASEB Journal*, 10(1), 93-101.

Pauling, L. (1960). *The Nature of the Chemical Bond*, Cornell University Press, Ithaca, NY.

Permyakov, E. A. (1993). *Luminescent Spectroscopy of Proteins*, CRC Press, Ann Arbor.

Reproduced with permission of the copyright owner. Further reproduction prohibited without permission.

Privalov, P. L. (1992). "Physical Basis of the Stability of the Folded Conformations of Proteins." Protein Folding, T. E. Creighton, ed., W. H. Freeman and Company, New York, 83-126.

Thomas, P. J., Qu, B.-H., and Pedersen, P. L. (1995). "Defective Protein Folding as a Basis of Human Disease." *Trends in Biochemical Science*, 20, 456-459.

Voet, D., and Voet, J. G. (1990). *Biochemistry*, John Wiley & Sons, New York, New York.

Woody, R. W. (1994). "Contributions of Tryptophan Side Chains to the Far-Ultraviolet Circular Dichroism of Proteins." *European Biophysics Journal*, 23, 253-262.

Reproduced with permission of the copyright owner. Further reproduction prohibited without permission.

CHAPTER II

THE TRIPLET STATE AND PROTEIN CONFORMATION

Introduction

As mentioned in the previous chapter, luminescence can be used as a probe of protein conformation. Luminescence may occur due to decay from the excited singlet state, fluorescence, or decay from the triplet state, phosphorescence (Fig. 2.1). Phosphorescence emission requires intersystem crossing from the excited singlet state to the lower energy triplet state and then decay from the triplet state to the singlet ground state. Both of these processes are spin forbidden and the major source of mixing of the triplet and singlet state is spin-orbit coupling (Lower and El-Sayed 1966). In tryptophan (Trp) the spin forbidden nature leads to phosphorescence lifetimes of milliseconds to seconds compared to nanoseconds for fluorescence. This longer lifetime makes the Trp triplet state a particularly sensitive probe of protein conformation.

Singlet and Triplet States

The electron spin has quantum number (s) of 1/2 and projection (m_s) unto the quantization direction (usually chosen to be the z axis) of +1/2 for spin up (α) and -1/2 for spin down (β). The two spin states may be expressed, in matrix notation, as:

$$\alpha = \begin{pmatrix} 1 \\ 0 \end{pmatrix} \quad \beta = \begin{pmatrix} 0 \\ 1 \end{pmatrix} \tag{2.1}$$

In a two electron system, the electrons will either have the same spin orientations (both spin up for example) corresponding to the triplet state or opposite spins (spin up and spin down) corresponding to the singlet state. In the singlet state, the electrons may occupy the same

Reproduced with permission of the copyright owner. Further reproduction prohibited without permission.

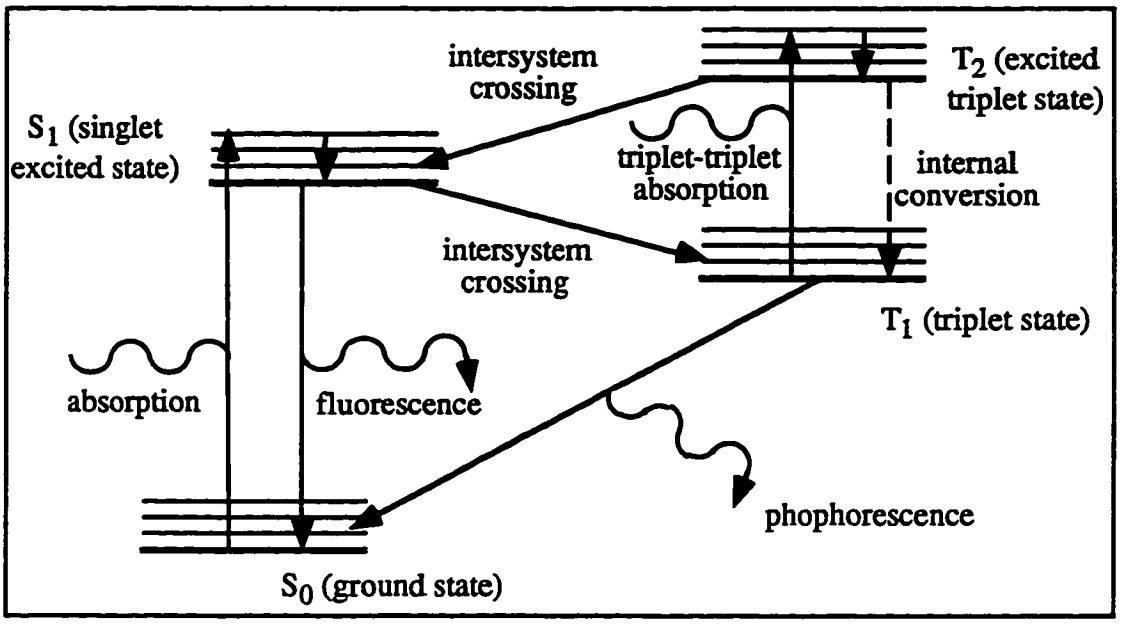

Figure 2.1. Energy level diagram showing some possible excitation and relaxation mechanisms for tryptophan

molecular orbital, but in the triplet state they must occupy different orbitals due to the Pauli exclusion principle. The spin wave functions for the singlet and triplet states in which only one of the two paired electrons is excited may be expressed as (McGlynn et al. 1969):

Singlet: $$\frac{1}{2}[\phi_1(1)\phi_2(2)+\phi_1(2)\phi_2(1)]\,[\alpha(1)\beta(2)-\alpha(2)\beta(1)]$$
$$S=0 \quad M_S=0 \qquad (2.2a)$$

Triplet: $$\frac{1}{\sqrt{2}}[\phi_1(1)\phi_2(2)-\phi_1(2)\phi_2(1)]\,\alpha(1)\alpha(2) \qquad (2.2b)$$
$$S=1 \quad M_S=1$$
$$\frac{1}{2}[\phi_1(1)\phi_2(2)-\phi_1(2)\phi_2(1)]\,[\alpha(1)\beta(2)+\alpha(2)\beta(1)]$$
$$S=1 \quad M_S=0$$
$$\frac{1}{\sqrt{2}}[\phi_1(1)\phi_2(2)-\phi_1(2)\phi_2(1)]\,\beta(1)\beta(2)$$
$$S=1 \quad M_S=-1$$

where the (1) and (2) denote the electrons, ϕ denotes a molecular orbital and the subscript refers to excitation state so that 1 is the ground state and 2 is the first excited state. S and M_S are the spin quantum numbers for the combined, two electron system. Note that the names of the states arise from the multiplicity (2S+1) of the states i.e. the number of possible values of M_S. The singlet state spin state is antisymmetric and in order for the total

Reproduced with permission of the copyright owner. Further reproduction prohibited without permission.

wave function describing the electronic state to be antisymmetric the orbital wave function must be symmetric; the opposite is true for the triplet state. To go from a singlet state to a triplet state requires a spin flip which cannot occur in the absence of some perturbing force, in this case spin-orbit coupling.

Spin-Orbit Coupling

An electron with spin angular momentum, **s**, has a magnetic moment, μ given by (Lower and El-Sayed 1966):

$$\mu = -\left[\frac{|e|}{m_e c}\right]\mathbf{s} \qquad (2.3)$$

where e is the charge on the electron, m_e is the mass of the electron and c is the speed of light. This spin magnetic moment interacts with the magnetic field due to the motion of the electron relative to the nucleus to produce spin-orbit coupling (Lower and El-Sayed 1966, McGlynn et al. 1969). The perturbation of the Hamiltonian due to spin orbit coupling, $\mathbf{H}_{SO}$, may be classically expressed as (Lower and El-Sayed 1966):

$$\mathbf{H}_{so} = -\mu \bullet (\mathbf{EXv}) \qquad (2.4)$$

EXv is the magnetic field produced by the velocity, **v**, of the electron in the electric field, **E**, of the nucleus. In quantum mechanics, **EXv** may be expressed in terms of the orbital angular momentum, **L**, of the electron. For a molecule with M nuclei and N electrons, it is necessary to sum contributions from the various electrons and nuclei leading to an approximation of $\mathbf{H}_{SO}$ as (Michl and Bonacic-Koutecky 1990):

$$\mathbf{H}_{so} = \frac{e^2}{2m^2c^2}\sum_{j=1}^{N}\sum_{\alpha=1}^{M}\frac{Z_\alpha}{|\mathbf{r}_{\alpha j}|}\mathbf{l}_j \bullet \mathbf{s}_j \qquad (2.5)$$

$|e|Z_\alpha$ is the charge of the αth nucleus and $\mathbf{r}_{\alpha j}$ is the position vector of the jth electron of the αth nucleus. Note that this version of the spin-orbit Hamiltonian neglects interaction between single electrons and other electrons in the molecule which may be important in some systems (McGlynn et al. 1969). The appearance of Z in equation 2.5 indicates that spin-orbit coupling is larger in heavier atoms; in these atoms, the electrons are also closer to

Reproduced with permission of the copyright owner. Further reproduction prohibited without permission.

the nucleus again increasing the spin-orbit coupling (McGlynn et al. 1969; Michl and Bonacic-Koutecky 1990).

Spin-orbit coupling perturbs the pure electronic spin states of electrons in a molecule. This perturbation means that the singlet states, ${}^1\psi$, acquire some triplet character and vice versa (Lower and El-Sayed 1966):

$${}^1\psi_0 = {}^1\psi_0^\circ + \sum_j \delta_{0j}\, {}^3\psi_j^\circ \qquad (2.6)$$

$${}^3\psi_1 = {}^3\psi_1^\circ + \sum_k \delta_{1k}\, {}^1\psi_k^\circ \qquad (2.7)$$

${}^3\psi_j^\circ$ is the jth unperturbed triplet state, the sums are carried out over all the vibrational substates in the triplet or singlet state under consideration and the perturbations, δ, are calculated according to first order perturbation theory so that (Lower and El-Sayed 1966):

$$\delta_{oj} = \frac{\left\langle {}^1\psi_0^\circ \middle| H_{so} \middle| {}^3\psi_j^\circ \right\rangle}{\left| {}^1E_0 - {}^3E_j \right|} \qquad (2.8)$$

where E designates the energy of the unperturbed state. It is this mixing of spin states that allows intersystem crossing to occur.

Once intersystem crossing has occurred from the first excited singlet state to the triplet state, there must be a radiative transition to the singlet ground state in order for phosphorescence to be observed. Radiative transitions are electronic transitions and to first order are due to the electron dipole operator, er (Cantor and Schimmel 1980; McGlynn et al. 1969). Thus the probability, P, of a radiative transition from the first triplet state down to the singlet ground state is (Lower and El-Sayed 1966; McGlynn et al. 1969):

$$P = \left| \left\langle {}^3\psi_1 \middle| \sum_i e\mathbf{r}_i \middle| {}^1\psi_0 \right\rangle \right|^2 \qquad (2.9)$$

where the wave functions are given by equations 2.6 and 2.7 and r is the position operator. Interactions between the pure, unperturbed spin states do not contribute to the probability of a transition so that, to first order, the probability of phosphorescence may be expressed as (Lower and El-Sayed 1966; McGlynn et al. 1969):

Reproduced with permission of the copyright owner. Further reproduction prohibited without permission.

$$P=\left|\sum_k \delta_{1k}\left\langle {}^1\psi_k^\circ\left|\sum_i e\mathbf{r}_i\right|{}^1\psi_0^\circ\right\rangle+\sum_j \delta_{0j}\left\langle {}^3\psi_1^\circ\left|\sum_i e\mathbf{r}_i\right|{}^3\psi_j^\circ\right\rangle\right|^2 \qquad (2.10)$$

Unfortunately, all of the above quantities are very difficult to calculate for molecules such as Trp much less for a Trp residue in a protein.

Non-radiative Decay of the Triplet State:

In the absence of external quenchers, the observed phosphorescence lifetime, τ_p, (i.e. the observed radiative lifetime of the triplet state) is dependent on the intrinsic radiative rate constant, k_r, and the nonradiative rate constant, k_{nr} (Schauerte et al. 1996):

$$\frac{1}{\tau_p}=k_r+k_{nr} \qquad (2.11)$$

Nonradiative decay occurs due to overlap between the vibrational states of the excited and ground states (Lower and El-Sayed 1966). Vibrational overlap is influenced by the geometry of the triplet and ground states, the vibrational frequencies of the two states, the size of the molecule as well as the energy gap between the two states (Lower and El-Sayed 1966). Changes in vibrational overlap which do not result in alterations of the electronic wavefunctions will still affect τ_p due to modifications of the rate of nonradiative decay.

For the Trp triplet state, the nonradiative term is believed to arise from out of plane motions of the residue's indole ring (Lower and El-Sayed 1966). The amplitude of this motion is dependent on the rigidity of the Trp residue's environment. For instance, Trp residues in tightly packed, rigid protein cores have a smaller range of motion and thus much longer phosphorescence lifetimes than do Trp residues which are solvent exposed. Strambini and Gonnelli demonstrated that the phosphorescence lifetime of N-acetyltryptophanamide is strongly correlated to the viscosity of the solvent in which it is dissolved (Strambini and Gonnelli 1985; Strambini and Gonnelli 1995). The effect of the rigidity of the environment on the Trp triplet state makes this state a particularly sensitive

Reproduced with permission of the copyright owner. Further reproduction prohibited without permission.

probe of protein folding, since as a protein folds and rigidity increases out of plane motion become progressively more restricted.

Quenching Mechanisms:

In fluid systems, such as those used for protein experiments, there is almost never a lack of external quenchers. These quenchers lead to a modification of equation 2.11 (Schauerte et al. 1996):

$$\frac{1}{\tau_p} = k_r + k_{nr} + k_q[Q] \qquad (2.12)$$

where k_q is the quenching rate constant and [Q] is the concentration of external quencher. The mechanisms of external quenching include collisions, exchange interactions, electron transfer and energy transfer.

Exchange effects are very short range and depend on the electrostatic interactions between the charge distributions of donor and acceptor molecules (Dexter 1953). In an exchange interaction, two molecules swap electrons due to overlap of their charge distributions. This mechanism varies exponentially with distance (Dexter 1953):

$$k_e \propto e^{-2r/L} \qquad (2.13)$$

k_e is the exchange rate constant, r is the distance between the donor and acceptor and L is the effective Bohr radius (~0.8 to 1 Å) for the excited donor and ground state acceptor molecules. Given the dependence on the Bohr radii, exchange interactions can be ruled out if quenching occurs over long distances.

Electron transfer also depends exponentially on the distance, r, between the donor and acceptor molecules (Canters and Kamp 1992; Marcus and Sutin 1985):

$$k_{et} \propto e^{-\beta r} \qquad (2.14)$$

k_{et} is the electron transfer rate and β is a measure of the overlap of the electronic wave functions of the acceptor and donor (Canters and Kamp 1992). Other factors which influence the electron transfer rate are the relative orientations of the molecules, the dielectric constant of the solvent and the redox potential of the donor-acceptor pair (Marcus

Reproduced with permission of the copyright owner. Further reproduction prohibited without permission.

and Sutin 1985). The redox potential may be varied by changing the oxidation state of the acceptor and this manipulation will change the quenching rate if electron transfer is the relevant quenching mechanism.

Energy transfer may occur due to dipole-dipole interactions between the excited molecule and an external quencher; this type of transfer is called Förster energy transfer. The Förster energy transfer rate, k_T, depends inversely on the sixth power of the distance between the donor and acceptor chromophores, due to the dipolar nature of the interaction (Cantor and Schimmel 1980; Förster 1948; Förster 1966; Mersol 1992):

$$k_T = \frac{1}{\tau_D}\left(\frac{R_o}{r}\right)^6 \qquad (2.15)$$

τ_D is the lifetime of the donor molecule in the absence of the acceptor and R_0 is the separation between donor and acceptor at which the transfer efficiency is fifty percent. R_0 is defined as:

$$R_o = 9.79X10^3\left(\frac{J\kappa^2\phi_D}{n^4}\right)^{1/6} \text{ Å} \qquad (2.16)$$

ϕ_D is the emission quantum yield of the donor in the absence of acceptor and n is the refractive index of the solution. J is the spectral overlap integral between the emission of the donor, $F(\lambda)$, and the absorption of the acceptor (which is dependent on the extinction coefficient, $\varepsilon(\lambda)$):

$$J = \frac{\int F(\lambda)\varepsilon(\lambda)\lambda^4 d\lambda}{\int F(\lambda)d\lambda} \qquad (2.17)$$

where λ is the wavelength of light. In the absence of spectral overlap there is no Förster energy transfer nor are there exchange interactions.

The κ^2 term in equation 2.16 depends on the relative orientations of the dipoles of the donor and acceptor molecules:

$$\kappa^2 = (\cos\gamma - 3\cos\alpha\cos\beta)^2 \qquad (2.18)$$

γ is the angle between the two dipole transition moments, α is the angle between the donor dipole moment and the line connecting the center of the two molecules and β is the angle

Reproduced with permission of the copyright owner. Further reproduction prohibited without permission.

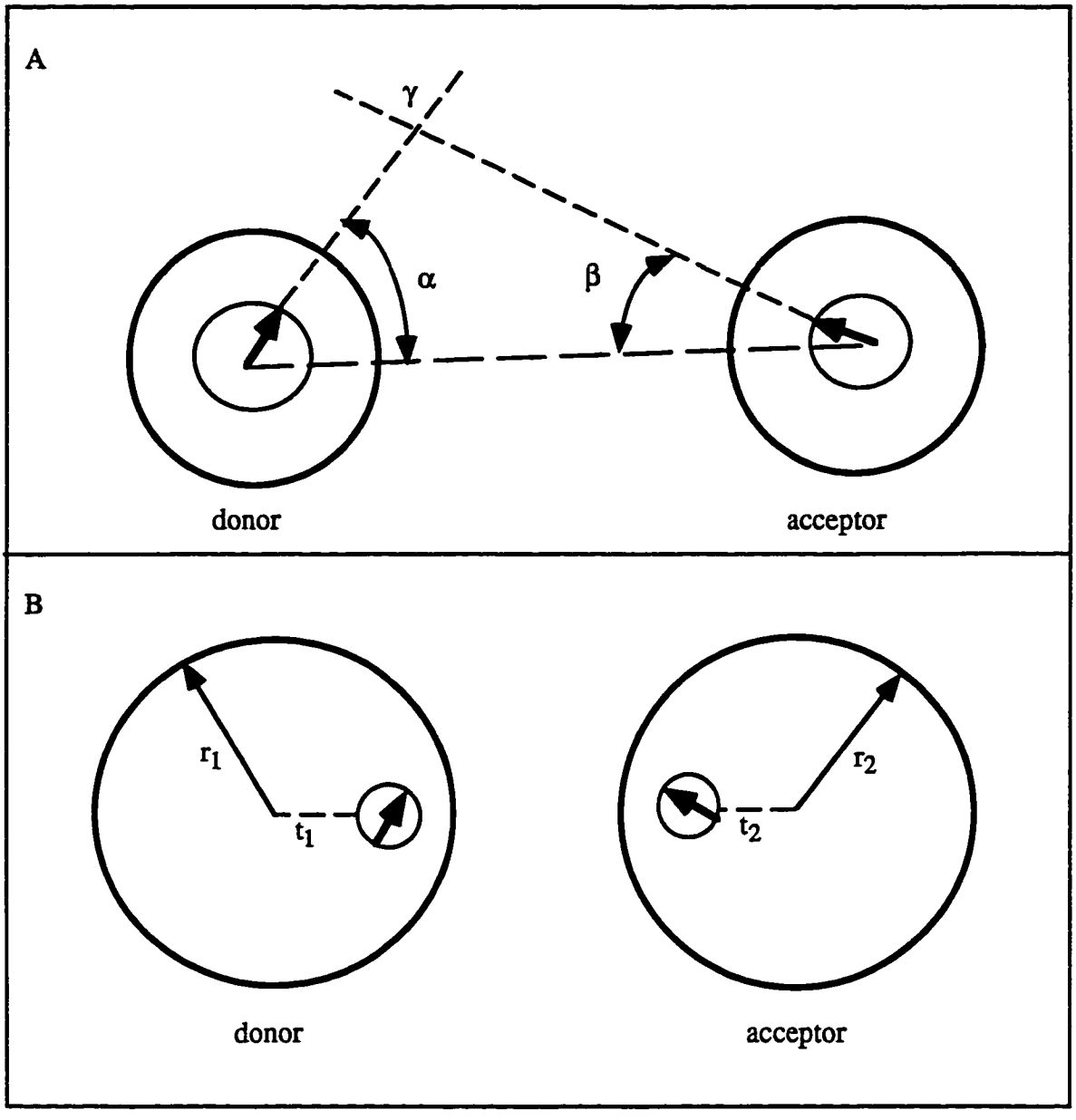

Figure 2.2. A. Acceptor and donor molecules with on center dipoles. The angles shown are those used for calculating κ^2 (equation 2.18). B. The geometry for donor and acceptor molecules with off center dipoles (equation 2.21).

between the connecting line and the acceptor dipole moment (Fig. 2.2). For a spherically symmetric donor-acceptor pair (Fig. 2.2A), Brownian motion can randomize the orientation of the donor and acceptor pair leading to a κ^2 equal to 2/3 as long as the time scale for the Brownian motion is longer than the excited state lifetime of the donor. If the orientations are not randomized, either due to steric hindrance (Fig. 2.2B) or to short

Reproduced with permission of the copyright owner. Further reproduction prohibited without permission.

excited state lifetimes, κ^2 is between 0 and 4 (Stryer 1978) and can be derived using equation 2.18 for various geometries (Mersol et al. 1992).

In the absence of other quenching mechanisms, the distance between the donor and acceptor dipole moments may be measured by monitoring the quenching rate at different concentrations of acceptor. The slope of the plot of quenching rate versus acceptor concentration (see equation 2.12) is the bimolecular rate of Förster energy transfer. Assuming that κ^2 is 2/3, all the other quantities for the calculation of R_0 (equation 2.16) are measurable and the distance between the donor and acceptor dipoles may be calculated from equation 2.15. Thus, Förster energy transfer can serve as a "spectroscopic ruler".

All of the above discussion assumes that the distribution of donors and acceptors is static during the excited state lifetime of the donor molecule (τ_D). However, phosphorescence is a long lived phenomenon which allows time for donor and acceptor molecules to diffuse changing the average separation and affecting the rate of energy transfer. In three dimensions, the mean square distance diffused in time t is 6Dt where D is the sum of the donor and acceptor diffusion coefficients; thus for diffusion to be important for Förster energy transfer $6D\tau_D$ must be larger than the square of the mean intermolecular distance between donor and acceptor molecules (s^2) (Thomas et al. 1978). The value of D for proteins is on the order of 10^{-7} cm^2/sec, and if the acceptor molecule is present at concentrations of 0.1 mM or more then Förster energy transfer is enhanced by diffusion only if the lifetime of the donor molecules is greater than 1 millisecond (Thomas et al. 1978).

This type of diffusion enhanced energy transfer where $6D\tau_D >> s^2$ is referred to as Förster energy transfer in the rapid diffusion limit and is characterized by the fact that all donors see the same distribution of acceptors. The rate of energy transfer is given by (Mersol 1992):

$$k_t = \frac{1}{V_D}\rho_A \int V_D \int \frac{1}{\tau_D}\left\langle\left(\frac{R_o}{r}\right)^6\right\rangle_\Omega dV_A \qquad (2.19)$$

Reproduced with permission of the copyright owner. Further reproduction prohibited without permission.

V_D and V_A are the volumes available to donor and acceptor molecules respectively, ρ_A is the density of acceptors and $\langle\ \rangle_\Omega$ is the angular averaging over the allowed orientations of the donor and acceptor. As an example, let the donor and acceptor be represented by spheres with centered dipoles (Fig. 2.2A) if κ^2 is 2/3 then k_t is determined as follows (Thomas et al. 1978):

$$k_t = \frac{\rho_A}{\tau_D}\int_a^\infty \left(\frac{R_o}{r}\right)^6 dr \int_0^\pi \sin\theta d\theta \int_0^{2\pi} d\phi = \frac{4\pi}{3}\frac{\rho_A}{\tau_D} R_o^6 a^{-3} \qquad (2.20)$$

where a is the distance of closest approach between the donor and acceptor dipoles and equals the sum of the radii of the two spheres (for the derivation with $\kappa^2 \neq 2/3$ see Mersol 1992). As another important example Mersol (1992) derived the equation for k_t in the case of two spherical molecules with radii r_1 for the donor and r_2 for the acceptor and off-center chromophores:

$$k_t = \frac{4\pi}{3}\frac{\rho_A}{\tau_D} R_o^6 \frac{(a+t_1+t_2)^3\left(a^2+2at_1+2at_2+2t_1t_2\right)}{a^2(a+2t_1)^2(a+2t_2)^2(a+2t_1+2t_2)^2} \qquad (2.21)$$

where again κ^2 is assumed to be 2/3, a is the distance of closest approach and t_1 and t_2 are the offsets of the dipoles from the center of the spheres for the donor and acceptor molecules respectively (see Fig. 2.2B).

Quenching the Trp Triplet State:

Quenchers of the Trp triplet state range from small molecules such as oxygen or nitric oxide to other amino acids in the protein under study. Oxygen and nitric oxide have quenching rates which are smaller than expected if they were to diffuse through proteins and collisionally quench the Trp triplet state (Strambini 1987; Vanderkooi 1992) and thus quenching by these small molecules seems to be a longer range process. This comparison is based on rates for the free diffusion of oxygen in aqueous solutions as well as fluorescence results indicating that the quenching rate for oxygen is approximately forty percent of that expected for free diffusion of oxygen in aqueous solution (Lakowicz 1983). It is not clear whether this is an appropriate model for quenching of phosphorescent Trps

Reproduced with permission of the copyright owner. Further reproduction prohibited without permission.

since the viscosity of the environment surrounding a phosphorescing Trp is expected to be greater than that of an aqueous solution.

The amino acids histidine, His, and tyrosine, Tyr, will quench the Trp triplet state if they are within 7 Å of the Trp (Gonnelli and Strambini 1995). Cystine, Cys, residues both in and out of disulfide bonds will also quench phosphorescence by short range mechanisms (Gonnelli and Strambini 1995). Disulfide bonds appear to quench Trp phosphorescence by short range electron transfer (Li et al. 1989). Quenching of Trp triplet states by other Trp residues is a longer range process with an exponential dependence on distance (Gonnelli and Strambini 1995) indicating a possible role for exchange interactions. The quenching of the Trp triplet state by these amino acids is another factor that makes phosphorescence a sensitive probe of conformation. The distance of a Trp residue from Cys, His, Tyr or other Trp residues will change as the protein conformation is altered by protein folding or unfolding affecting the phosphorescence lifetime.

A Sample Application

Trp phosphorescence from proteins with lifetimes of seconds was originally detected in rigid glasses at liquid nitrogen temperatures (Longworth 1971). In 1974 Saviotti and Galley demonstrated that the lifetime of Trp phosphorescence in liver alcohol dehydrogenase at room temperature is dependent on the concentration of dissolved oxygen present. Room temperature phosphorescence (RTP) has since been observed in a number of proteins in fluid solutions and in the absence of oxygen (Gonnelli and Strambini 1995; Vanderkooi 1992). The RTP lifetime of a Trp residue can vary 3 to 4 orders of magnitude depending on the location of the Trp relative to the solvent (Schauerte et al. 1996) and the presence or absence of quenchers.

The longest observed Trp RTP lifetime comes from the protein *Escherichia coli* alkaline phosphatase (AP). AP is a dimeric enzyme with three Trp residues per monomer (Wyckoff et al. 1983) and an RTP lifetime on the order of 2 seconds. The RTP signal of

Reproduced with permission of the copyright owner. Further reproduction prohibited without permission.

AP was assigned to Trp 109 by Strambini (1987) because the emission had been identified as arising from only a single Trp residue per monomer which had to be in a rigid environment as evidenced by the long RTP lifetime.

In order to verify this assignment and to test the utility of Förster energy transfer to locate phosphorescing Trp residues within proteins, particularly proteins with multiple Trp residues, Mersol and coworkers (1991, 1992) investigated the RTP of AP in the presence and absence of external quenchers. The phosphorescing Trp in AP served as the donor for Förster energy transfer, and, initially, Mersol used small dye molecules as acceptors. The quenching of these dyes was found to be independent of the amount of spectral overlap indicating that some process other than Förster energy transfer was responsible for the quenching (Mersol 1992; Mersol et al. 1991). Therefore, instead of dye molecules, the heme proteins horse skeletal muscle myoglobin (Mb) and horse heart cytochrome c (cyt c) were used as acceptors. The heme absorption overlaps the phosphorescence of Trp.

Mersol and coworkers modeled the donor and acceptor proteins as spheres with off center dipoles (Fig. 2.2B) and used equation 2.21 for the diffusion-enhanced rate of Förster energy transfer. Equation 2.21 can be used to determine the offset (t_1) of the emitting Trp from the center of AP. The known quantities were determined in the following manner.

The rate of Förster energy transfer per millimolar acceptor $\left(\frac{k_t}{\rho_A}\right)$ was determined from the slope of Stern-Volmer plots i.e. plots of measured RTP decay rate constants versus quencher concentration (see equation 2.10). τ_D was determined from the RTP decay of AP in the absence of heme proteins. Radii (r_2 in equation 2.21) of 15.2 Å and 17.4 Å were used for cyt c and Mb respectively with offsets (t_2) of 9.7 Å and 7.8 Å for the heme group from the proteins' center (for a derivation of these distances see Mersol (1991)). The radius used for AP was 30 Å (r_1).

Reproduced with permission of the copyright owner. Further reproduction prohibited without permission.

R_0 was calculated according to equation 2.16 using a value of 2/3 for κ^2 and the refractive index of the solution. As noted previously, a κ^2 of 2/3 is not strictly applicable to the off center geometry due to steric hindrance (Fig. 2.2B). However, since the donor and acceptor chromophores are not close to the surface using 2/3 rather than a calculated value of κ^2 results in only a small error (Mersol et al. 1991). The radiative efficiency was calculated by dividing the RTP lifetime in the absence of acceptor, 1.9 seconds, by an estimated radiative lifetime of 11.5 seconds (Mersol 1992). The overlap integral (J) was calculated by summing over the product of the normalized phosphorescence spectrum of AP; the normalized absorption spectrum of the heme protein in the region from 390 to 590 nm (only the heme group absorbs in this wavelength range) and the wavelength to the fourth. This sum was divided by the sum of the normalized phosphorescence (equation 2.17).

From the data on quenching of RTP by various concentrations of Mb the distance of the emitting Trp below the surface of AP, t_1, was calculated to be 16 Å by Mersol and coworkers. This value of t_1 was not affected by varying the pH above and below the pI of Mb, indicating that changing the charge of Mb did not alter the transfer rate. Additionally, the calculated distance between the heme in Mb and the emitting Trp in AP was beyond the distance at which exchange interactions between the two molecules would be important. Finally, this location of the emitting Trp in AP is in good agreement with Strambini's assignment of the long lived RTP of AP to Trp 109 (Gonnelli and Strambini 1995; Strambini 1987).

The value of t_1 calculated from the cyt c quenching data was 8 Å. This low value was proposed to arise from either the inadequacy of modeling AP, Mb and cyt c as spheres or from electrostatic interactions between cyt c and AP. Horse heart cytochrome c has 19 lysine residues leading to an overall charge of +8 at pH 7.2 (Goldkorn and Shejter 1979). This large positive charge could lead to electrostatic interactions between cyt c and AP

Reproduced with permission of the copyright owner. Further reproduction prohibited without permission.

which, due to the high pI of 10.7 (Lehninger 1982), could not be reversed by performing experiments at pHs above and below the pI as was done for Mb.

However, it is possible to significantly change the charge of cyt c by acetylating the protein. Acetylation neutralizes the charge of each lysine residue modified (Finkelstein et al. 1981). As an extension of the work of Mersol and coworkers, and to determine whether or not electrostatics were a factor in the quenching of AP by reduced cyt c, RTP experiments were performed using AP and acetylated, reduced cyt c.

Materials & Methods

Escherichia coli AP type III-S was obtained from Sigma Chemical Co. as a crystalline suspension in 2.5 ammonium sulfate solution. Crystallized horse heart cytochrome was purchased from Boehringer Mannheim Biochemicals. CM Sephadex C-50 was obtained from Pharmacia Fine Chemicals, diethylenetriamine pentaacetic acid (DETAPAC), a chelating agent, picrylsulfonic acid (TNBS) and sodium dithionite were also purchased from Sigma. All chemicals were used without further purification

Cytochrome c acetylation

Cyt c was acetylated according to the method of Takemori and coworkers as modified by Finkelstein and coworkers (Finkelstein et al. 1981; Takemori et al. 1962). A 10 ml solution containing 2 gm of anhydrous sodium acetate was prepared, cooled to 0° C and 100 mg of cyt c was added. Once the cyt c was dissolved, 0.16 ml of acetic anhydride was added dropwise, the solution was stirred on ice for 40 minutes and transferred to dialysis tubing. The cyt c was dialyzed at 4°C against 1 liter of 10 mM potassium phosphate, 0.1 mM DETAPAC pH 7.4 for 24 hours with 3 changes of solution . The acetylated cytochrome c was then passed through a CM Sephadex column pre-equilibrated with 10 mM potassium phosphate, 0.1 mM DETAPAC pH 7.4 in order to remove the unaltered cyt c.

Reproduced with permission of the copyright owner. Further reproduction prohibited without permission.

The acetylated cyt c was concentrated in Centricon-10 microconcentrators (Amicon) by centrifugation for approximately 1 1/2 hour at 4750 rpm. The concentrated, acetylated cyt c was diluted with Tris-HCl buffer, pH 7.5 and centrifuged again to obtain a final solution of acetylated cyt c in Tris-HCl buffer, pH 7.5 for use in the phosphorescence experiments. The final concentration of acetylated cyt c ([ac. cyt c]) was determined by:

$$[\text{ac.cyt c}] = \frac{(OD_{red} - OD_{ox})}{\varepsilon} \qquad (2.22)$$

where OD is the measured optical density at 550 nm, red refers to the reduced protein, ox refers to the oxidized protein and ε is the reduced minus oxidized extinction coefficient which equals 19.5 mM^{-1} cm^{-1} at 550 nm (Lambeth et al. 1981).

The degree of modification of cytochrome c was determined using the trinitro-benzenesulfonic acid (TNBS) method of Finkelstein, et al (1981). Following the Sephadex column, 2 ml of the acetylated cyt c was dialyzed for four hours against 500 ml of 4% sodium carbonate buffer pH 8.7, and the concentration of acetylated cyt c was determined

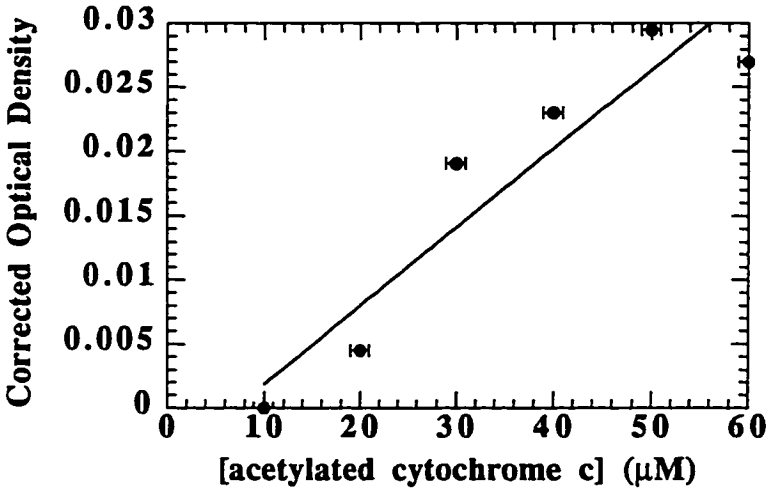

Figure 2.3. Optical density (OD) versus the concentration of acetylated cytochrome c. The OD values were corrected by subtracting off the OD of a cyt. c without TNBS blank and the OD of a TNBS blank. All ODs are the average of two experiments and the error bars are the standard deviations of the averages. The line shown is a least squares fit to the data with a slope of $6.1X10^{-4}$ μM^{-1}

Reproduced with permission of the copyright owner. Further reproduction prohibited without permission.

as described above. 5 to 20 nmoles modified cyt c and then 50 µl of 1% TNBS in water (stored on ice) were added to 4% sodium carbonate buffer for a final volume of 0.5 ml (a concentration of 10-60 µM acetylated cytochrome c was thus obtained). The samples were then incubated at 50° C for 5 minutes as were blanks containing sodium carbonate buffer with and without 50 µl TNBS. After 5 minutes samples were removed from the water bath and put on ice in order to stop the reaction and to prevent the decomposition of TNBS into picric acid.

The percent acetylation was determined by diluting 50 µl of sample with 950 µl distilled water and immediately reading the absorbance at 360 nm using a Shimadzu Model UV-260 spectrophotometer. The same procedure was repeated for native cytochrome c including and excluding the addition of TNBS. The slope of absorbance vs. concentration was determined for native cytochrome c without TNBS. The value of absorbance for the blank containing only TNBS and the value of absorbance for given concentrations of native cytochrome c without TNBS were subtracted from the data for acetylated and native cytochrome c incubated with TNBS. From this corrected data, the percent acetylation was calculated using the equation of Azzi, et al (1975):

$$\% \text{ modification} = 100\left(1 - \frac{S_{acetylated}}{S_{native}}\right) \qquad (2.23)$$

where S is the slope of the plot of absorbance vs. concentrations for acetylated and native cytochrome c corrected as described above. The slopes were determined to be $1.8X10^{-3}$ μM^{-1} for unmodified cyt c and $6.1X10^{-4}$ μM^{-1} for acetylated cyt c (Fig. 2.3). The subtraction of the cyt c and TNBS controls added some noise to the data.

Phosphorescence:

Deoxygenation and phosphorescence studies were conducted as described by Mersol (1991, 1992). AP was prepared at a concentration of 0.5 mg/ml in 0.4% ß-D glucose, 50 mM Tris-HCl pH 7.5; 0.4% ß-D glucose was also added to the cyt c. 300 µl

Reproduced with permission of the copyright owner. Further reproduction prohibited without permission.

of AP were placed in a quartz vacuum cuvette and 500 µl of concentrated cyt c were placed in a glass test tube. To both the AP and the cyt c was added 1 µl of 20 mg/ml glucose oxidase and 2 mg/ml catalase. Glucose oxidase helped to deoxygenate the solution by catalyzing the reaction of oxygen and ß-D glucose to produce gluconolactone and hydrogen peroxide which was scavenged by the catalase (Englander et al. 1987). Deoxygenation was performed by covering the protein solutions with a stream of ultrapure Argon while stirring. After approximately 15 minutes under Argon the samples were removed and covered with a layer of heavy mineral oil to prevent oxygen contamination. Millimolar concentrations of sodium dithionite dissolved in Tris-HCl buffer, pH 7.5 were then added to both the AP and the cyt c in order to reduce the cyt c and to help prevent oxygen contamination. A phosphorescence experiment was conducted with the AP and then increasing amounts of native or acetylated cyt c were added for quenching experiments.

Phosphorescence data were collected using the setup described by Mersol (1991, 1992) (Fig. 2.4). The second harmonic of a Spectra-Physics Nd:YAG (model DCR-11) provided a 7-9 nsec pulse at 532 nm. This pulse pumped a dye laser (Quanta-Ray PDL-3)

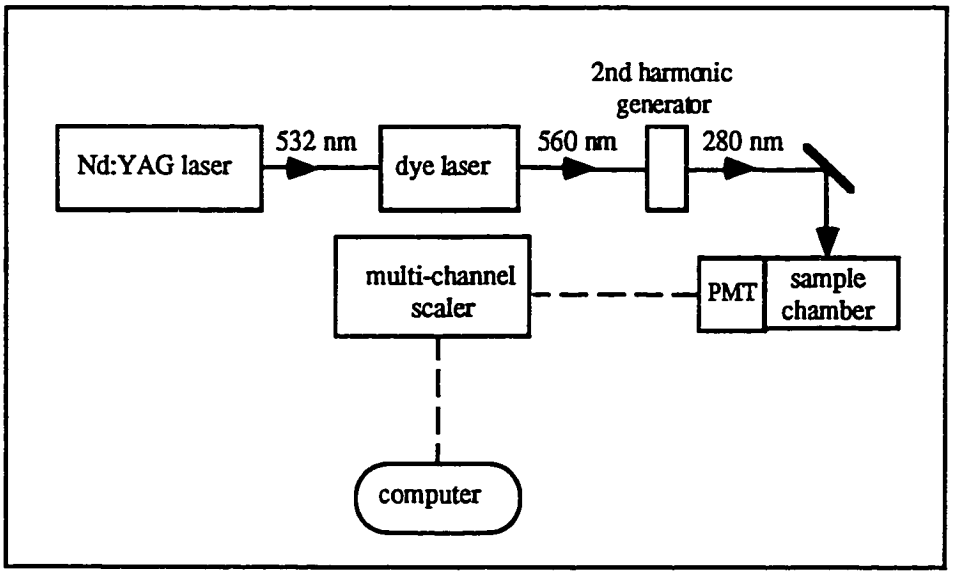

Figure 2.4. Setup for monitoring phosphorescence lifetimes.

Reproduced with permission of the copyright owner. Further reproduction prohibited without permission.

containing the dye Rhodamine 590 which has a peak emission at 560 nm. The 560 nm light then passed through a second harmonic generating crystal (Inrad) yielding the 280 nm pulse which excites the sample. Emission was collected through a band-pass filter centered at 450 nm, the peak of Trp phosphorescence emission, and detected by a Hammatsu R3550 photomultiplier tube (PMT) operated in photon counting mode. The signal from the PMT was sent into a Pacific Instruments Model AD6 amplifier/discriminator, collected by an ACEMCS multichannel scaler card (EG&G Ortec) and displayed on a personal computer. A mechanical shutter triggered by the laser Q switch, gated out the first 2 milliseconds of light from the sample to avoid contamination from protein fluorescence, stray laser light and cuvette luminescence.

The phosphorescence measurements were fit to single exponentials using a Marquardt χ^2 method as implemented by the program Fldec (PTI):

$$N = N_o e^{(-t/\tau)} \qquad (2.24)$$

N is the number of photons collected in photon counting mode, N_0 is the number of counts emitted immediately following excitation, t is the time elapsed since excitation of the sample and τ is the lifetime.

Results

The degree of acetylation of cyt c as determined from the TNBS assay was 65 ± 10 percent. The large uncertainty is due to the scatter in the absorbance data partly because of the very small difference in absorbance between the acetylated cyt c and the controls. Sixty five percent acetylation corresponds to modifying approximately 12 of the 19 lysine residues in cyt c leading to a change in cyt c charge from +8 to -4 which would seriously affect any electrostatic interactions.

Time resolved RTP experiments were performed with AP and various concentrations of reduced cyt c in both its acetylated and unaltered form. Representative phosphorescence decays shown in figure 2.5 exhibit the phosphorescence quenching

Reproduced with permission of the copyright owner. Further reproduction prohibited without permission.

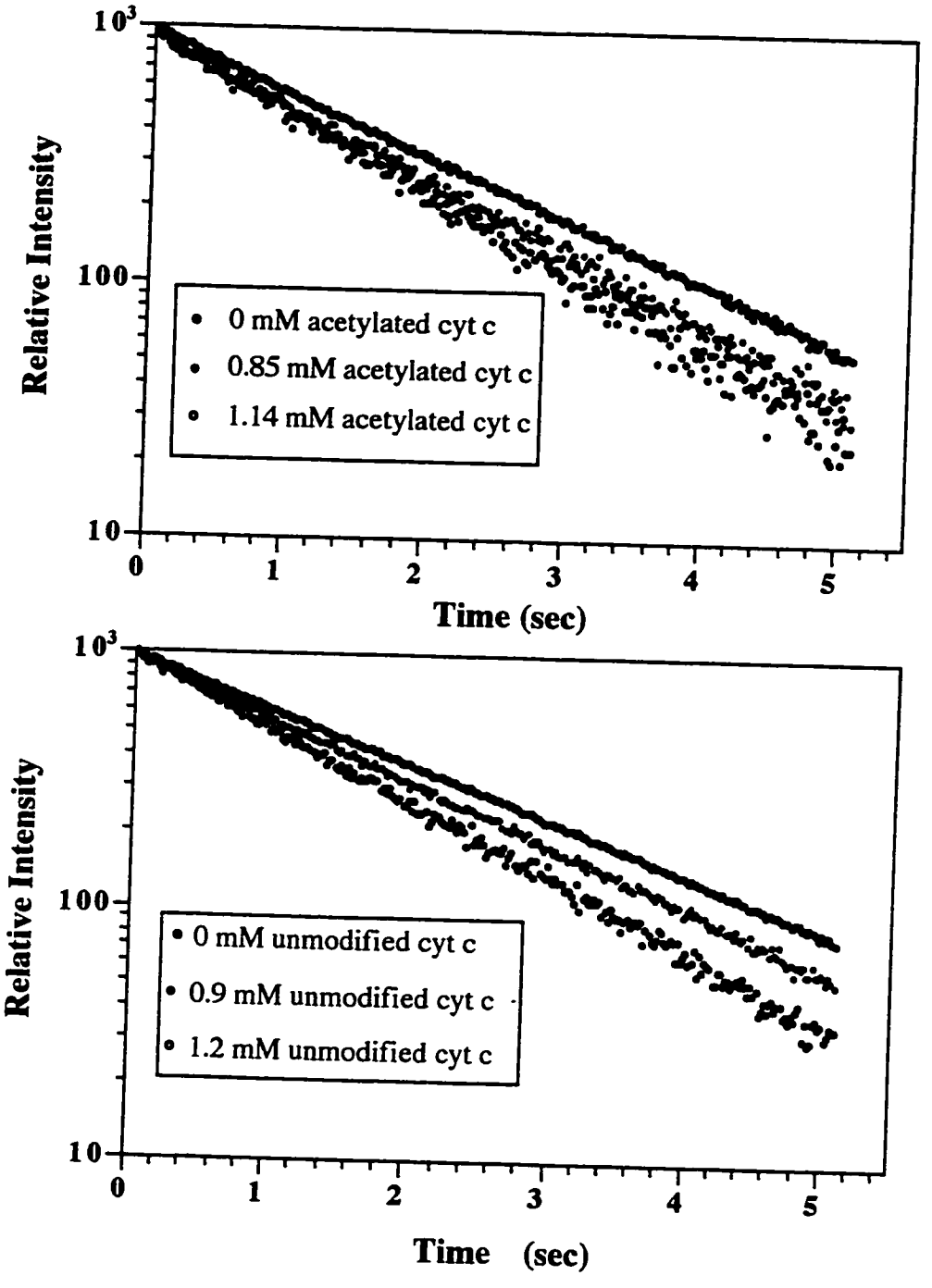

Figure 2.5. Quenching of AP phosphorescence by acetylated and unmodified cyt c. 0.5 mg/ml AP in 50 mM Tris 0.4% β-D glucose pH 7.5. Every 2nd data point is displayed

Reproduced with permission of the copyright owner. Further reproduction prohibited without permission.

which occurs with increasing concentrations of cyt c. Using lifetimes from these data a bimolecular quenching rate constant, $\frac{k_t}{\rho_A}$, of 0.12 ± 0.02 mM^{-1} s^{-1} was determined for acetylated cyt c and a $\frac{k_t}{\rho_A}$ of 0.14 ± 0.01 mM^{-1} s^{-1} was calculated for unmodified cyt c (Fig. 2.6).

Discussion & Conclusions

The values of $\frac{k_t}{\rho_A}$ for acetylated and unaltered cyt c were not significantly different indicating that the acceptor charge does not play a role in the quenching of AP phosphorescence by reduced cyt c. It should be noted that the values of $\frac{k_t}{\rho_A}$ obtained are larger than the value of 0.10 mM^{-1} s^{-1} reported by Mersol (1991, 1992) for reduced cyt c. The source of the discrepancy is unclear, but could possibly arise from slight oxygen contamination leading to quenching of AP phosphorescence.

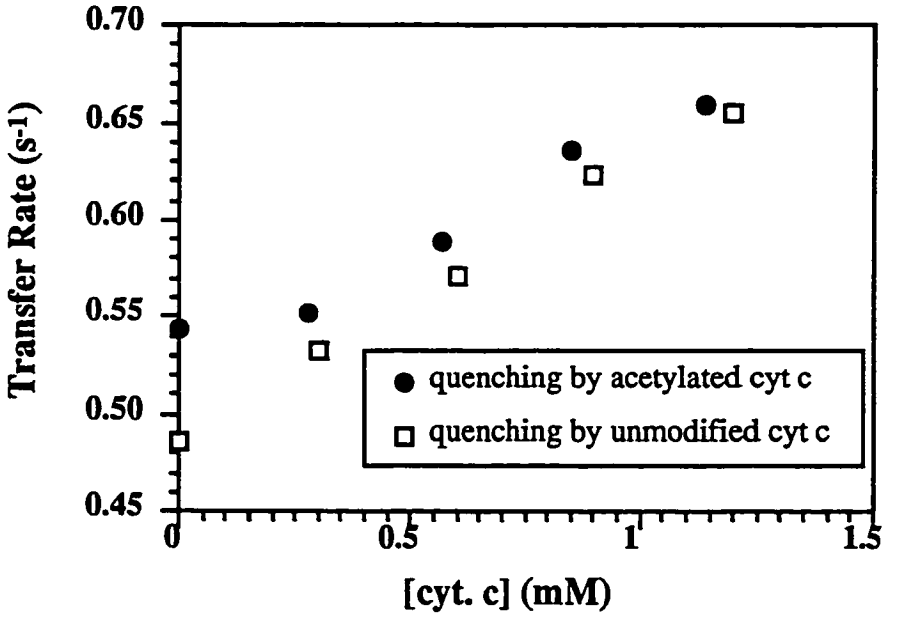

Figure 2.6. AP phosphorescence quenching rate versus concentration of cyt c for both acetylated and unmodified cyt c. Acetylated cyt c data are the average of three experiments, and unmodified cyt c data are the average of two experiments.

Reproduced with permission of the copyright owner. Further reproduction prohibited without permission.

This experiment seems to rule out electrostatic interactions in the quenching of AP phosphorescence by cyt c. If electrostatic interactions are unimportant then the discrepancy between the expected value of t_1 and the value obtained for cyt c experiments by Mersol (1991, 1992) may be due to exchange interactions or to the inadequacy of the 2 sphere model used to interpret the data (Fig 2.2B). As discussed by Mersol (1991, 1992) a more appropriate approximation for the cyt c - AP interaction would be to model the proteins as ellipsoids with the same volume as that used for the spherical approximation. Ellipsoids have both a minor and major axis and although the quenching rate will decrease when the chromophores interact along the long axes, interaction along the short axes will significantly increase the Förster energy transfer rate due to the r^{-6} dependence of the quenching rate (Mersol 1992; Mersol et al. 1991). The heme in cyt c touches the surface of the protein (Mersol 1992; Mersol et al. 1991) and if this occurs at a particularly non-spherical site on the protein it is possible that modeling cyt c as an ellipsoid and AP as a sphere will solve the problem as well as the 2 ellipsoid approach.

This experiment and those performed by Mersol and coworkers both demonstrate the utility and difficulties of using phosphorescence and Förster energy transfer to determine the location of Trp residues within proteins. It is possible to use Förster energy transfer to monitor protein conformation changes since the quenching rate will be altered as the location of the Trp residue shifts with respect to the solvent. However, it is easier to use the intrinsic change in Trp phosphorescence lifetime which occurs due to shifts in nonradiative, collisional and exchange mechanism quenching of Trp residue within proteins as the protein conformation is altered.

Reproduced with permission of the copyright owner. Further reproduction prohibited without permission.

References

Azzi, A., Montecucco, C., and Richter, C. (1975). "The Use of Acetylated Ferricytochrome *c* for the Detection of Superoxide Radicals Produced in Biological Membranes." *Biochemical and Biophysical Research Communications*, 65(2), 597-603.

Canters, G. W., and Kamp, M. v. d. (1992). "Protein-mediated Electron Transfer." *Current Opinion in Structural Biology*, 2, 859-869.

Cantor, C. R., and Schimmel, P. R. (1980). *Biophysical Chemistry Part II: Techniques for the Study of Biological Structure and Function*, W. H. Freeman and Company, New York.

Dexter, D. L. (1953). "A Theory of Sensitized Luminescence in Solids." *Journal of Chemical Physics*, 21(5), 836-850.

Englander, S. W., Calhoun, D. B., and Englander, J. J. (1987). "Biochemistry without Oxygen." *Analytical Biochemistry*, 161, 300-306.

Finkelstein, E., Rosen, G. M., Patton, S. E., Cohen, M. S., and Raukman, E. J. (1981). "Effect of Modification of Cytochrome c on its Reactions with Superoxide and NADPH: Cytochrome P-450 Reductase." *Biochemical and Biophysical Research Communications*, 102(3), 1008-1015.

Förster, T. (1948). "Intermolecular Energy Migration and Fluorescence (Zwischenmolekulare Energiewanderung und Fluoreszenz)." *Annalen der Physik*, 2, 55-75.

Förster, T. (1966). "Delocalized Excitation and Excitation Transfer." Modern Quantum Chemistry, O. Sinanoïglu, ed., Academic Press, New York, 93-137.

Goldkorn, T., and Shejter, A. (1979). "Electrostatic Effects on the Kinetics of Oxidation-Reduction Reactions of c-type Cytochromes." *Journal of Biological Chemistry*, 254, 12562-12566.

Gonnelli, M., and Strambini, G. B. (1995). "Phosphorescence Lifetime of Tryptophan in Proteins." *Biochemistry*, 34, 13847-13857.

Lakowicz, J. R. (1983). *Principles of Fluorescence Spectroscopy*, Plenum Press, New York.

Lambeth, J. D., Jack R. Lancaster, J., and Kamin, H. (1981). "Steroidogenic Electron Transport by Adrenodoxin Reductase and Adrenodoxin." *The Journal of Biological Chemistry*, 256(8), 3674-3678.

Lehninger, A. L. (1982). *Biochemistry*, Worth Publishers, New York.

Li, Z., Lee, W. E., and Galley, W. C. (1989). "Distance Dependence of the Tryptophan-Disulfide Interaction at the Triplet Level from Pulsed Phosphorescence Studies on a Model System." *Biophysical Journal*, 56, 361-367.

Reproduced with permission of the copyright owner. Further reproduction prohibited without permission.

Longworth, J. W. (1971). "Luminescence of Polypeptides and Proteins." Excited States of Proteins and Nucleic Acids, R. F. Steiner and I. Weinryb, eds., Plenum Press, New York, 319-484.

Lower, S. K., and El-Sayed, M. A. (1966). "The Triplet State and Molecular Electronic Processes in Organic Molecules." *Chemical Reviews*, 66, 199-241.

Marcus, R. A., and Sutin, N. (1985). "Electron Transfers in Chemistry and Biology." *Biochimica et Biophysica Acta*, 811, 265-322.

McGlynn, S. P., Azumi, T., and Kinoshita, M. (1969). *Molecular Spectroscopy of the Triplet State*, Prentice-Hall, Inc., Englewood Cliffs, New Jersey.

Mersol, J. V. (1992). "Room Temperature Tryptophan Phosphorescence Spectroscopy as a Probe of Protein Structure and Dynamics," Ph.D., University of Michigan, Ann Arbor.

Mersol, J. V., Steel, D. G., and Gafni, A. (1991). "Quenching of Tryptophan Phosphorescence in *Escherichia coli* Alkaline Phosphatase by Long-Range Transfer Mechanisms to External Agents in the Rapid-Diffusion Limit." *Biochemistry*, 30, 668-675.

Mersol, J. V., Wang, H., Gafni, A., and Steel, D. G. (1992). "Consideration of Dipole Orientation Angles Yields Accurate Rate Equations for Energy Transfer in the Rapid Diffusion Limit." *Biophysical Journal*, 61, 1647-1655.

Michl, J., and Bonacic-Koutecky, V. (1990). *Electronic Apects of Organic Photochemistry*, John Wiley & Sons, New York.

Saviotti, M. L., and Galley, W. C. (1974). "Room Temperature Phosphorescence and the Dynamic Aspects of Protein Structure." *Proceedings of the National Academy of Sciences, USA*, 71, 4154-4158.

Schauerte, J. A., Steel, D. G., and Gafni, A. (1996). "Time Resolved Room Temperature Tryptophan Phosphorescence in Proteins." *Methods in Enzymology*, in press.

Strambini, G. B. (1987). "Quenching of Alkaline Phosphatase Phosphorescence by O2 and NO: Evidence for Inflexible Regions of Protein Structure." *Biophysical Journal*, 52, 23-28.

Strambini, G. B., and Gonnelli, M. (1985). "The Indole Nucleus Triplet-State Lifetime and its Dependence on Solvent Microviscosity." *Chemical Physics Letters*, 115, 196-200.

Strambini, G. B., and Gonnelli, M. (1995). "Tryptophan Phosphorescence in Fluid Solution." *Journal of the American Chemical Society*, 117(29), 7646-7651.

Stryer, L. (1978). "Fluorescence Energy Transfer as a Spectroscopic Ruler." *Annual Review of Biochemistry*, 47, 819-846.

Takemori, S., Wada, K., Ando, K., Hosokawa, M., Sekuzu, I., and Okunuki, K. (1962). "Studies on Cytochrome *a* with Chemically Modified Cytochrome *c* and Basic Proteins." *The Journal of Biochemistry*, 52(1), 28-37.

Reproduced with permission of the copyright owner. Further reproduction prohibited without permission.

Thomas, D. D., Carlsen, W. F., and Stryer, L. (1978). "Fluorescence Energy Transfer in the Rapid-Diffusion Limit." *Proceedings of the National Academy of Sciences, U.S.A.*, 75(12), 5746-5750.

Vanderkooi, J. M. (1992). "Tryptophan Phosphorescence from Proteins at Room Temperature." Topics in Fluorescence Spectroscopy, Volume 3: Biochemical Applications, J. R. Lakowicz, ed., Plenum Press, New York, 113-136.

Wyckoff, H. W., Handschumacher, M., Murthy, H. M. K., and Sowadski, J. M. (1983). "The three dimensional structure of alkaline phosphatase from E. Coli." *Advances in Enzymology*, 55, 453-480.

Reproduced with permission of the copyright owner. Further reproduction prohibited without permission.

CHAPTER III

PHOSPHORESCENCE AND TRANSIENT ABSORPTION

Introduction

Measurements of changes in tryptophan (Trp) phosphorescence lifetimes at room temperature when combined with other techniques for probing protein conformation such as assaying for enzyme activity have proven useful for the identification of folding intermediates (Mersol et al. 1993; Subramaniam et al. 1995). Unfortunately, many proteins have Trp residues which do not phosphoresce at room temperature hindering the widespread use of room temperature phosphorescence as a means of studying protein conformation. An alternate method for measuring the triplet state lifetime is transient absorption.

Transient absorption has been used to observe the triplet state of Trp residues in proteins (Ghiron et al. 1988; Grossweiner and Usui 1971; Sudhakar et al. 1995; Sudhakar et al. 1993). These experiments take advantage of the fact that the peak absorption by the lowest energy Trp triplet state occurs around 450 nm (Bent and Hayon 1975) well to the red of the absorption of the ground state Trp. To perform transient absorption experiments, a protein is excited from the ground state by a pulse of UV light, and then the population of the triplet state is probed by monitoring the transmission through the sample of 450 nm light. When the triplet state is depopulated there is no longer any absorbance at 450 nm.

Determination of the triplet state lifetime by transient absorption is complicated by the fact that photoexcitation can lead to electron ejection and other processes that result in

Reproduced with permission of the copyright owner. Further reproduction prohibited without permission.

absorbing species other than the triplet state. Among these species are solvated electrons (e_{aq}^-) whose broad absorption peaks around 700 nm (Fielden and Hart 1967), and Trp radical species both charged and uncharged (Fig. 3.1). The multitude of possible absorbers complicates absorption measurements while providing a window into the chemistry which occurs following photoexcitation.

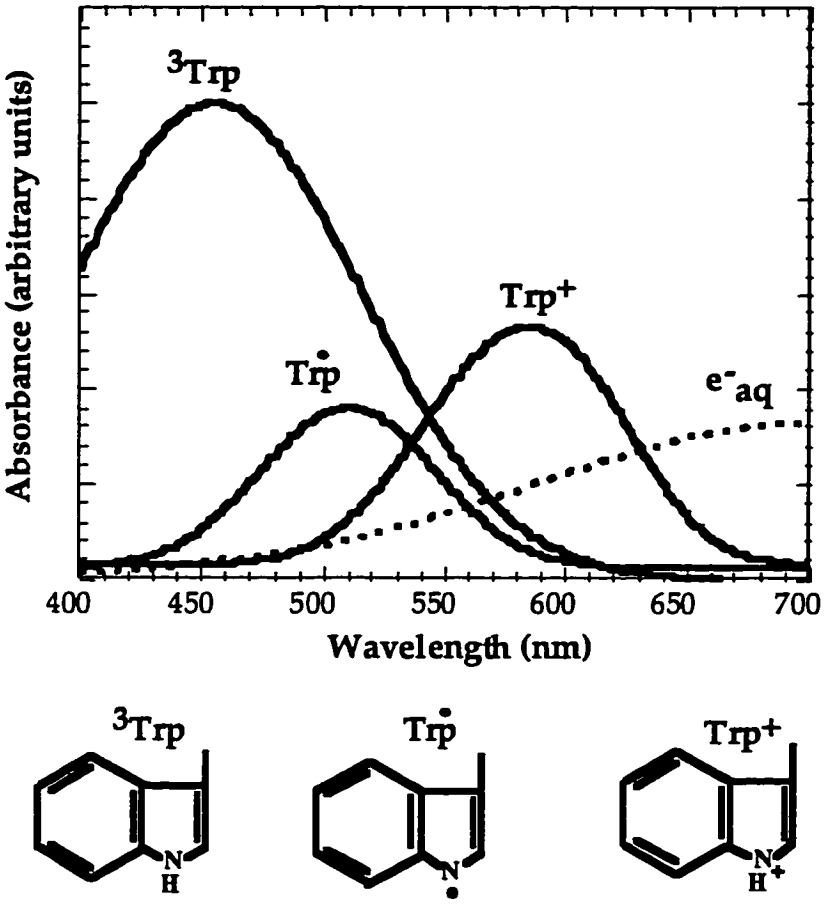

Figure 3.1. Idealized transient absorption spectra of the Trp triplet state (^{3}Trp), neutral radical ($\dot{Trp}$), cation radical (Trp^+) and solvated electron (e_{aq}). The spectra are adapted from Redpath et al (1975) and Grossweiner et al (1976).

Separation of the contributions of various species to the transient absorption can be at least partially accomplished by comparing the absorption of aerated solutions with those of deoxygenated solutions. In general, triplet states are so rapidly depopulated due to

Reproduced with permission of the copyright owner. Further reproduction prohibited without permission.

quenching by oxygen that their absorption will not be detected on time scales of microseconds or longer, and e^-_{aq} are rapidly scavenged by molecular oxygen. The transient absorption of radical species is not seriously affected by the presence of oxygen although the signal from the radicals may be decreased if a significant proportion of the radicals result from photochemistry of the triplet state.

In order to determine the efficacy of measuring Trp triplet state lifetimes by transient absorption a comparison was made to lifetimes obtained from room temperature phosphorescence for *Escherichia coli* alkaline phosphatase (AP). In addition, the Trp triplet state of rabbit phosphoglycerate kinase (PGK), a protein which is not phosphorescent at room temperature, was studied using transient absorption.

Materials and Methods

E. coli AP type III was obtained from Sigma Chemical Co. as a suspension in ammonium sulfate. Aliquots of the suspension were centrifuged, the supernatant was removed and the pellet was dissolved in 50 mM Tris buffer pH 7.5. The protein solution was diluted to 2 ml, placed in a Centricon 30 (Amicon Corp.) and concentrated down to 300-500 µl. The dilution step was repeated at least twice to ensure salt removal.

Rabbit muscle PGK in lyophilized form was purchased from Sigma Chemical Co. PGK was dissolved in 20 mM HEPES pH 7.5 and the salt was removed as described for AP.

The optical density at 280 nm of AP and PGK solutions was determined using a Shimadzu UV-visible recording spectrometer (model UV-260). For all experiments described here optical densities at 280 nm of between 0.3 and 0.4 and path lengths of 1 cm were used.

Samples were deoxygenated by flowing ultra pure argon gas through sealed 1 cm by 1 cm quartz cuvettes. Prior to entering the cuvette, the argon was purged of residual oxygen by bubbling the gas through solutions of amalgamated zinc, 0.1 M vanadyl sulfate

Reproduced with permission of the copyright owner. Further reproduction prohibited without permission.

and water respectively (Englander et al. 1987). The argon was allowed to stream through the cuvette for several hours. Upon removal from the argon system, the cuvette's stopper was sealed with silicon grease to prevent leakage of air into the sample.

Rate Equations

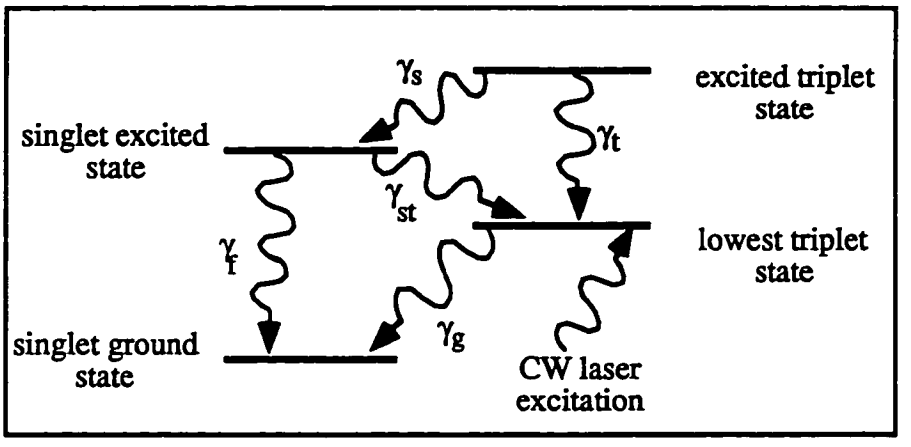

Figure 3.2. Decay processes which are important for transient absorption experiments aimed at measuring the lifetime of the lowest triplet state.

The changes in populations of the lowest triplet state, $\dot{n}_1$, and of the excited triplet state, $\dot{n}_2$, are expressed as:

$$\dot{n}_1 = -\gamma_g n_1 + \gamma_{st} n_s + \gamma_t n_2 - \frac{I\sigma}{\hbar\omega}(n_1 - n_2) \qquad (3.1)$$

$$\dot{n}_2 = -(\gamma_t + \gamma_s) n_2 + \frac{I\sigma}{\hbar\omega}(n_1 - n_2) \qquad (3.2)$$

n denotes a population with 1, 2 and s referring to the lowest triplet state, excited triplet state and excited singlet state respectively. γ_g is the rate of decay from the first excited triplet state to the singlet ground state (this quantity is directly measured by phosphorescence), γ_{st} is the intersystem crossing rate from the singlet state to the lowest triplet state, γ_t is the rate of decay from the higher level triplet state to the lowest level triplet state and γ_s accounts for intersystem crossing from the excited triplet state to the excited singlet state. I is the laser intensity; σ is the absorption cross section and $\hbar\omega$ is the energy at frequency ω. $\frac{I\sigma}{\hbar\omega}$ is multiplied by n_1 to account for absorption and by n_2 to account for

Reproduced with permission of the copyright owner. Further reproduction prohibited without permission.

stimulated emission. Generally, the second term in equation 3.1, which accounts for intersystem crossing from the singlet state, is negligible for times longer than a few microseconds after the UV excitation pulse since the transitions from the excited triplet state to the excited singlet state, which would repopulate the excited singlet state, and from the excited singlet state to the lowest triplet state are both spin forbidden (see ch. II).

In order for a transient absorption experiment to successfully measure the lifetime of the triplet state, the γ_S term must be negligible compared to the γ_t term in equation 3.2. If this is not the case, the lowest triplet state will be depopulated faster than occurs in the absence of transient absorption. If the γ_S term is significant, the measured triplet state lifetime will decrease with increasing probe beam intensity (up to some saturating value) as more population is lost to the excited singlet state and the measured lifetime will be shorter than the same quantity as measured by phosphorescence. Additionally, the system will display delayed fluorescence due to repopulation of the excited singlet state.

Instrumentation

Phosphorescence data were collected using a setup similar to that described by Mersol et al (1991) (Fig 3.3). The second harmonic of a Spectra-Physics Nd:YAG (model DCR-11) provided a 7-9 nsec pulse at 532 nm. This pulse pumped a dye laser (Quanta-Ray PDL-3) containing the dye Rhodamine 590 which has a peak emission at 560 nm. The 560 nm light then passed through a second harmonic generating crystal (Inrad) yielding the 280 nm pulse which excited the sample. The sample's emission at 450 nm, the peak of Trp phosphorescence emission, was separated by an optical monochromator (ISA HR-320) and detected by a Hamamatsu R3550 photomultiplier tube (PMT) operating in photon counting mode. The signal from the PMT was sent into a Pacific Instruments Model AD6 amplifier/discriminator, collected by an ACEMCS multichannel scaler card (EG&G Ortec) and displayed on a personal computer.

Reproduced with permission of the copyright owner. Further reproduction prohibited without permission.

The transient absorption apparatus (Fig. 3.3) used a laser for both the pump and probe beams. A laser beam probe allowed the collection of data from small (300 - 500 μl)

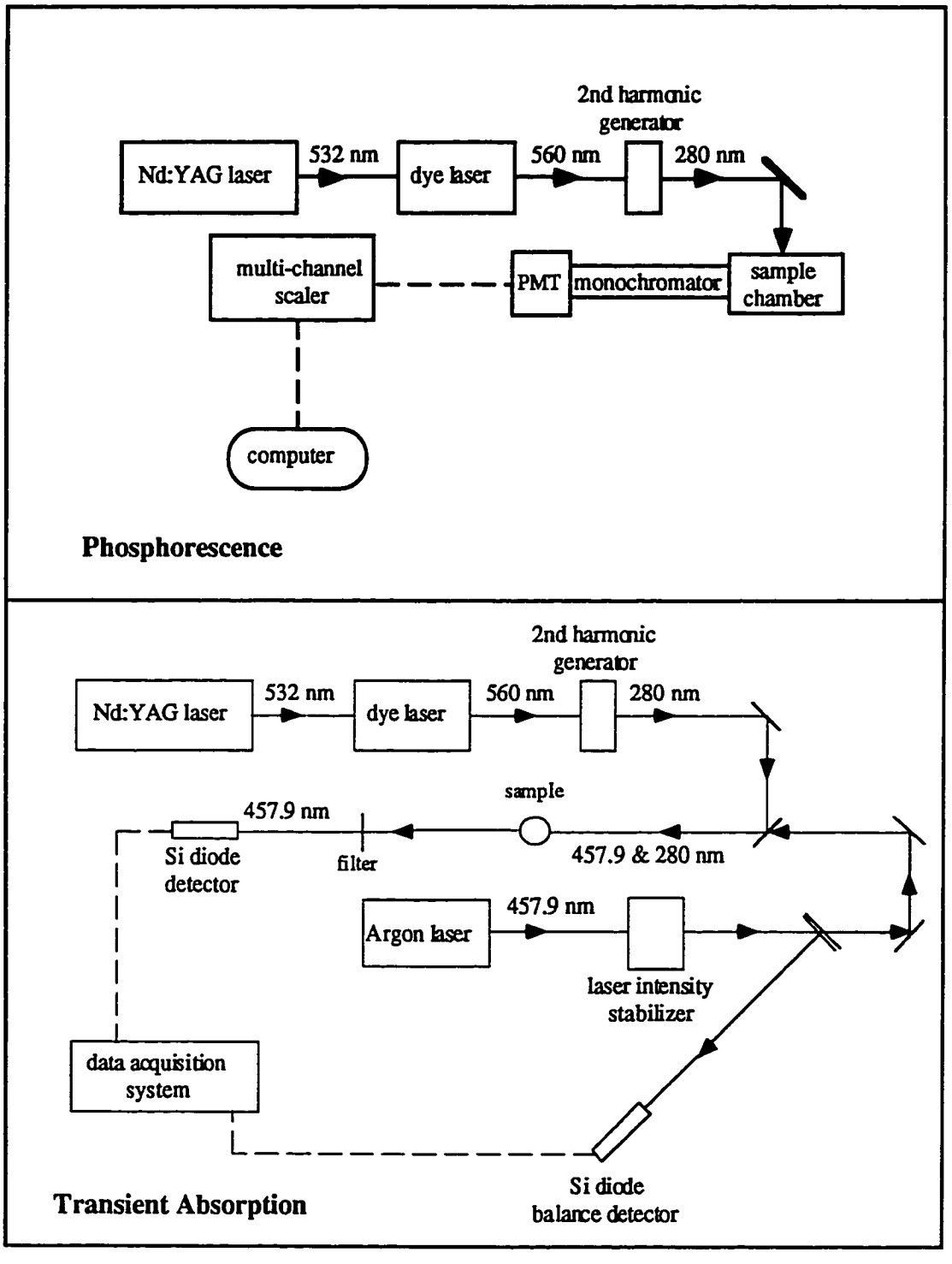

Figure 3.3. Schematic of the phosphorescence and transient absorption apparatuses.

Reproduced with permission of the copyright owner. Further reproduction prohibited without permission.

samples of proteins, permitted the detector to be positioned far from the sample so that scattered light from sample emission did not interfere with the measurements (Chan and Austin 1984) and made it easy to obtain time resolved kinetics. The probe beam for this system was provided by an argon laser (Spectra Physics model 166) which has a line at 457.9 nm near the peak of Trp triplet absorption. A 280 nm pulse for exciting the sample from the ground state was provided as described for the phosphorescence setup. The excitation pulse was reflected by a dichroic filter and together with the light from the argon laser passed through the sample. The 280 nm light was blocked by a filter after the sample.

Before meeting the 280 nm light, the argon laser beam passed through a laser intensity stabilizer (Thor Labs model CR200) which uses a liquid crystal and a feedback loop to keep the transmitted light intensity relatively constant. Neutral density filters after the laser intensity stabilizer insured that the argon beam power was 0.5 mW or less. Approximately 50% of the laser beam was then reflected to a balance silicon diode detector in order to provide a measure of the laser intensity before the beam traversed the sample. The laser intensity stabilizer was necessary because we were trying to detect a 1% or less peak to baseline change in a large DC offset. Without the laser intensity stabilizer the desired signal was swamped by the noise from the argon laser.

The signals from the two diodes were collected by an Analogic Data 6000 Universal Waveform Analyzer (D6000), basically a cross between a computer and an oscilloscope. When triggered by the Q-switch of the Nd:YAG, the D6000 collected data at a sample interval selected by the experimenter. The D6000 digitized both sets of data and divided the signal from the detector after the sample by the correlated signal from the balance detector in order to further reduce the noise. By pulsing the Nd:YAG laser once and monitoring the intensity of the CW beam from the Argon laser it was possible to collect transient absorption kinetics.

Reproduced with permission of the copyright owner. Further reproduction prohibited without permission.

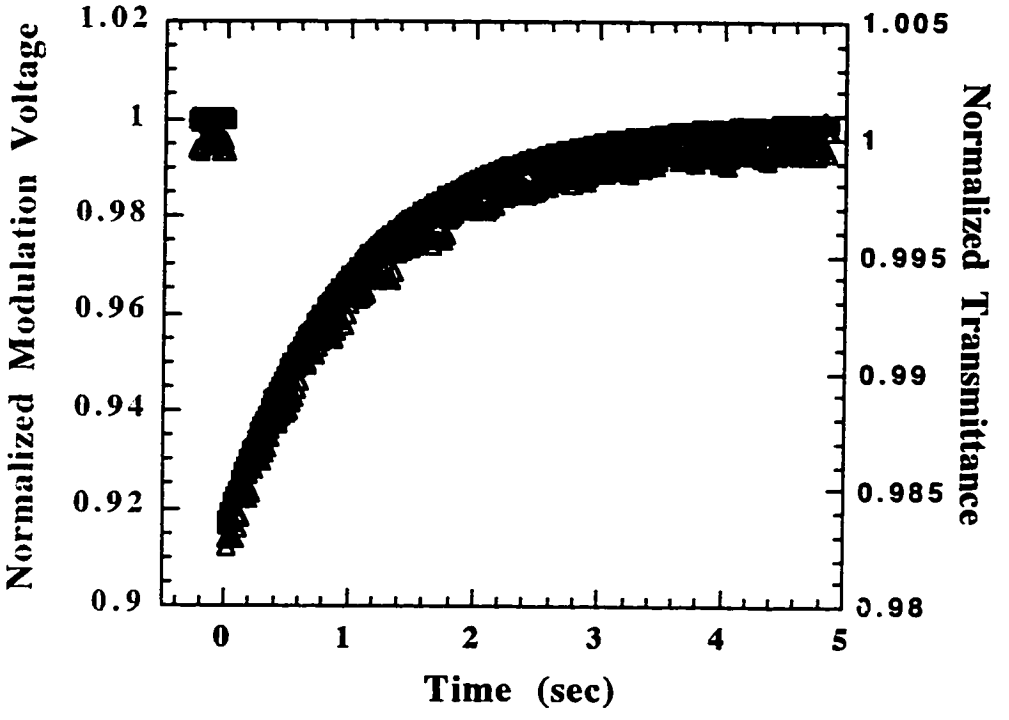

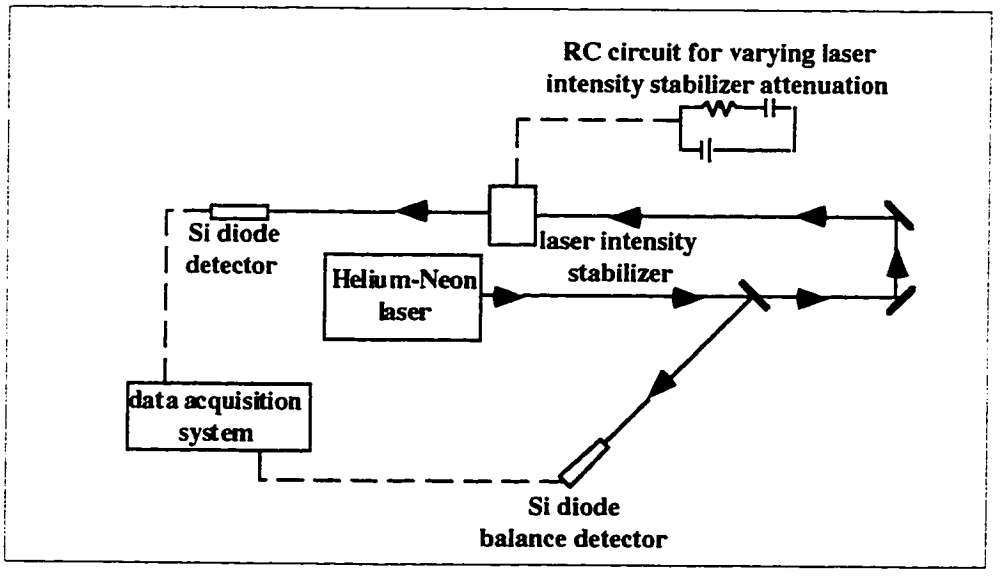

Figure 3.4. Data and apparatus for RC circuit simulated data. The signal directly from the RC circuit is in gray (A=0.084 and τ=1.065 sec) and the Si diode signal divided by the signal from the balance diode is in black (A=0.0177 and τ=1.071 sec).

Reproduced with permission of the copyright owner. Further reproduction prohibited without permission.

In order to check that the electronics worked properly, the Argon laser was replaced with a Helium-Neon (HeNe) laser (Uniphase) which was much less noisy than the Argon. This replacement allowed the use of the laser intensity stabilizer (LIS) as a "sample". By driving the LIS with an RC circuit, the intensity of the HeNe light could be modulated and the decrease followed by exponential increase of laser intensity mimicked the signal seen in a transient absorption experiment (Fig. 3.4). As in a transient absorption experiment, the light was balance-detected so that half of the HeNe laser light was split off prior to modulation by the LIS and the signal from the diode past the LIS was divided by the balance signal. The discharge of the capacitor was triggered by the Q-switch of the Nd-YAG laser and both the voltage from the RC circuit and the light detected by the Si diode were monitored. The RC time constant was adjusted using a variable resistor.

Both the HeNe and the voltage data were fit to:

$$y = C - Ae^{-t/\tau} \qquad (3.3)$$

where C is a constant which was determined by the average of the pretrigger baseline and was not fit. The fitted parameters were A, the amplitude, and τ, the lifetime, which should equal the RC time constant. Data were fit using the Levenberg-Marquardt method as implemented by the program Table Curve (Jandel Scientific). The lifetime values for the HeNe data were within eight percent of the lifetime values for the voltage data. Given that the HeNe data was approximately twice as noisy as the voltage data and that the light data had a range that was at least eight times smaller than that for the RC data directly from the circuit (Fig. 3.4), this agreement seems reasonable.

Data Analysis

The phosphorescence measurements can be fit to a sum of exponentials:

$$N(t) = \sum_i N_{oi} e^{(-t/\tau_i)} \qquad (3.4)$$

Reproduced with permission of the copyright owner. Further reproduction prohibited without permission.

t is the time elapsed since excitation of the sample, N is the number of photons collected from time t to t+Δt in photon counting mode, N_{oi} is the number of counts emitted by the ith species immediately following excitation and τ_i is the lifetime of the ith species. Transient absorption experiments measure the transmission of the sample, I_S, which, for optically thin samples is given by the Beer-Lambert law (Cantor and Schimmel 1980)

$$I_s = aI_o 10^{-\left(\sum_i \varepsilon_i C_i e^{(-t/\tau_i)}\right)\ell} \tag{3.5}$$

$$\begin{aligned} \frac{I_s}{I_b} &= \frac{a}{(1-a)}\left(1 - \ln(10)\left(\sum_i \varepsilon_i C_i e^{(-t/\tau_i)}\right)\ell\right) \\ &= \frac{a}{(1-a)}\left(1 - \sum_i A_i e^{(-t/\tau_i)}\right) \end{aligned} \tag{3.6}$$

I_0 is the initial light intensity of the argon beam prior to splitting the beam, a is the fraction of the argon intensity which is incident on the sample; ℓ is the path length, 1 cm for these experiments; ε_i is the extinction coefficient of the ith absorbing species; C_i is the concentration of the ith species; τ_i is the ith lifetime and A_i is the ith amplitude. If the optical density (the exponent in equation 3.5) of the transient species is small (<0.1) equation 3.5 may be expanded as equation 3.6. This approximation is valid for the data presented here since the transient absorption is less than five percent which corresponds to an optical density of 0.02 or less. The form of equation 3.6 also includes the division of I_S by the intensity monitored by the balance detector, I_b. Nonlinear least square fits of the phosphorescence data to equation 3.4 and the transient absorption data to equation 3.6 were performed by the program Table Curve.

The transient absorption data contained flat regions due to the limits of digitization of the Analogic. These flat regions led to residuals (experimental data minus fit) which were not randomly distributed about zero as expected for a good fit to the data (inset Fig. 3.6). Computer data, simulating the flat areas was generated to ensure that the digitization did not change the fit. The fits were unaffected by the simulated digitization.

Reproduced with permission of the copyright owner. Further reproduction prohibited without permission.

Results

AP is a dimer containing three Trp residues per subunit (Wyckoff et al. 1983). The room temperature phosphorescence of AP has been extensively studied(Mersol 1992; Mersol et al. 1991; Papp and Vanderkooi 1989; Strambini 1987) and has been shown

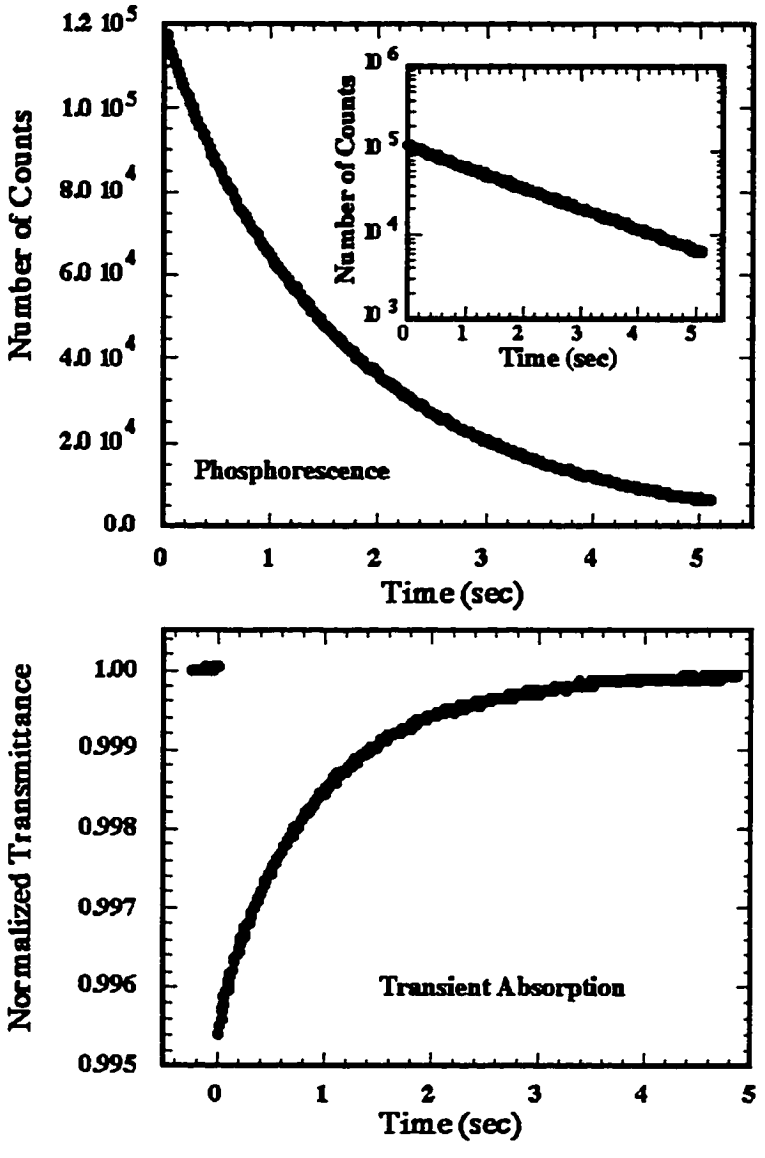

Figure 3.5. Room temperature phosphorescence and transient absorption of 6 μM deoxygenated AP in 50 mM Tris pH 7.5. The phosphorescence is the sum of 300 UV laser shots and the transient absorption is the average of 300 shots. The inset shows the phosphorescence data on a log scale.

Reproduced with permission of the copyright owner. Further reproduction prohibited without permission.

to arise from Trp 109 (Mersol et al. 1991; Strambini 1987). The room temperature phosphorescence lifetime of AP in well deoxygenated solutions is on the order of 2 seconds and its lifetime in aerated solutions is approximately 3 milliseconds. Due to the long triplet state lifetime, we expected that on time scales of milliseconds and longer the absorption of the 457.9 nm line of the argon laser would be dominated by the triplet state since the peak of Trp triplet-triplet absorption occurs around 450 nm (Bent and Hayon 1975) (Fig. 3.1). This assumption was confirmed by experiments comparing the absorption at 457.9 nm and 514.5 nm of deoxygenated, photoexcited AP. The absorption of the 514.5 nm light was approximately one third that of the 457.9 nm laser line (data not shown).

Table 3.1: Amplitude and lifetime determinations for room temperature phosphorescence and transient absorption data of 6 μM AP in 50 mM Tris pH 7.5. Phosphorescence fits are to equation 3.4 and transient absorption fits are to equation 3.6 except as indicated. The data for the deoxygenated sample is displayed in figure 3.5.

Experiment Type	Amplitude	Lifetime (sec)	% intensity
Phosphorescence†	6.62×10^{2}	2.58×10^{-3}	100
Transient Absorption†	1.7×10^{-3}	2.9×10^{-3}	100
Phosphorescence#	1.31×10^{5}	1.79	99
	5.52×10^{3}	0.47	1
Transient absorption#	2.33×10^{-3}	1.33	70
	2.16×10^{-3}	0.60	30
	1.04×10^{-3}	1.79*	41.5
	5.91×10^{-5}	0.47*	0.6
	3.36×10^{-3}	0.77	57.9

†aerated samples #deoxygenated samples

*These lifetimes were held fixed according to equation 3.7

Experiments performed on aerated solutions of AP demonstrated good agreement between lifetimes determined by phosphorescence and those from transient absorption (Table 3.1). However, for deoxygenated AP samples, the relationship between the long

Reproduced with permission of the copyright owner. Further reproduction prohibited without permission.

lifetime component for transient absorption and that for phosphorescence was not consistent from experiment to experiment. In some experiments the long decay component in the transient absorption data was much longer than that seen in phosphorescence and for some data sets the transient absorption lifetime was shorter than the phosphorescence lifetime as in the data set displayed (Fig. 3.5 and Table 3.1). We therefore decided to constrain the transient absorption fit using the amplitudes and lifetimes from phosphorescence plus an additional component:

$$\text{normalized transmittance} = 1 - A\left(\frac{A_{1p}}{A_{2p}}e^{-t/\tau_{1p}} + e^{-t/\tau_{2p}}\right) - Be^{-t/\tau} \quad (3.7)$$

where A_{1p} and A_{2p} are the amplitudes from the fit to phosphorescence and τ_{1p} and τ_{2p} are the lifetimes. A, B and τ are adjustable parameters. Without the additional exponential term the transient data could not be fit by this equation.

The goodness of fit was comparable to that for the unconstrained results. The value of τ (eqn 3.7) ranged from 9 to 700 milliseconds. This additional lifetime for the transient absorption presumably results from a dark state such as a tryptophan radical species or perhaps even some dark triplet state from one of the two other Trp residues in AP.

Given the long lifetime of AP, a possible experimental source of discrepancies between the phosphorescence and transient absorption data is diffusion of excited molecules out of the small region probed in the transient absorption experiments. In phosphorescence experiments, the luminescence from one entire side of the cuvette is collected so that diffusion is not a factor. As a first test of this possibility, the spot size of the argon and UV beams in the transient absorption setup were increased. This modification did not lead to significant changes in the relationship between the phosphorescence and transient absorption lifetimes for the same sample probed with two different spot sizes.

To further investigate the possibility of diffusion, the transient absorption and phosphorescence of AP in 30 percent glycerol were measured and compared to results for

Reproduced with permission of the copyright owner. Further reproduction prohibited without permission.

AP in the absence of glycerol. In the full strength UV beam, the transient absorption long lifetimes were consistently longer than the phosphorescence lifetimes. This relationship was true for experiments conducted on the same day for AP with and without glycerol. Both the glycerol and spot size experiments fail to indicate a role for diffusion in the discrepancies between the phosphorescence and transient absorption lifetimes of AP.

However, these experiments did reveal the importance of photodamage in transient absorption experiments. In 30 percent glycerol, fifty 280 nm laser pulses led to a fifty percent decrease of transient absorption signal strength. When the intensity of the UV pulse was lowered by half, reduction in signal was still seen but it decreased to twenty percent. AP in solution without glycerol showed a 25 percent decrease in signal if the sample was not moved between shots. The long lifetimes for samples which were not moved or shaken between laser pulses were consistently shorter than those which were moved.

Rabbit muscle PGK is a monomeric enzyme containing 4 Trp residues (Fifis and Scopes 1978) none of which exhibit a long lived phosphorescence lifetime. The transient absorption of rabbit PGK at 457.9 nm did reveal a long lived component (Fig. 3.6 and Table 3.2). This transient was virtually indistinguishable in aerated and deoxygenated solution (data not shown) and the amplitude of the long lived transient increased upon changing the probe wavelength from 457.9 to 514.5 nm. These data suggest that the long lived transient absorption of rabbit PGK arises from a state other than the Trp triplet state. One to two percent of the transient absorption signal from rabbit PGK was contributed by a short lived component which seemed to disappear when oxygen was introduced into the sample. This small component was present in the 514.5 nm data, but even large changes in the amplitude of this component were not resolvable due to its small contribution to the data. It is, therefore, impossible to say whether this was a contribution from the Trp triplet state.

Reproduced with permission of the copyright owner. Further reproduction prohibited without permission.

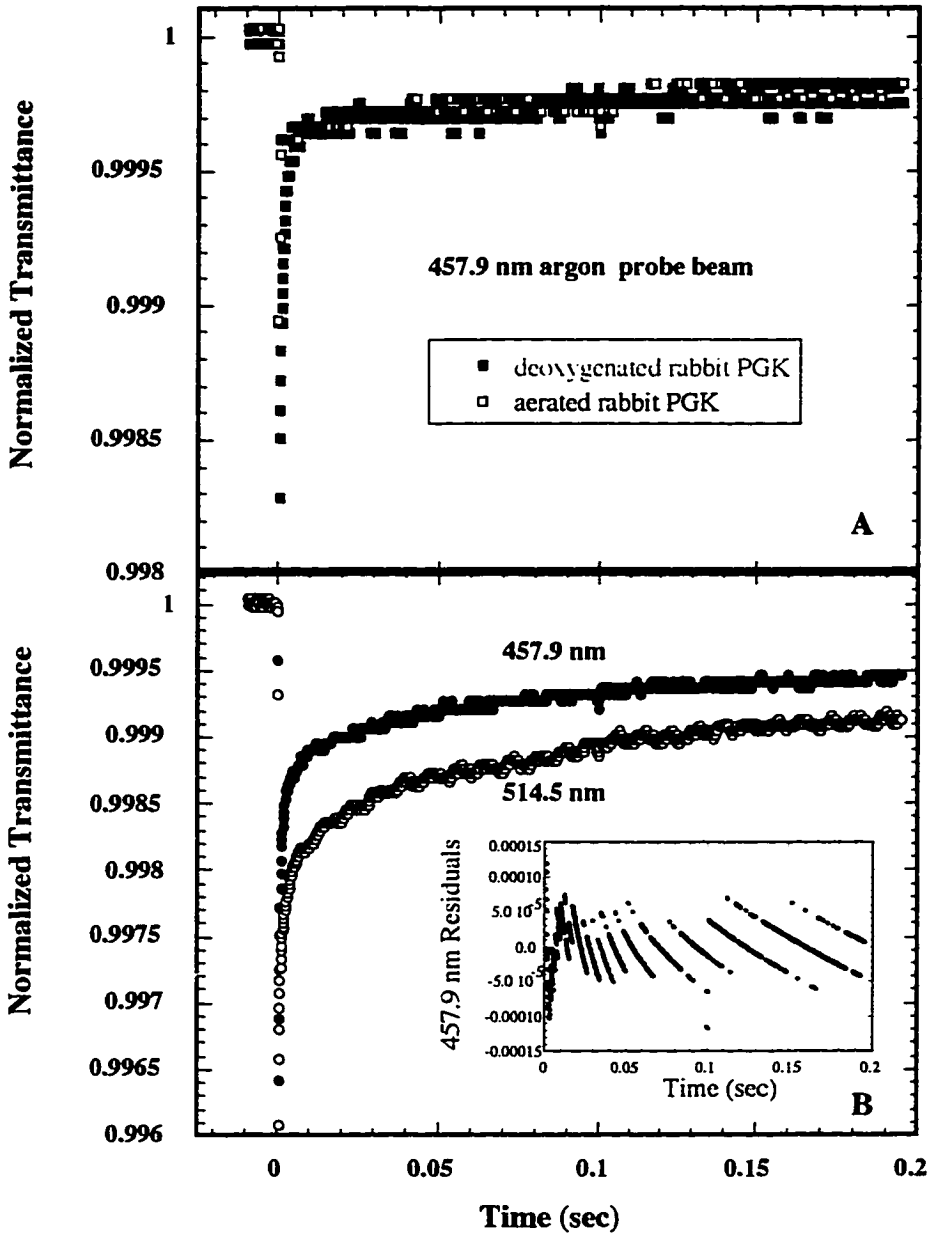

Figure 3.6. Transient absorption of 15 μM rabbit PGK in 20 mM HEPES pH 7.5 at room temperature. The persistence of the long component in aerated solution is shown in A, and the increase of the signal, for a deoxygenated sample, upon changing the probe wavelength from 457.9 to 514.5 nm is shown in B. The inset in B displays the residuals for the fit to the 457.9 nm data; lifetimes and amplitudes for the data are given in Table 3.2.

Reproduced with permission of the copyright owner. Further reproduction prohibited without permission.

All of the fits to the transient absorption data were extremely sensitive to the initial values of lifetimes and amplitudes entered into the fitting program. This sensitivity is due to a combination of the small dynamic range of the transient absorption data (particularly in comparison to the phosphorescence data) and the difficulty of fitting a smooth curve to a curve containing flat regions due to the digitization. Despite these complications, the 95 percent confidence limits, as calculated by the program Table Curve, were within, at most, plus or minus 15 percent of the fitted parameters.

Table 3.2: Amplitudes and lifetimes for 3 exponential fits to the transient absorption experiments on deoxygenated 15 μM rabbit muscle PGK in 20 mM HEPES pH 7.5 at room temperature. Fits are to equation 3.6 and the data are displayed in the bottom panel of figure 3.6.

Probe Wavelength (nm)	Amplitude (X 10^{-3})	lifetime (msec)	% intensity	average lifetime (msec)
457.9	0.834	440	96	
	0.519	23	3	
	4.08	0.6	1	70
514.5	1.40	373	96.9	
	0.679	21	2.7	
	1.50	1.3	0.3	151

Discussion

Comparisons of Trp triplet state lifetimes at room temperature as obtained from phosphorescence and from transient absorption have been made by Strambini and Gonnelli (1995). Their results for indole derivatives indicate that triplet lifetimes as measured by transient absorption are shorter than those measured by phosphorescence. They attribute this discrepancy to impurities in the solutions as well as complications due to triplet-triplet quenching and the production of photoproducts which would be seen in the transient absorption measurements.

Our results for AP demonstrate that there is a discrepancy between triplet state lifetimes determined by transient absorption and those determined by phosphorescence for

Reproduced with permission of the copyright owner. Further reproduction prohibited without permission.

Trp residues in proteins. AP lifetimes as determined solely from the transient absorption data fail to agree with the triplet state lifetimes determined from phosphorescence experiments. However, unlike the results for indole derivatives (Strambini and Gonnelli 1995) there is no consistent relationship between the phosphorescence and transient absorption lifetimes.

The absence of a Trp triplet state transient absorption signal from rabbit PGK was unexpected. Although we see no significant phosphorescence intensity from rabbit PGK, a long lived room temperature phosphorescence lifetime has been observed in yeast PGK (Cioni et al. 1993; Gonnelli and Strambini 1995). This lifetime is attributed to Trp 333 (yeast numbering) which is an evolutionarily conserved residue (Mori et al. 1986; Watson and Littlechild 1990); therefore, we expected to also see a long triplet state lifetime in rabbit PGK. It is possible that any long lived dark tryptophan triplet state was masked by the long lived transient which we did observe.

The long lived PGK transient cannot arise directly from either the Trp triplet state or e_{aq} since it is present with an apparently unmodified lifetime in both deoxygenated and aerated solutions. It must, therefore, arise from either the Trp neutral or cation radical. The peak of the neutral radical absorption occurs at 510 nm with an ε of 1750 M^{-1} cm^{-1} (Redpath et al. 1975) while the cation radical peak absorption is at 570 nm with an ε of 2600 M^{-1} cm^{-1} (Redpath et al. 1975) (see Fig. 3.1). Due to the difference in extinction coefficient, the doubling of the transient absorption signal between 457.9 nm and 514.5 nm is not sufficient to distinguish between the two species.

One of the goals of this work was to use triplet state transient absorption to follow protein folding. The question, therefore, arose as to whether the long lived transient in rabbit PGK, despite it's non-triplet state nature, could be used as a probe of folding. Preliminary experiments conducted on rabbit PGK in 2 M guanidine hydrochloride showed that the lifetime of the long lived transient more than doubled compared to native PGK in denaturant-free buffer, but that the peak to peak amplitude of the signal was almost halved

Reproduced with permission of the copyright owner. Further reproduction prohibited without permission.

(data not shown). These preliminary results indicate that long lived states other than the triplet state might be useful as probes of protein conformation.

Conclusions

The use of a laser pump-probe system for the study of transient absorption following photoexcitation allows the use of small sample volumes and low protein concentrations. This method of measuring transient absorption also permits the collection of data on longer time scales than fluorescence from proteins which show little or no phosphorescence. The longer lived transient signals should be more sensitive to environmental perturbations than shorter lived signals.

Transient absorption experiments are much more complicated than luminescence experiments due to the small signal strength and contributions from various photochemically generated species such as the Trp neutral radical. These additional contributions can, as seems to be the case for PGK, be a help as well as a hindrance by providing long lived states which cannot be detected luminescently.

In order to build on and aid in the interpretation of the findings presented here, some instrumentation improvements are necessary. First, to better the quality of the data a more sensitive digitizer or more amplification is essential to remove or at least reduce the digitization error present in the data. Additionally, it might be helpful to divide the sample signal by the balance signal prior to digitization. It is also possible to increase the signal strength by increasing the protein concentration, but such an increase would lead in inhomogeneities in the absorption of the 280 nm beam through the sample as well as increasing the probability of protein-protein interactions which could lead to processes such as triplet-triplet annihilation. Faster time resolution, hundreds of nanoseconds for instance, would allow the collection of data with a larger dynamic range improving the reliability of the fits. Finally, the ability to use a variety of wavelengths rather than only 457.9 and

Reproduced with permission of the copyright owner. Further reproduction prohibited without permission.

514.5 nm by using a tunable laser with a wider wavelength range would allow positive identification of the transiently absorbing species present.

With such improvements, the contribution of the triplet state to both AP and PGK transients could be unequivocally identified as could the species responsible for the long lived transient absorption in PGK. The identification of specific transiently absorbing species in different proteins should lead to a better understanding of triplet state photochemistry and the affects of local environment on Trp residues. Transient absorption signals from both the Trp triplet state and other photochemical species could serve as probes of protein conformation which could be used in addition to luminescence experiments.

Reproduced with permission of the copyright owner. Further reproduction prohibited without permission.

References

Bent, D. V., and Hayon, E. (1975). "Excited State Chemistry of Aromatic Amino Acids and Related Peptides. III. Tryptophan." *Journal of the American Chemical Society*, 97(10), 2612-2619.

Cantor, C. R., and Schimmel, P. R. (1980). *Biophysical Chemistry Part II: Techniques for the Study of Biological Structure and Function*, W. H. Freeman and Company, New York.

Chan, S. S., and Austin, R. H. (1984). "Laser Photolysis in Biochemistry." Methods of Biochemical Analysis, D. Glick, ed., John Wiley & Sons, New York.

Cioni, P., Puntoni, A., and Stramibini, G. B. (1993). "Tryptophan phosphorescence as a monitor of the solution structure of phosphoglycerate kinase from yeast." *Biophysical Chemistry*, 46, 47-55.

Englander, S. W., Calhoun, D. B., and Englander, J. J. (1987). "Biochemistry without Oxygen." *Analytical Biochemistry*, 161, 300-306.

Fielden, E. M., and Hart, E. J. (1967). "Activation Energy of the Hydrated Electron + Water Reaction and the Ultra-Violet Absorption Spectrum of the Hydrated Electron." *Faraday Society Transactions*, 63, 2975-2982.

Fifis, T., and Scopes, R. K. (1978). "Purification of 3-phosphoglycerate kinase from diverse sources by affinity elution chromatography." *Biochemical Journal*, 175, 311-319.

Ghiron, C., Bazin, M., and Santus, R. (1988). "Characterization of the indole triplet excited state in proteins utilizing laser flash photolysis." *Journal of Biocheimical and Biophysical Methods*, 15, 337-348.

Gonnelli, M., and Strambini, G. B. (1995). "Phosphorescence Lifetime of Tryptophan in Proteins." *Biochemistry*, 34, 13847-13857.

Grossweiner, L. I., and Usui, Y. (1971). "Flash photolysis and inactivation of aqueous lysozyme." *Photochemistry and Photobiology*, 13, 195-214.

Mersol, J. V. (1992). "Room Temperature Tryptophan Phosphorescence Spectroscopy as a Probe of Protein Structure and Dynamics," Ph.D. thesis, University of Michigan, Ann Arbor.

Mersol, J. V., Steel, D. G., and Gafni, A. (1991). "Quenching of Tryptophan Phosphorescence in *Escherichia coli* Alkaline Phosphatase by Long-Range Transfer Mechanisms to External Agents in the Rapid-Diffusion Limit." *Biochemistry*, 30, 668-675.

Mersol, J. V., Steel, D. G., and Gafni, A. (1993). "Detection of Intermediate Protein Conformations by Room Temperature Tryptophan Phosphorescence Spectroscopy During Denaturation of Escherichia coli Alkaline Phosphatase." *Biophysical Chemistry*, 48(2), 281-291.

Reproduced with permission of the copyright owner. Further reproduction prohibited without permission.

Mori, N., Singer-Sam, J., and Riggs, A. D. (1986). "Evolutionary conservation of the substrate-binding cleft of phosphoglycerate kinases." *FEBS Letters*, 204(2), 313-317.

Papp, S., and Vanderkooi, J. M. (1989). "Tryptophan Phosphorescence at Room Temperature as a Tool to Study Protein Structure and Dynamics." *Photochemistry and Photobiology*, 49(6), 775-784.

Redpath, J. L., Santus, R., Ovadia, J., and Grossweiner, L. I. (1975). "The Oxidation of Tryptophan by Radical Anions." *International Journal of Radiation Biology*, 27(2), 201-204.

Strambini, G. B. (1987). "Quenching of Alkaline Phosphatase Phosphorescence by O2 and NO: Evidence for Inflexible Regions of Protein Structure." *Biophysical Journal*, 52, 23-28.

Strambini, G. B., and Gonnelli, M. (1995). "Tryptophan Phosphorescence in Fluid Solution." *Journal of the American Chemical Society*, 117(29), 7646-7651.

Subramaniam, V., Bergenhem, N. C., Gafni, A., and Steel, D. G. (1995). "Phosphorescence reveals a continued slow annealing of the protein core following reactivation of Escherichia coli alkaline phosphatase." *Biochemistry*, 34(4), 1133-1136.

Sudhakar, K., Phillips, C. M., Owen, C. S., and Vanderkooi, J. M. (1995). "Dynamics of parvalbumin studied by fluorescence emission and triplet absorption spectroscopy of tryptophan." *Biochemistry*, 34, 1355-1363.

Sudhakar, K., Phillips, C. M., Williams, S. A., and Vanderkooi, J. M. (1993). "Excited states of tryptophan in cod parvalbumin: Identification of a short-lived emitting triplet state at room temperature." *Biophysical Journal*, 64, 1503-1511.

Watson, H. C., and Littlechild, J. A. (1990). "Isoenzymes of phosphoglycerate kinase: evolutionary conservation of the structure of this glycolytic enzyme." *Biochemical Society Transactions*, 18, 187-190.

Wyckoff, H. W., Handschumacher, M., Murthy, H. M. K., and Sowadski, J. M. (1983). "The three dimensional structure of alkaline phosphatase from E. Coli." *Advances in Enzymology*, 55, 453-480.

Reproduced with permission of the copyright owner. Further reproduction prohibited without permission.

CHAPTER IV

EARLY EVENTS IN PROTEIN FOLDING

The triplet state methods described thus far, allow an experimenter to look at protein folding and conformational changes on time scales of seconds or longer. However, there is much theoretical and experimental evidence that important events in protein folding occur on much shorter time scales. Of particular interest are "early events" in protein folding which occur on time scales of microseconds or less. On the most general level, early events could be important by helping to restrict the number of available conformations leading to a resolution of Levinthal's paradox (see ch. I).

There are various models of protein folding all of which make predictions about what happens in the early stages. Amongst these are the diffusion-collision model, the framework model , the jigsaw model and the molten globule model. Additionally there are models based upon computer simulations.

The diffusion-collision model of Karplus and Weaver postulates that small, transient regions of secondary structure, called microdomains, form at the beginning of folding. These microdomains then collide with each other due to diffusion of the polypeptide chain (Karplus and Weaver 1994). The framework model of Kim and Baldwin also postulates that secondary structure is formed early in protein folding (Kim and Baldwin 1982). That some parts of proteins can form isolated bits of secondary structure is supported by the experiments of Dyson and others who have shown that some peptide fragments from proteins will form secondary structure in solution (Jing et al. 1995; Waltho et al. 1993; Wright et al. 1988).

Reproduced with permission of the copyright owner. Further reproduction prohibited without permission.

The jigsaw puzzle model states that there are numerous independent pathways for protein folding implying that there are no obligate intermediates in protein folding (Harrison and Durbin 1985). In this model, if one watched a single protein fold a number of times, the conformation at the end would be constant, but the pathway would vary. In contrast, the molten globule model suggests that a protein forms a "substantial" amount of secondary structure and then passes through a compact, solvated intermediate state which lacks rigid side chain packing (Ptitsyn 1992). The molten globule model is based on experimental observations of "molten globule" intermediates (compact intermediates displaying substantial secondary structure, lacking a cooperative thermal unfolding transition and lacking well defined tertiary structure) for some proteins.

Computer based molecular dynamics simulations can be used to simulate the protein folding pathway. However, molecular dynamics simulations are limited by the amount of computer memory available and the speed of computation. Usually, only 10^2 to 10^5 atoms may be considered and the time scale of the molecular dynamics experiments are restricted to nanoseconds at the most (van Gunsteren and Mark 1992). Simulations which use atomic models and full representations of the solvent (solvent-protein interactions are extremely important for protein folding or unfolding) have thus far concentrated on unfolding rather than folding and have used extreme pHs, high temperatures or artificial energy terms to force the unfolding to occur within the time scale of the simulation (Karplus and Sali 1995). Another approach to the problem is to simplify the model by using lattice models. In most lattice models, proteins are represented as short (~30 amino acid) heteropolymers which are constrained to fold on square lattices (Karplus and Sali 1995). These lattice models are quite simplified, but they do allow the study of protein folding within the constraints imposed by a computer.

Based on such simple, exact lattice models of protein folding, Dill and coworkers predict that nonlocal interactions contain the information necessary for protein folding and that secondary structure formation is a consequence of folding not the driving force behind

Reproduced with permission of the copyright owner. Further reproduction prohibited without permission.

it (Chan and Dill 1994; Dill et al. 1995). One important factor in this model is the inclusion of both hydrophobic and polar residues which leads to fewer compact conformations than seen in homopolymers (Dill et al. 1995). In addition, in these models it is possible that formation of too much secondary structure early in folding can actually slow down protein folding due to steric hindrance (Chan and Dill 1994).

In order to distinguish between different theories of protein folding, protein folding experiments must attempt to address the following questions. When does secondary structure form? Is there a protein folding pathway, i.e. do specific, kinetic intermediates exist? Is hydrophobic collapse differentiable from secondary structure formation? Finally, are the answers to these questions protein dependent?

In order to answer any of these questions, an experimentalist must be able to observe the initial stages of protein folding and secondary structure formation. Secondary structure can be formed on time scales of microsecond or less as indicated by studies of helix-coil transitions in polypeptides. In these studies, the transition from random coil to α helical conformations was observed to occur in tens to hundreds of nanoseconds (Bösterling and Engel 1979; Burke et al. 1965; Cummings and Eyring 1975; Inoue et al. 1979; Tsuji et al. 1976). Additional evidence comes from stopped flow experiments with proteins, in which a denatured protein solution is mixed with buffer in order to dilute out the denaturant and allow the protein to refold. Mixing the two solutions takes at least one millisecond and is referred to as the dead time of the experiment. For many proteins a "burst phase" of protein folding occurs within the dead time (Chiba et al. 1994; Elöve et al. 1992; Jennings and Wright 1993; Kuwajima et al. 1987; Sugawara et al. 1991). For example, in experiments using apomyoglobin denatured in urea, 64% of the ellipticity at 222 nm was regained in the dead time (5 msec) of the stopped flow experiment (Jennings and Wright 1993).

How then, is it possible to study secondary structure formation and make comparisons to theory? Protein refolding may be slowed down by performing experiments

Reproduced with permission of the copyright owner. Further reproduction prohibited without permission.

at low temperatures and high (1 M and higher) residual concentrations of denaturants such as guanidine hydrochloride (Chen et al. 1992; Chen et al. 1989). However, since denaturants are known to interact with proteins either by binding to the protein or by changing the accessible surface area (Creighton 1993; Myers et al. 1995) it is unclear how these high residual concentrations would affect the mechanisms of protein folding.

Another approach to measuring fast rate constants associated with protein folding is to use dynamic NMR (Huang and Oas 1995). For a protein with a two state transition, the NMR line shape of the partially unfolded protein will be broadened and shifted since each protein molecule will sample the unfolded and folded states during the NMR experiment (Huang and Oas 1995). Using the line shapes of the fully folded state, the fully unfolded state and the interconverting state, the rate constants for folding and unfolding at various concentrations of denaturant, such as urea, may be determined from the broadened, shifted NMR resonances. Then, from a plot of the natural log of the rate constants (ln(k)) versus urea concentration the rate constants at 0 M urea can be ascertained. Huang and Oas (1995) used this technique to study the folding of an N terminal domain fragment of λ repressor, they found a folding rate constant of 3600±400 s^{-1} indicating that this λ repressor fragment folds on a submillisecond time scale.

Dynamic NMR does not measure the folding rate directly and the extrapolation of the folding rate to 0 M urea assumes that a plot of ln(k) versus urea concentration is linear which may not be true (Huang and Oas 1995). Furthermore, a two state transition is assumed and like other NMR experiments, only small proteins can be investigated using this technique.

In order to investigate the burst phase in a time resolved manner, an experimental system must be devised which changes one or more solution parameter (i.e. pH, temperature, pressure, etc.) in microseconds or less. Such studies have been conducted on the heme protein cytochrome c (cyt c) using nanosecond laser photolysis (Jones et al. 1993). In these experiments, cyt c was unfolded in the presence of carbon monoxide (CO)

Reproduced with permission of the copyright owner. Further reproduction prohibited without permission.

and guanidine hydrochloride (Gdn-HCl). In 4.6 M Gdn-HCl, photodissociation of the CO allowed cyt c to refold. The "dead time" of this experiment corresponded to the nanosecond width of the laser pulse since CO photodissociates in <1 picosecond (Jones et al. 1993). In these experiments, changes in heme ligation indicating conformational alterations were observed on the microsecond time scale. Unfortunately, since this procedure relies on a specific cyt c ligand and on the fact that the heme prosthetic group is covalently bound to cyt c, it is not applicable to most proteins.

Measurements of helix-coil transitions in the 1960s and 1970s used a variety of fast methods for perturbing solutions. One of the most common was the electric field jump. Electric field jumps can be made to occur within nanoseconds with relaxation rates of nanoseconds to milliseconds (Eyring and Hemmes 1986). Electric field jumps will trigger protein conformational changes if the folding involves a net change in charge or a net change in dipole moment (Eyring and Hemmes 1986) as occurs in α helix formation. One problem with electric field jumps, aside from the short duration of the perturbation, is that jumps in the electric field could change the kinetics and mechanism of protein folding since highly charged and α helical regions of the protein would be most affected by the change in electric field. It is possible, however, that electric field experiments would be pertinent for membrane bound proteins since there is an electric potential across the cell membrane.

Another possibility is to improve the dead time of mixing experiments such as stopped flow. Improvement in dead time is possible using the continuous flow method in which two liquids are mixed by forcing them through a small (25 μm in diameter) nozzle (Takahashi et al. 1995) or around a small (~100 μm radius) sphere at velocities of around 10 m/sec (Regenfuss et al. 1985). The jet emitted from the nozzle is then optically probed at different positions along its path to yield time resolved data (Regenfuss et al. 1985; Takahashi et al. 1995). The dead time depends on the nozzle used and can be as low as 20 microseconds (Takahashi et al. 1995). Hofrichter and coworkers have conducted protein

Reproduced with permission of the copyright owner. Further reproduction prohibited without permission.

folding experiments using continuous flow and preliminary results indicate that the shear forces at the nozzle complicate the results (Chan et al. 1996).

Temperature jumps have also been used to study helix-coil transitions of polypeptides (Lumry et al. 1964). These investigators produced the temperature jump by electric discharge and high (millimolar to molar) salt concentrations were needed to conduct the current and heat up the solution (Czerlinski and Eigen 1959). Such high salt concentrations limit the proteins and protein conformations that can be studied. The dead time of the Lumry experiment was 20 microseconds (Lumry et al. 1964), and even more modern setups which use Joule heating to jump the temperature have heating times of microseconds (Hi-Tech 1995).

All of the above experimental methods have dead times which are too long (stopped flow or electrical discharge temperature jumps), do not directly measure folding rates (steady state techniques such as dynamic NMR), perturb the system in ways which may affect the folding rates (high residual denaturant concentrations, electric field jumps or continuous flow) or are applicable to an extremely limited number of proteins (flash photolysis of cyt c). One solution to all of these problems is to use a short (nanoseconds or less) laser pulse to perturb a solution characteristic such as pH or temperature. In such experiments, absorption of the laser pulse causes an extremely rapid change in some property of the solution. The dead time of such an experiments is dependent on the temporal width of the laser pulse and the solution response. This approach is analogous to the cyt c experiments of Jones and coworkers (1993), but instead of changing a specific protein ligand a general solution property is changed and the method is generally applicable.

One disadvantage of these optical techniques is that, unlike mixing experiments, all changes to the solution characteristics are transient. Therefore, care must be taken to ensure that measurements are conducted in regions of stable temperature or pH. Additionally, low optical densities must be used so that changes are homogenous across the

Reproduced with permission of the copyright owner. Further reproduction prohibited without permission.

sample. However, the amount of material required for the transient experiments is much less than that required for stopped flow and experiments take less time. The following chapters describe applications of laser based techniques to studies of early events in protein folding.

Reproduced with permission of the copyright owner. Further reproduction prohibited without permission.

References

Bösterling, B., and Engel, J. (1979). "Kinetic Studies on the Helix-Coil Transition of Fluorescent Labeled Poly(-L-Lysine) by the Temperature-Jump Technique." *Biophysical Chemistry*, 9, 201-209.

Burke, J. J., Hammes, G. G., and Lewis, T. B. (1965). "Ultrasonic Attenuation Measurements of Poly-L-Glutamic Acid Solutions." *The Journal of Chemical Physics*, 42(10), 3520-3525.

Chan, C.-K., Hu, Y., Takahashi, S., Rousseau, D. L., Eaton, W. A., and Hofrichter, J. (1996). "Protein Folding Studied by Ultrafast Mixing." *Biophysical Journal*, 70, A177.

Chan, H. S., and Dill, K. A. (1994). "Transition States and Folding Dynamics of Proteins and Heteropolymers." *Journal of Chemical Physics*, 100(12), 9238-9257.

Chen, B.-L., Baase, W. A., Nicholson, H., and Schellman, J. A. (1992). "Folding Kinetics of T4 Lysozyme and Nine Mutants at 12°C." *Biochemistry*, 31, 1464-1476.

Chen, B.-l., Baase, W. A., and Schellman, J. A. (1989). "Low-Temperature Unfolding of a Mutant of Phage T4 Lysozyme. 2. Kinetic Investigations." *Biochemistry*, 28, 691-699.

Chiba, K., Ikai, A., Kawamura-Konishi, Y., and Kihara, H. (1994). "Kinetic Study on Myoglobin Refolding Monitored by Five Optical Probe Stopped-Flow Methods." *Proteins: Structure, Function, and Genetics*, 19, 110-119.

Creighton, T. E. (1993). *Proteins: Structures and Molecular Properties*, W. H. Freeman and Company, New York.

Cummings, A. L., and Eyring, E. M. (1975). "Helix-Coil Transition Kinetics in Aqueous Poly(α,L-Glutamic Acid)." *Biopolymers*, 14, 2107-2114.

Czerlinski, V. G., and Eigen, M. (1959). "Ein Temperatursprungmethode zur Untersuchung Chemischer Relaxation." *Zeitschrift für Elektrochemie*, 63, 652-661.

Dill, K. A., Bromberg, S., Yue, K., Fiebig, K. M., Yee, D. P., Thomas, P. D., and Chan, H. S. (1995). "Principles of Protein Folding - A Perspective from Simple Exact Models." *Protein Science*, 4, 561-602.

Elöve, G. A., Chaffotte, A. F., Roder, H., and Goldberg, M. E. (1992). "Early Steps in Cytochrome *c* Folding Probed by Time-Resolved Circular Dichroism and Fluorescence Spectroscopy." *Biochemistry*, 31, 6876-6883.

Eyring, E. M., and Hemmes, P. (1986). "Electric Field Methods." Techniques in Chemistry, C. F. Bernasconi, ed., John Wiley & Sons, New York, 219-246.

Reproduced with permission of the copyright owner. Further reproduction prohibited without permission.

Harrison, S. C., and Durbin, R. (1985). "Is there a Single Pathway for the Folding of a Polypeptide Chain?" *Proceedings of the National Academy of Sciences USA*, 82, 4028-4030.

Hi-Tech, S. (1995). "Description of TJ-64 temperature jump apparatus." .

Huang, G. S., and Oas, T. G. (1995). "Submillisecond Folding of Monomeric λ repressor." *Proceedings of the National Academy of Sciences, USA*, 92, 6878-6882.

Inoue, S., Sano, T., Yakabe, Y., Ushio, H., and Yasunaga, T. (1979). "Kinetic Studies of the Helix-Coil Transition in Aqueous Solutions of Poly(L-Lysine)." *Biopolymers*, 18, 681-691.

Jennings, P. A., and Wright, P. E. (1993). "Formation of a molten globule intermediate early in the kinetic folding pathway of apomyoglobin." *Science*, 262, 892-896.

Jing, G.-z., Zhou, B., Xie, L., Liu, L.-j., and Liu, Z.-g. (1995). "Comparative Studies of the Conformation of the N-terminal Fragments of Staphylococcal Nuclease R in Solution." *Biochimica et Biophysica Acta*, 1250, 189-196.

Jones, C. M., Henry, E. R., Hu, Y., Chan, C.-K., Luck, S. D., Bhuyan, A., Roder, H., Hofrichter, J., and Eaton, W. A. (1993). "Fast Events in Protein Folding Initiated by Nanosecond Laser Photolysis." *Proceedings of the National Academy of Sciences, U.S.A.*, 90, 11860-11864.

Karplus, M., and Sali, A. (1995). "Theoretical Studies of Protein Folding and Unfolding." *Current Opinion in Structural Biology*, 5, 58-73.

Karplus, M., and Weaver, D. L. (1994). "Protein Folding Dynamics: The Diffusion-Collision Model and Experimental Data." *Protein Science*, 3, 650-668.

Kim, P. S., and Baldwin, R. L. (1982). "Specific Intermediates in the Folding Reactions of Small Proteins and the Mechanism of Protein Folding." *Annual Review of Biochemistry*, 51, 459-489.

Kuwajima, K., Yamaya, H., Miwa, S., Sugai, S., and Nagamura, T. (1987). "Rapid Formation of Secondary Structure Framework in Protein Folding Studied by Stopped-Flow Circular Dichroism." *FEBS Letters*, 221, 115-118.

Lumry, R., Legare, R., and Miller, W. G. (1964). "The Dynamics of the Helix-Coil Transition in Poly-α,L-Glutamic Acid." *Biopolymers*, 2, 489-500.

Myers, J. K., Pace, C. N., and Scholtz, J. M. (1995). "Denaturant *m* Values and Heat Capacity Changes: Relation to Changes in Accessible Surface Areas of Protein Folding." *Protein Science*, 4, 2138-2148.

Ptitsyn, O. B. (1992). "The Molten Globule State." Protein Folding, T. E. Creighton, ed., W. H. Freeman and Company, New York, 243-300.

Regenfuss, P., Clegg, R. M., Fulwyler, M. J., Barrantes, F. J., and Jovin, T. M. (1985). "Mixing Liquids in Microseconds." *Review of Scientific Instruments*, 56(2), 283-290.

Reproduced with permission of the copyright owner. Further reproduction prohibited without permission.

Sugawara, T., Kuwajima, K., and Sugai, S. (1991). "Folding of Staphylococcal Nuclease A Studied by Equilibrium and Kinetic Circular Dichroism Spectra." *Biochemistry*, 30, 2698-2706.

Takahashi, S., Ching, Y.-c., Wang, J., and Rousseau, D. L. (1995). "Microsecond Generation of Oxygen-bound Cytochrome c Oxidase by Rapid Solution Mixing." *Journal of Biological Chemistry*, 270(15), 8405-8407.

Tsuji, Y., Yasunaga, T., Sano, T., and Ushio, H. (1976). "Kinetic Studies of the Helix-Coil Transition in Aqueous Solutions of Poly(α-L-glutamic acid) Using the Electric Field Pulse Method." *Journal of the American Chemical Society*, 98, 813-818.

van Gunsteren, W. F., and Mark, A. E. (1992). "On the Interpretation of Biochemical Data by Molecular Dynamics Computer Simulation." *European Journal of Biochemistry*, 204, 947-961.

Waltho, J. P., Feher, V. A., Merutka, G., Dyson, H. J., and Wright, P. E. (1993). "Peptide Models of Protein Folding Initiation Sites. 1. Secondary Formation by Peptides Corresponding to the G- and H-Helices of Myoglobin." *Biochemistry*, 32, 6337-6347.

Wright, P. E., Dyson, H. J., and Lerner, R. A. (1988). "Conformation of Peptide Fragments of Proteins in Aqueous Solution: Implications for Initiation of Protein Folding." *Biochemistry*, 27(19), 7167-7175.

Reproduced with permission of the copyright owner. Further reproduction prohibited without permission.

CHAPTER V
pH JUMPING

Introduction

To observe early events in protein folding or unfolding a well defined change in solution characteristics must be induced in microseconds or less. Changes in solution pH can lead to changes in protein conformation and shifts in solution pH may be triggered optically on such time scales.

Transient changes in pH may be initiated by photoexcitation of aromatic alcohols or heterocyclic compounds (Gutman 1984; Kosover and Huppert 1986; Pines et al. 1986). In the excited state, the pKs of aromatic alcohols (heterocyclic compounds) are much lower (higher) than in the ground state resulting in proton ejection (acceptance). In order for an aromatic alcohol to be protonated prior to photoexcitation, the pH of the solution must be below the ground state pK of the alcohol; whereas a heterocyclic compound should be deprotonated necessitating a solution pH above the ground state pK. The ground state pKs of pH jumping compounds studied by Gutman are in the neutral range between pH 5 and 9 (Gutman 1984; Pines et al. 1986).

In this pH region most proteins are in their native state so that any pH jump experiments would investigate protein unfolding rather than folding. However, charged polyamino acids may undergo a transition from random coil to structured states when the pH is changed from neutral. For example, poly-L-glutamic acid (PGA) is transformed from a random coil to a stable α helix when the pH is lowered below 5 (Stryer and Blout 1961) and poly-L-lysine undergoes a similar transition when the pH is raised to 11

Reproduced with permission of the copyright owner. Further reproduction prohibited without permission.

(Bösterling and Engel 1979). The rate constants for helix formation of these polyamino acids are known to be about 10^7 s^{-1} from experiments performed using electric field jumps (Cummings and Eyring 1975; Inoue et al. 1979; Sano and Yasunaga 1980; Tsuji et al. 1976), ultrasonic relaxation (Burke et al. 1965) and temperature jumps (Eggers and Funck 1976; Lumry et al. 1964).

Optical detection of the change in protein or polypeptide conformation due to the pH jump is complicated by the absorbance of the pH jumping compounds in the UV and the high pH jumper concentration (hundreds of micromolar) necessary to significantly change the pH. One way around this problem is to monitor the properties of dyes which interact with the polyamino acid or protein, but absorb light in the visible rather than the ultraviolet. These dyes must be sensitive to conformational changes of the macromolecules.

Acridine orange (AO) is a cationic dye which intercalates in DNA helices as well as in some charged α helices (Gafni et al. 1973; Stryer and Blout 1961). In particular, upon lowering the pH of a solution of AO and PGA from neutral to below pH 5 the circular dichroism (CD) of AO from 360 to 560 nm becomes structured displaying three well defined ellipticity bands which may be used as a monitor of PGA helicity (Myhr 1968; Stryer and Blout 1961). This change in AO circular dichroism is due to the formation of a right handed superhelix of AO molecules around the right handed PGA α helix (Hatano et al. 1973; Imae and Ikeda 1976). The PGA-AO complex seemed to be an ideal model system for use in pH jump experiments.

Materials and Methods

PGA sodium salt; acridine orange, hemizinc chloride salt (AO); bromcresol green (BG); sodium chloride (NaCl); sodium hydroxide (NaOH) and hydrochloric acid (HCl) were purchased from Sigma Chemical Co. The pH jumper 8-hydroxypyrene-1,3,6-trisulfonic acid (HPTS) was purchased from Fisher Scientific. 4-(bromomethyl)-6,7-dimethoxycoumarin (BrDMC) was purchased from Molecular Probes. All chemicals were

Reproduced with permission of the copyright owner. Further reproduction prohibited without permission.

used without further purification. All experiments were performed at room temperature in unbuffered solutions. A buffered solution would significantly decrease the amplitude of a pH jump. The pH of samples was adjusted with HCl and NaOH.

Spectroscopy

The absorption spectrum and the circular dichroism (CD) spectrum of PGA and AO are reported to be affected by the order in which the dye and polymer are mixed (Myhr 1968). For all experiments, the AO solution was added to the PGA solution while slowly stirring.

Absorption measurements were performed on a Shimadzu UV-260, a UV-visible recording spectrometer complete with reference channel. Absorption spectra were collected using quartz cuvettes with a path length of 1 cm and water in the reference channel. The absorption baseline was collected with water in the reference and sample cuvettes.

Steady state fluorescence spectra were collected on a SPEX Fluorolog consisting of a 450 W Xenon lamp, model 1681 0.22 m focal length excitation spectrometer, model 1680 0.22 m focal length emission double spectrometer, a Hamamatsu R928 side-on PMT in photon counting mode for the sample signal, and a Hamamatsu R508 side-on PMT in analog mode for the reference signal. The reference PMT voltage was 500 kV and the sample PMT voltage was 900 kV. The signal for the reference was given by a solution of rhodamine.

CD measurements were conducted on a Jasco J-720 spectropolarimeter located in the University of Michigan protein core facility. A quartz cuvette with a path length of 1 cm was used for all measurements. (+)-10-camphor sulfonic acid (Sigma Chemical Co.) was used as a standard to calibrate the CD machine. CD spectra were collected from 560 to 360 nm for solutions of AO and AO plus PGA, and from 560 to 425 nm for most samples containing HPTS. Five traces were accumulated for all the data displayed at a rate of 200 nm/min.

Reproduced with permission of the copyright owner. Further reproduction prohibited without permission.

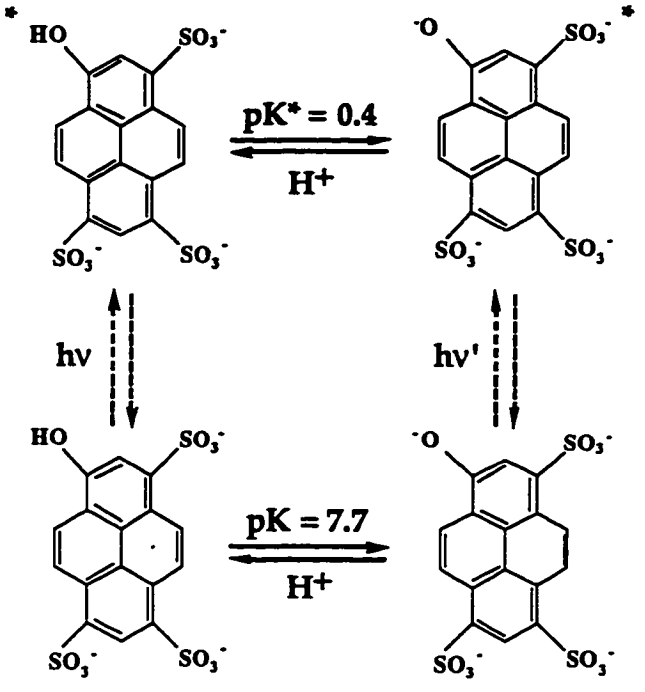

Figure 5.1. The photoexcitation of HPTS leading to a pH jump. The star indicates the excited state.

Laser induced pH jump:

An unbuffered solution of HPTS with a pH less than the ground state pK is mainly in the protonated form in the ground state. If the initial pH is also greater than the excited state pK (pK*), upon photoexcitation the shift in pK leads to a change in the equilibrium and deprotonation is much more likely (figure 5.1, for pK equations see appendix C). HPTS is a particularly efficient pH jumper because its pK* is 0.4 (Smith et al. 1979) while its pK is 7.7 (Gutman et al. 1981). The proton dissociation rate, k_{off}, of excited HPTS may be calculated from pK* assuming that the proton association rate, k_{on}, is diffusion limited and using the fact that when the pH equals pK* (see appendix C), the equilibrium constant, K, equals the hydrogen ion concentration:

$$K = \frac{k_{off}}{k_{on}} = [H^+] \qquad (5.1)$$

$$k_{off} = k_{on} 10^{-pH} = (4X10^{10} M^{-1}s^{-1})\, 10^{-0.4} M = 1.59X10^{-10} s \qquad (5.2)$$

Reproduced with permission of the copyright owner. Further reproduction prohibited without permission.

Thus, the proton off rate is approximately 60 picoseconds which is within the error bars of the experimentally determined value of 31 picoseconds (Smith et al. 1979), and well within the excited state lifetime of 6.3 nsec at pH 7 (Smith et al. 1979).

The duration and amplitude of the pH jump were measured by detecting the change in absorption at 632.8 nm of the pH indicator bromcresol green (BG) according to the protocol of Gutman, et al (1981). The peak of the BG absorbance occurs at 618 nm, and as can be seen from figure 5.2, the absorbance of BG between 500 and 700 nm substantially changes with pH. The useful pH range for BG is from pH 3.8 to pH 5.4 (Sigma Chemical).

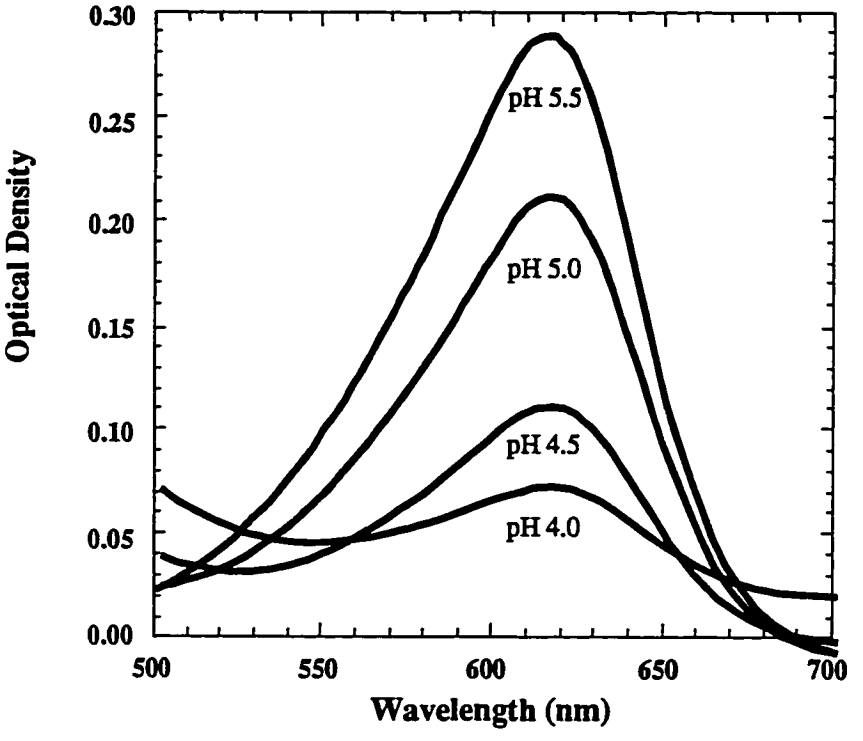

Figure 5.2. Absorbance of 10 μM bromcresol green in 1 mM sodium acetate. The path length was 1 cm and the reference sample was water. The negative absorbance around 700 nm is due to a slight baseline shift.

Samples of HPTS (the pH jumper) and BG were prepared in 10 mM NaCl pH 6.2. Repeated pulsing of the HPTS with 355 nm light resulted in absorbance changes and variations in the magnitude of the pH jump. To avoid these problems, the sample was

Reproduced with permission of the copyright owner. Further reproduction prohibited without permission.

placed in a Hellma quartz flow cell with a 3 mm path length. The flow rate (Biorad pump) was 113 to 190 ml/hour.

The instrument used to collect the data (Fig. 5.3) was a modified from that of Gutman, et al (1981). In preparation for an experiment, the 8-10 nanosecond, 355 nm pump pulse from a frequency tripled Spectra-Physics DCR-11 Nd-YAG laser and the 632.8 He-Ne laser (Uniphase) probe beam were aligned collinearly. Laser spot sizes were less than 1 mm^2. The transmission of the 632.8 nm beam through the sample cell was monitored by a silicon photodiode terminated at 50 ohms to give a response time of 10 nsec. The signal from the diode was amplified and then displayed on a 200 MHz digital oscilloscope (Gould) and stored on a Macintosh computer. The electronic filter on the Gould oscilloscope was used to filter out noise in the 4-10 MHz range and above.

To perform an experiment, the HPTS was photoexcited by a 355 nm laser pulse, and the transient change in transmission at 632.8 nm of the bromcresol green was monitored. The time between 355 nm laser shots was 1.1 sec and all experiments were conducted with a 0.4 μsec pretrigger during which no change in the transmission was seen. All the pH jump data are the average of 256 photoexcitations.

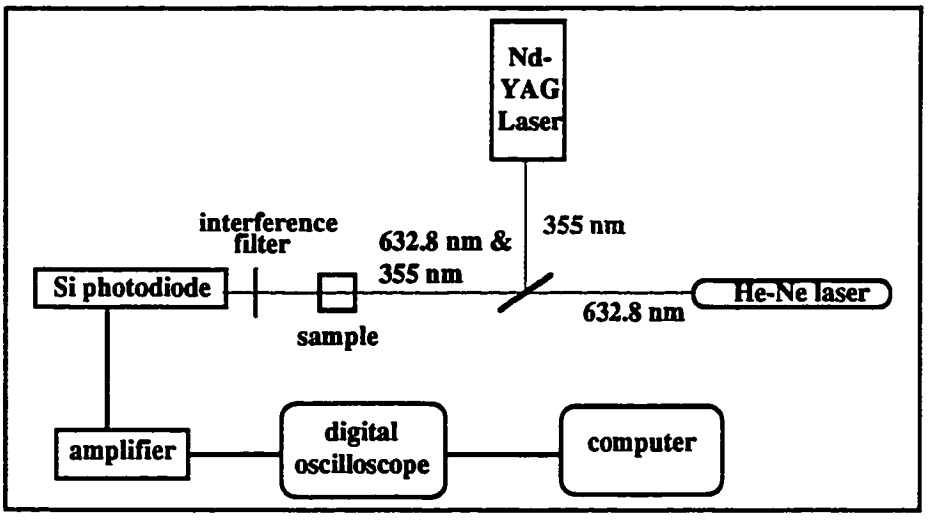

Figure 5.3. Schematic of the apparatus used to initiate and monitor the pH jump. The nanosecond 355 nm pulse from the Nd-YAG photoexcited HPTS led to the pH jump which was monitored by the change in transmission of the 632.8 nm laser beam. For more details see the text.

Reproduced with permission of the copyright owner. Further reproduction prohibited without permission.

pH jump data analysis:

The proton concentration ($[H^+]$) was calculated from the measured change in transmission at 632.8 nm. The pH jump is a transient phenomenon and the changes in $[H^+]$ are derived from the following differential equation (Gutman et al. 1981):

$$H^+ + In^- \underset{k_{off}}{\overset{k_{on}}{\rightleftharpoons}} HIn \tag{5.3}$$

$$-\frac{d[In^-]}{dt} = \frac{d[HIn]}{dt} = k_{on}[In^-][H^+] - k'_{off}[HIn] \tag{5.4}$$

$$[H^+](t) = \frac{\left(\frac{d[HIn](t)}{dt}\right) + k'_{off}[HIn](t)}{k_{on}[In^-](t)} \tag{5.5}$$

where In^- is the alkaline form of the pH indicator, HIn is the protonated form of the pH indicator, k_{on} is the proton on rate, k_{off} is the proton off rate and k'_{off} is the apparent proton off rate. The apparent proton off rate is used in equation 5.4 because some of the protons are directly transferred from BG back to HPTS. The off rate measured in this experiment is then, the actual off rate of the pH indicator plus a proton transfer term (Gutman et al. 1981). Equation 5.5 is only correct as long as $[H^+](t)$ is much greater than the equilibrium proton concentration (Gutman et al. 1981). If the transient proton concentration is close to the equilibrium proton concentration then contributions of protons from water and from BG must be considered.

The Si photodiode measured the time resolved transmission, T(t), of the sample. The transmission data were converted to the time resolved change in optical density, $\Delta OD(t)$, using Beer's law (equation 1.5) and then to $[In^-](t)$:

$$\Delta OD(t) = \log_{10}\left(\frac{T_{base}}{T(t)}\right) - \log_{10}\left(\frac{T_{HPTSbase}}{T_{HPTS}(t)}\right) \tag{5.6}$$

Reproduced with permission of the copyright owner. Further reproduction prohibited without permission.

$$\Delta[In^-](t) = \frac{\Delta OD(t)}{(0.3\ cm)(33X10^3\ M^{-1}cm^{-1})} \qquad (5.7)$$

where T_{base} is the baseline transmission prior to the 355 nm pulse, $T_{HPTS}(t)$ is the time resolved transmission seen in a solution containing only HPTS (i.e. no BG) , $T_{HPTSbase}$ is the baseline transmission for the HPTS data, 0.3 cm is the path length of the flow cell and $33 \times 10^3\ M^{-1}\ cm^{-1}$ is the extinction coefficient of In^- for BG (Gutman et al. 1981). The second term in equation 5.6 corrects for changes due only to the HPTS and unrelated to changes in BG absorption.

Before calculating [HIn](t) the transmission baseline prior to photoexcitation was used to calculate the equilibrium concentration of In^- (analogously to equation 5.7). Then, the published values (Gutman et al. 1981) of k_{on} and k_{off} were used to calculate the equilibrium concentration of HIn:

$$[HIn]_{eq} = \frac{k_{on}}{k_{off}}[H^+]_{eq}[In^-]_{eq} \qquad (5.8)$$

$$[\text{total indicator}] = [HIn]_{eq} + [In^-]_{eq} \qquad (5.9)$$

where eq refers to equilibrium values (values prior to photoexcitation) and $[H^+]_{eq}$ is calculated from the starting pH (6.2 in this case). The total indicator concentration from equation 5.9 and the time resolved $[In^-](t)$ from equation 5.7 were used to calculate [HIn](t).

The time resolved data were imported into the data analysis and graphing program Kaleidagraph (Synergy Software). A 5 point moving average of the [HIn](t) was taken and then the derivative of the smoothed data was taken in order to determine d[HIn](t)/dt. The smoothing was necessary because Kaleidagraph takes a derivative according to:

$$\frac{dy}{dx} = \frac{y_{i+1} - y_i}{x_{i+1} - x_i} \qquad (5.10)$$

Reproduced with permission of the copyright owner. Further reproduction prohibited without permission.

and this formula tends to magnify the noise in [HIn](t). The final term for equation 5.5, k'_{off}, was calculated from fitting the [HIn](t) data to:

$$[HIn](t) = [HIn]_{eq} + Ae^{-k'_{off}t} \qquad (5.11)$$

where A and k'_{off} are the fitted parameters. The published value of 5×10^{10} M^{-1} s^{-1} was used for k_{on}.

Results

The equilibrium pHs used for these experiments were determined by two factors. First, in order for the pH jump to work, HPTS must be mostly protonated prior to photoexcitation so the pH of the solution must be less than the pK of HPTS. Second, the magnitude of the pH jump must be large enough to induce a random coil - α helical transition in PGA. An initial pH of 6.2 was chosen because according to Stryer and Blout (1961) at pH 6.2 PGA is entirely random coil and this pH is more than one pH unit below the ground state pK of HPTS.

HPTS experiments:

Using the setup in figure 5.3 a pH jump of almost 2 pH units was achieved with a 355 nm pulse energy of 30 mJ (fig. 5.4). At a BG concentration of 57 μM, HPTS concentration of 200 μM and a pulse energy of 30 mJ, a maximum pH jump of 4.27 ± 0.05 was reached 230 nsec after the 355 nm pulse. A plot of maximum pH vs. 355 nm laser energy was linear (inset figure 5.4) indicating that the sample was not saturated at the 355 nm energies used. Note that the pH does not extrapolate to pH 6.2 at zero mJ of laser energy due to the assumption that the transient pH is much greater than the equilibrium pH.

Reproduced with permission of the copyright owner. Further reproduction prohibited without permission.

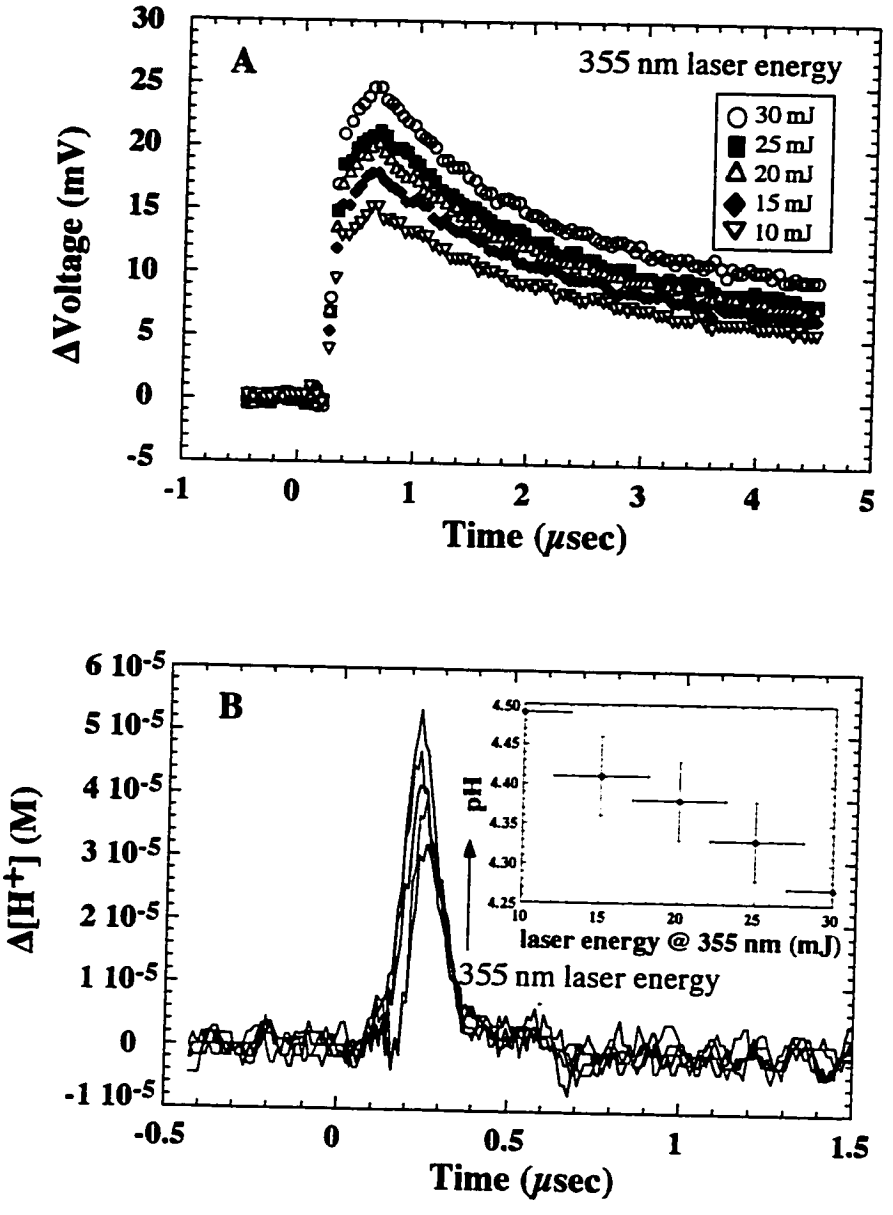

Figure 5.4. (A) Change in transmission at 632.8 nm of a solution containing 10 mM NaCl, 57 μM BG and 200 μM HPTS. All data are the average 256 laser pulses at 355 nm used to excite the HPTS and initiate the pH jump. (B) Change in proton concentration as seen by the BG at various 355 nm laser intensities. Calculated from the data in (A). The inset shows the maximum change in pH versus 355 nm laser energy.

Reproduced with permission of the copyright owner. Further reproduction prohibited without permission.

PGA & AO:

PGA is available with various average molecular weights depending on the degree of polymerization. Most previous studies on the interaction of PGA with AO used PGA with average molecular weights of 50,000 to 110,000 (Ballard et al. 1966; Hatano et al. 1973; Stryer and Blout 1961; Yamaoka and Resnik 1966); therefore in order to facilitate comparisons with the literature, PGA with an average molecular weight of 83,000 (as determined by Sigma Chemical Co. using viscosity) was used for these experiments. PGA with an average molecular weight of 17,500 was also tried but it showed less structure, based on CD, than did the longer chains of PGA (data not shown).

Another chemical variable of importance is the molar ratio between polymer residues and the dye (P/D). If the dye concentration is too large there will be free dye in solution as well as electrostatically attached to the PGA (Hatano et al. 1973; Myhr 1968) . Higher dye concentrations have also been shown to cause aggregation (Imae and Ikeda 1976; Myhr 1968), and there is some evidence that, at pH 4.5, P/Ds of less than 10 can disrupt the PGA α helix (Hatano et al. 1973) For these experiments the P/D ratio was in the range 40:1 to 55:1.

AO shows significant changes in absorption between 350 and 600 nm depending on whether it is in a monomeric or dimeric form (Lamm and Neville 1965; Zanker 1952). AO concentrations used for these experiments were between 10 and 50 μM, a range in which the absorption is mainly from monomeric AO at both pH 6.2 and 4.3 with an absorption peak at 491 nm and a shoulder in the absorption beginning at around 470 nm (figure 5.5). Upon the addition of PGA, at either pH 6.2 or 4.3, the absorption spectrum of AO blue shifts giving a peak of 456 nm for pH 6.2 and 451 nm for pH 4.3 (figure 5.5). This blue shift corresponds to stacking of the dye (AO) on the polymer (PGA) (Ballard et al. 1966; Hatano et al. 1973; Imae and Ikeda 1976; Myhr 1968) and is in agreement with the published absorption spectra (Hatano et al. 1973; Stryer and Blout 1961).

Reproduced with permission of the copyright owner. Further reproduction prohibited without permission.

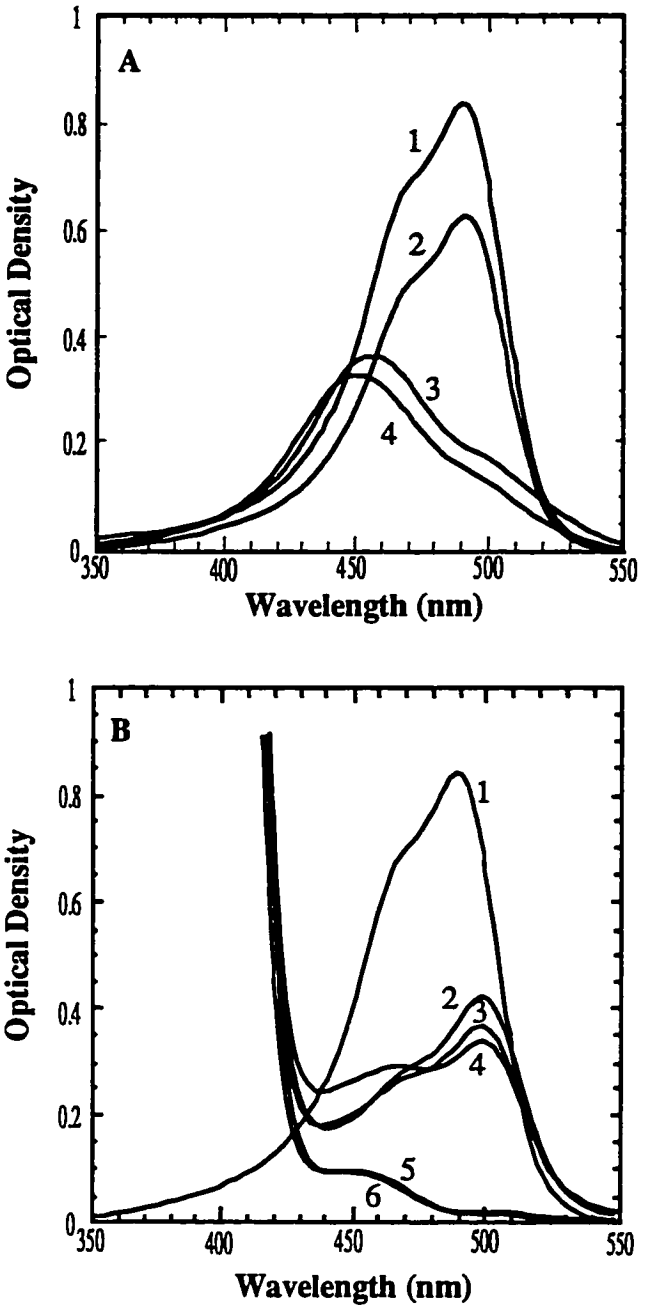

Figure 5.5. (A) Absorption spectra of AO with and without PGA. 25 μM AO pH 4.3 (curve 1), 25 μM AO pH 6.2 (curve 2), 25 μM AO and PGA pH 4.3 P/D=54 (curve 3) and 25 μM AO and PGA pH 6.2 P/D=54 (curve 4). (B) Absorption spectra of HPTS with and without PGA and/or AO. 25 μM AO pH 4.3 for reference (curve 1); 200 μM HPTS and 25 μM AO pH 6.2 (curve 2); 200 μM HPTS, 25 μM AO and PGA pH 4.3 P/D=54 solution mixed at pH 6.2 and titrated to pH 4.3 (curve 3); 200 μM HPTS, 25 μM AO and PGA pH 6.2 P/D=54 solution mixed at pH 6.2 (curve 4); 200 μM HPTS and PGA pH 6.2 (curve 5) and 200 μM HPTS pH 6.2 (curve 6). All solutions were in water and were titrated with NaOH and HCl.

Reproduced with permission of the copyright owner. Further reproduction prohibited without permission.

Comparisons of the fluorescence emission spectra of AO by itself to AO plus PGA were complicated by shifts in the absorption spectra. Emission spectra excited at 490 nm showed that the addition of PGA to AO decreased the fluorescence intensity, as expected since the absorption of AO plus PGA at 490 nm is lower than that of AO alone, but did not significantly shift the emission peak from 529 nm (uncorrected value). At a P/D ratio of 54, mixtures of AO and PGA at pH 6.2 displayed greater emission than those at pH 4.3 (figure 5.6). At pH 4.3 the emission spectrum for PGA + AO excited at 455 nm was red shifted almost 10 nm (uncorrected) (figure 5.6). At both pH 4.3 and 6.2 the samples excited at 455 nm showed an additional shoulder around 620 which is much weaker at pH 6.2. At pH 4.3 the strength of the shoulder was dependent on whether the samples were mixed at pH 6.2 and then titrated to pH 4.3 or mixed at pH 4.3. In the latter case, the shoulder was much more prominent. A similar, band was seen by Myhr for both coil complexes at pH 8 and helix complexes at pH 4.5 (Myhr 1968).

The CD between 360 and 560 nm of AO alone showed little reproducible structure (data not shown). PGA by itself showed no CD in this region since it has no absorption in the visible wavelength range (data not shown). However, addition of AO to a PGA solution led to a well defined CD signal at pH 4.3 where PGA is helical (figure 5.7). This signal was characterized by two positive ellipticity bands at 436 and 522 nm respectively and a negative band at 465 nm (figure 5.7) in agreement with published CD spectra (Hatano et al. 1973; Imae and Ikeda 1976). At pH 6.2 no reproducible structure was expected, but in some samples, a peak was observed around 440 nm and a valley near 475 nm. The midpoint of the coil to helical transition in water is located at pH 6 (Myhr 1968), and it is possible that at pH 6.2 there was still some residual helical structure.

The magnitude of the CD was very dependent on whether the pH of the solutions was adjusted before or after mixing the PGA and AO (data not shown) indicating that the system is not at equilibrium but rather is in some metastable state. This effect has some serious consequences for a pH jump experiment in which the baseline pH (pH 6.2 for the

Reproduced with permission of the copyright owner. Further reproduction prohibited without permission.

Figure 5.6. Uncorrected fluorescence emission spectra of AO with and without HPTS or PGA. The emission of samples excited at 490 nm was monitored from 500 to 700 nm. The emission of samples excited at 455 nm was recorded from 465 to 665 nm. Data were collected at 1 nm intervals, but only every 5th point is displayed. All samples were in water and were mixed at pH 6.2 and titrated to pH 4.3. (A) Fluorescence excited at 490 or 455 nm of 25 μM AO with and without 200 μM HPTS. (B) Fluorescence of 25 μM AO in the presence of PGA P/D=54 with and without 200 μM HPTS. Samples were excited at 490 nm. (C and D) Fluorescence of 25 μM AO in the presence of PGA P/D=54 with and without 200 μM HPTS. Samples were excited at 455 nm. Note the large increase in fluorescence when HPTS was added at pH 6.2.

Reproduced with permission of the copyright owner. Further reproduction prohibited without permission.

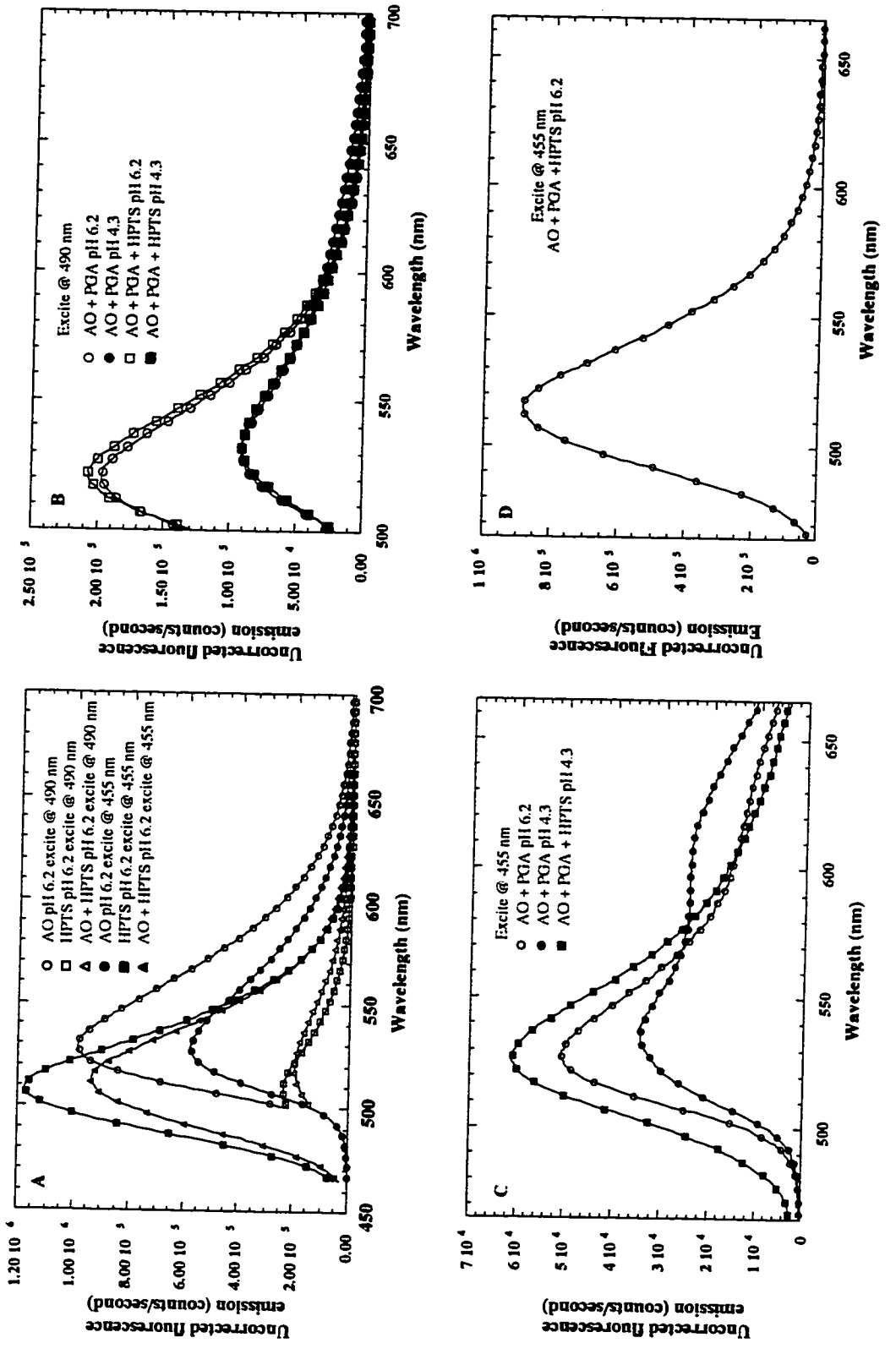

Reproduced with permission of the copyright owner. Further reproduction prohibited without permission.

HPTS experiments described above) may be adjusted before or after mixing, but the pH of the solution during the jump corresponds to mixing and then adjusting the pH.

Adding HPTS:

Addition of 200 to 250 μM HPTS to a pH 6.2 solution containing PGA and AO at P/D of 54 caused the peak in the absorption spectrum to red shift to 500 nm (figure 5.5). 200 μM HPTS alone showed absorbances of less than 0.1 between 450 and 650 nm. However, a solution containing only AO and HPTS showed an absorption peak similar to that of solutions containing AO, HPTS and PGA leading to the conclusion that HPTS interacts with AO at pH 6.2. This same shift in absorption was seen in solutions at pH 4.3.

The fluorescence emission spectra of solutions containing both AO and HPTS were complicated by the fact that both molecules are fluorescent although 200 μM HPTS has only 2% absorption at 455 nm. Nonetheless, 200 μM HPTS showed considerable emission when excited at 455 and 490 nm. The peak of this emission was centered around 510 nm as expected for HPTS, but was much larger, particularly when excited at 455 nm, than expected (figure 5.6). This emission arises from the large fluorescence spectrometer bandwidth used to observe acridine orange fluorescence at these concentrations. The addition of HPTS to solutions containing AO and PGA caused a blue shift in the fluorescence compared to AO and PGA alone due to the HPTS fluorescence (figure 5.6).

The CD of HPTS + AO + PGA lacks structure at pH 6.2 (figure 5.7). Experiments in which solutions were mixed at pH 6.2 and then titrated to pH 4.3 showed negligible CD spectra. However, addition of HPTS at pH 4.3 to samples already at pH 4.3 showed only small decreases in CD again indicating a lack of equilibrium in the system.

Following the experiments involving HPTS , AO and PGA , a calculation of the HPTS to PGA ratio which would be necessary for a pH jump experiment was done to see if the HPTS concentration could be lowered in order to try to shift the equilibrium towards

Reproduced with permission of the copyright owner. Further reproduction prohibited without permission.

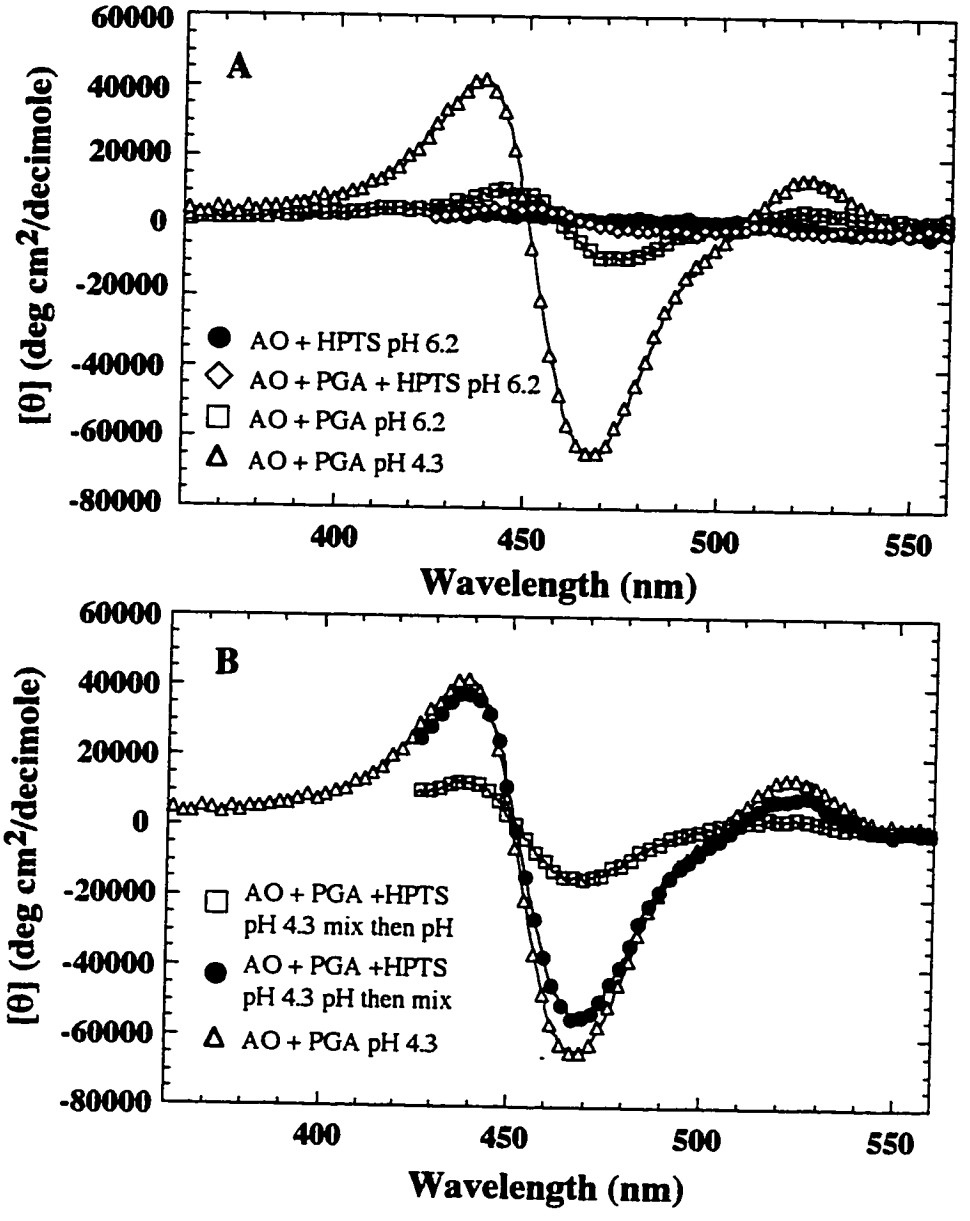

Figure 5.7. Circular Dichroism (CD) of AO with PGA and/or HPTS. (A) 25 μM AO with 200 μM HPTS pH 6.2 solutions mixed at pH 6.2 (•); 25 μM AO and PGA P/D=54 and 200 μM HPTS pH 6.2 solutions mixed at pH 6.2(◊); 25 μM AO and PGA P/D=54 pH 6.2 solutions mixed at pH 6.2 (□) and 25 μM AO and PGA P/D=54 pH 4.3 solution mixed at pH 4.3 (Δ). (B) 25 μM AO and PGA P/D=54 and 200 μM HPTS pH 4.3 solutions mixed at pH 6.2 and titrated to pH 4.3 (•); 25 μM AO and PGA P/D=54 and 200 μM HPTS pH 4.3 solutions mixed at pH 4.3 (□) and 25 μM AO and PGA P/D=54 pH 4.3 solution mixed at pH 4.3 (Δ). Path length for CD = 1 cm. [θ] for all the data was calculated using only the concentration of AO.

Reproduced with permission of the copyright owner. Further reproduction prohibited without permission.

the AO-PGA complex. At pH 4.3 thirty seven percent of the PGA monomers are protonated since the pK of the PGA side chain carboxylic acid is 4.07(Voet and Voet 1990). From the pH jump experiments, 200 μM HPTS decreased the pH from 6.2 to 4.3 corresponding to the release of 50 μM of protons or the deprotonation of twenty-five percent of the HPTS in solution. Thus, the ratio of HPTS to PGA monomers should be two to one. The experiments conducted with a P/D ratio of 54 had a much lower ratio of HPTS to PGA monomer. To try to accommodate the higher HPTS:PGA ratio experiments were conducted with a HPTS, AO and PGA and a P/D ratio of 10. In these experiments, the AO still interacted mainly with the HPTS (data not shown).

It has been shown that in solutions containing only PGA, the addition of NaCl will increase the helical content of the polypeptide (Satoh et al. 1981; Satoh et al. 1982). Addition of NaCl failed to induce a CD signal in the PGA:AO:HPTS sample that was mixed at pH 6.2 and titrated to pH 4.3 and even decreased the CD signal in the sample that was mixed at pH 4.3. The decrease in helical content may be due to the NaCl concentrations used (0.21 to 1.7 mM) and the helical content of PGA at pH 4.3. Under conditions where PGA is almost entirely random coil, NaCl concentrations up to tens of millimolar will encourage helix formation; however, as the percent of helical PGA increases in the absence of NaCl, the concentrations of NaCl which stabilize the α helix formation decrease so that above 88% helicity adding any NaCl disrupts the α helix (Satoh, et al. 1981; Satoh, et al. 1982).

Discussion

PGA and AO interact electrostatically and this interaction was disrupted by the presence of HPTS. At pH 6.2 HPTS has a charge of -3, PGA is also negatively charged and AO has a charge of +1 in solution (see appendix B for structures). Thus, it seemed likely that HPTS was out competing PGA for AO at pH 6.2.

Reproduced with permission of the copyright owner. Further reproduction prohibited without permission.

In protein titration studies, the titration curve for lowering the pH does not always superimpose on the reverse titration curve due to a coupling between a conformational change and the titration (Cantor and Schimmel 1980). The differences between samples titrated to pH 4.3 and those mixed at pH 4.3 showed a similar hysteresis perhaps indicating that there was some competition between AO binding and the PGA helix-coil transition when the pH was lowered from 6.2 to 4.3. The differences between samples titrated to pH 4.3 and those mixed at pH 4.3 also indicated that the equilibrium between HPTS, PGA and AO at pH 4.3 took hours or possibly even days to be reached. Testing how long it takes samples at pH 4.3 to reach equilibrium is difficult since PGA tends to precipitate out of solution over time (Myhr 1968).

One way around the HPTS-AO-PGA interaction would be to covalently rather than electrostatically bind a dye to PGA. A candidate dye must be able to covalently bind to the carboxylic group on glutamic acid, respond to changes in PGA conformation and not disrupt the helix-coil transition. In order to have a uniform pH jump across the sample, the solution must be optically thin at 355 nm and the "leftover" 355 nm photons must not bleach a covalently bound dye.

Attempts to covalently label PGA with the dye BrDMC met with no success. In a published report on labeling PGA with dansyl chloride it was found that the labeling was successful, but the labeled PGA aggregated when the pH of the solution was below 6.2 (Bösterling and Engel 1979).

Carboxylic acids are known to be particularly difficult to label. An alternative to labeling the carboxylic acids of PGA would be to incorporate an easily labeled amino acid such as cysteine into the PGA. Any dye covalently bound to this incorporated residue would have to meet the same criteria specified above for dyes bound to glutamic acid, but the number of possible dyes should be greater. The labeled polypeptide would have to be assayed for its ability to form an α helix and for its pH behavior.

Reproduced with permission of the copyright owner. Further reproduction prohibited without permission.

Aside from dye problems PGA poses other difficulties as a model for early events in protein folding. PGA is a homopolymer lacking any hydrophobic interaction. There is evidence from theoretical models (Dill et al. 1995) as well as experimental models (Kamtekar et al. 1993; Xiong et al. 1995) that one of the most important components of protein folding is the fact that proteins are heteropolymers rather than homopolymers. In particular, proteins are composed of hydrophobic and polar residues and this combination is likely to be necessary for protein folding (Dill et al. 1995).

PGA also exhibits opposite pH behavior compared to proteins, it folds at low pH and is random coil at neutral pH indicating that the interactions needed for structure formation are different. Additionally, since PGA lacks tertiary structure, it cannot model the role of tertiary structure in protein folding. Furthermore, the length of the helix in PGA is tens of residues; whereas in proteins, the average length of an α helix is only 10 amino acid residues (Branden and Tooze 1991).

Thus, it might be best to choose an entirely different system for pH jump studies. One possibility is to look at the helix-coil transition in small (around 15 amino acid residues) alanine based peptides which form α helices in solution (Marqusee and Baldwin 1987; Marqusee et al. 1989). These peptides either fold or unfold when the pH is lowered depending on the peptide composition (Bradley et al. 1990; Fairman et al. 1989; Marqusee and Baldwin 1987; Marqusee et al. 1989; Stellwagen et al. 1992) so that both helix-coil and coil-helix transitions could be studied as could the affect of specific residues on the folding or unfolding kinetics. Once again, labeling would be a potential problem and the short length of these polypeptides increases the likelihood that dyes or HPTS itself would interfere with the helix-coil transition.

Given the technical difficulties and fundamental concerns, it might be best to go directly to studying proteins rather than model systems. This approach limits the pH jump technique to studying unfolding. Care would have to be taken to insure that the HPTS does not interact with the protein being studied, and the protein would have to be labeled.

Reproduced with permission of the copyright owner. Further reproduction prohibited without permission.

The same dye criteria would apply, but the choice of residue to label and available dyes would be much larger.

Conclusions

Using aromatic alcohols, it is possible to transiently change the pH of a protein or polypeptide solution. Complications arise in using UV optical techniques to study protein folding or unfolding due to the absorption of the pH jumping alcohols in the UV. These complications may be overcome by monitoring conformationally sensitive optical properties of dyes bound to polypeptides or proteins rather than the macromolecules themselves. However, interactions between the dyes, aromatic alcohols and/or polypeptides and proteins complicate such experiments.

One solution to these difficulties is to eliminate the use of dyes by monitoring spectroscopic parameters other than those in the UV or visible range. This approach has been taken by Small, et al using a pH jump and photoacoustic measurements to study the folding of poly-L-lysine (Abbruzzetti et al. 1996; Small 1996). Additionally, the Small group uses a caged proton, 2-hydroxyphenyl 2-nitrophenylethyl phosphate, as a proton donor rather than an aromatic alcohol. A caged proton compound undergoes a chemical change following photoexcitation and proton dissociation which precludes recombination; hence the duration of the pH jump is only limited by diffusion making it longer than the pH jump attained with aromatic alcohols.

A fundamentally different approach to the problem of early folding studies relies on changing the method of initiating protein folding/unfolding rather than the spectroscopy. This alternative is described in the following chapter.

Reproduced with permission of the copyright owner. Further reproduction prohibited without permission.

References

Abbruzzetti, S., Masino, L., Viappiani, C., Vecli, A., Libertini, L. J., Small, E. W., Nandagopal, R., McRae, R., and Small, J. R. (1996). "Rapid, Photo-Induced Proton Transfer: Dependence on Acceptor Size, Shape and Concentration." *Biophysical Journal*, 70(2), A178.

Ballard, R. E., McCaffery, A. J., and Mason, S. F. (1966). "Electronic Spectrum, Optical Activity, and Structure of the Acridine Orange Complex with Poly-α,L-glutamic Acid." *Biopolymers*, 4, 97-106.

Bösterling, B., and Engel, J. (1979). "Kinetic Studies on the Helix-Coil Transition of Fluorescent Labeled Poly(-L-Lysine) by the Temperature-Jump Technique." *Biophysical Chemistry*, 9, 201-209.

Bradley, E. K., Thomason, J. F., Cohen, F. E., Kosen, P. A., and Kuntz, I. D. (1990). "Studies of Synthetic Helical Peptides Using Circular Dichroism and Nuclear Magnetic Resonance." *Journal of Molecular Biology*, 215, 607-622.

Branden, C., and Tooze, J. (1991). *Introduction to Protein Structure*, Garland Publishing, Inc, New York, New York.

Burke, J. J., Hammes, G. G., and Lewis, T. B. (1965). "Ultrasonic Attenuation Measurements of Poly-L-Glutamic Acid Solutions." *The Journal of Chemical Physics*, 42(10), 3520-3525.

Cantor, C. R., and Schimmel, P. R. (1980). *Biophysical Chemistry Part I: The Conformation of Biological Macromolecules*, W. H. Freeman and Company, San Francisco.

Cummings, A. L., and Eyring, E. M. (1975). "Helix-Coil Transition Kinetics in Aqueous Poly(α,L-Glutamic Acid)." *Biopolymers*, 14, 2107-2114.

Dill, K. A., Bromberg, S., Yue, K., Fiebig, K. M., Yee, D. P., Thomas, P. D., and Chan, H. S. (1995). "Principles of Protein Folding - A Perspective from Simple Exact Models." *Protein Science*, 4, 561-602.

Eggers, F., and Funck, T. (1976). "Relaxation Spectra (10^(-9) s $\leq \tau \leq$ 10 s)and Conformation Dynamics of Polyamino Acids." *Studia Biophysica*, 57, 101-104.

Fairman, R., Shoemaker, K. R., York, E. J., Stewart, J. M., and Baldwin, R. L. (1989). "Further Studies of the Helix Dipole Model: Effects of a Free α-NH_3 or α-COO^- Group on Helix Stability." *Proteins: Structure, Function and Genetics*, 5, 1-7.

Gafni, A., Schlessinger, J., and Steinberg, I. Z. (1973). "Fluorescence and Optical Activity of Acridine Dyes Bound to Poly-A and DNA." *Israel Journal of Chemistry*, 11, 423-434.

Reproduced with permission of the copyright owner. Further reproduction prohibited without permission.

Gutman, M. (1984). "The pH Jump: Probing of Macromolecules and Solutions by a Laser-Induced, Ultrashort Proton Pulse - Theory and Applications in Biochemistry." *Methods of Biochemical Analysis*, 30, 1-103.

Gutman, M., Huppert, D., and Pines, E. (1981). "The pH Jump: A Rapid Modulation of pH of Aqueous Solutions by a Laser Pulse." *Journal of the American Chemical Society*, 103, 3709-3713.

Hatano, M., Yoneyama, M., and Sato, Y. (1973). "Interaction of Poly-α,L-glutamic Acid with Acridine Orange." *Biopolymers*, 12, 895-903.

Imae, T., and Ikeda, S. (1976). "Circular Dichroism and Structure of the Complex of Acridine Orange and Poly(L-glutamic Acid)." *Biopolymers*, 15, 1655-1667.

Inoue, S., Sano, T., Yakabe, Y., Ushio, H., and Yasunaga, T. (1979). "Kinetic Studies of the Helix-Coil Transition in Aqueous Solutions of Poly(L-Lysine)." *Biopolymers*, 18, 681-691.

Kamtekar, S., Schiffer, J. M., Xiong, H., Babik, J. M., and Hecht, M. H. (1993). "Protein Design by Binary Patterning of Polar and Nonpolar Amino Acids." *Science*, 262, 1680-1685.

Kosover, E. M., and Huppert, D. (1986). "Excited State Electron and Proton Transfers." *Annual Review of Physical Chemistry*, 37, 127-156.

Lamm, M. E., and Neville, D. M. (1965). "The Dimer Spectrum of Acridine Orange Hydrochloride." *The Journal of Physical Chemistry*, 69(11), 3872-3877.

Lumry, R., Legare, R., and Miller, W. G. (1964). "The Dynamics of the Helix-Coil Transition in Poly-α,L-Glutamic Acid." *Biopolymers*, 2, 489-500.

Marqusee, S., and Baldwin, R. L. (1987). "Helix Stabilization by Glu-..Lys+ Salt Bridges in Short Peptides of *de novo* design." *Proceedings of the National Academy of Sciences, USA*, 84, 8898-8902.

Marqusee, S., Robbins, V. H., and Baldwin, R. L. (1989). "Unusually Stable Helix Formation in Short Alanine-Based Peptides." *Proceedings of the National Academy of Sciences, USA*, 86, 5286-5290.

Myhr, B. C. (1968). "Studies on the Structure and Optical Behavior of the Acridine Orange Complex with Poly-α,L-glutamic Acid," Ph. D., Iowa State University, Ames, Iowa.

Pines, E., Huppert, D., Gutman, M., Nachliel, N., and Fishman, M. (1986). "The pOH Jump: Determination of Deprotonation Rates of Water by 6-Methoxyquinoline and Acridine." *Journal of Physical Chemistry*, 90, 6366-6370.

Sano, T., and Yasunaga, T. (1980). "Kinetics of Helix-Coil Transition of Polypeptides in Solution by Relaxation Methods." *Biophysical Chemistry*, 11, 377-386.

Reproduced with permission of the copyright owner. Further reproduction prohibited without permission.

Satoh, M., Komiyama, J., and Iijima, T. (1981). "Dependence on Ionic Strength of Charge-Induced Coil-Helix Transition of Sodium Poly(L-Glutamate) in Aqueous Solution." *Biophysical Chemistry*, 14, 347-355.

Satoh, M., Komiyama, J., and Iijima, T. (1982). "Salt Effects on the Helix-Coil Transition of Sodium Poly(L-glutamate) in Aqueous Solution." *Biopolymers*, 21, 1927-1931.

Small, E. W. (1996). "Pulsed-laser Photoacoustics Hears Molecular Vibrartions." *Laser Focus World*, 32(3), S27-S35.

Smith, K. K., Kaufmann, K. J., Huppert, D., and Gutman, M. (1979). "Picosecond Proton Ejection: An Ultrafast pH Jump." *Chemical Physics Letters*, 64(3), 522-527.

Stellwagen, E., Park, S.-H., Shalongo, W., and Jain, A. (1992). "The Contribution of Residue Ion Pairs to the Helical Stability of a Model Peptide." *Biopolymers*, 32, 1193-1200.

Stryer, L., and Blout, E. R. (1961). "Optical Rotatory Dispersion of Dyes Bound to Macromolecules. Cationic Dyes: Polyglutamic Acid Complexes." *Journal of the American Chemical Society*, 83, 1411-1418.

Tsuji, Y., Yasunaga, T., Sano, T., and Ushio, H. (1976). "Kinetic Studies of the Helix-Coil Transition in Aqueous Solutions of Poly(α-L-glutamic acid) Using the Electric Field Pulse Method." *Journal of the American Chemical Society*, 98, 813-818.

Voet, D., and Voet, J. G. (1990). *Biochemistry*, John Wiley & Sons, New York, New York.

Xiong, H., Buckwalter, B. L., Shieh, H.-M., and Hecht, M. H. (1995). "Periodicity of Polar and Nonpolar Amino Acids is the Major Determinant of Secondary Structure in Self-Assembling Oligomeric Peptides." *Proceedings of the National Academy of Sciences*, 92, 6349-6353.

Yamaoka, K., and Resnik, R. A. (1966). "The Extrinsic Cotton Effect of Acridine Orange Bound to Native DNA and Helical Poly-α,L-glutamic Acid." *The Journal of Physical Chemistry*, 70(12), 4051-4066.

Zanker, V. (1952). "Über den Nachweis definierter reversibler Assoziate ("reversible Polymerisate") des Acridinorange durch Absorptions- und Fluoreszenzmessungen in wässriger Lösung." *Z. Physik. Chem.*, 199, 225-258.

Reproduced with permission of the copyright owner. Further reproduction prohibited without permission.

CHAPTER VI

TEMPERATURE JUMPS

Introduction

Studies of early events in protein folding may be conducted using laser induced temperature jumps. Proteins denature at both high and low temperature and thus temperature jumps may be used to trigger both folding and unfolding. Also, in contrast to the pH jumps discussed in the last chapter, no extrinsic dyes need be used in order to induce a temperature jump, and there is no interference with observations of intrinsic protein absorption and fluorescence.

Laser induced temperature jumps take advantage of the fact that water absorbs strongly in the near infrared (IR) (Fig. 6.1). The transition of water from the excited state back to the ground state is nonradiative and the excitation energy is dissipated as heat into the solution. Water thermalization occurs on the subnanosecond time scale (Anfinrud et al. 1989; Genberg et al. 1987; Lian et al. 1994) enabling the observation of temperature jump induced phenomena with a resolution of nanoseconds or longer. As an alternative to near IR absorption, dyes such as crystal violet may be used as energy transducers (Phillips et al. 1995). These dyes have the advantage of absorbing in the visible rather than the infrared, but such dyes also have strong absorbances in the ultraviolet (UV) making them difficult to use in experiments employing UV-visible spectroscopy to monitor protein conformational changes.

The effects of temperature on protein conformation may be described as follows. Heat denaturation is an entropically driven process; increases in temperature lead to higher

Reproduced with permission of the copyright owner. Further reproduction prohibited without permission.

thermal energies and increases in protein flexibility. The flexibility enlarges the conformational space available to the protein and some of the newly accessible conformations destabilize the hydrogen bonds which are sensitive to geometry (Creighton 1993). Cold denaturation is an enthalpically driven process. Physically, cold denaturation corresponds to the solvation of nonpolar residues by water which is more ordered at low temperatures (Creighton 1993). This solvation compensates for the enthalpy contributions of van der Waals and hydrogen bonding in the folded protein (Privalov 1990).

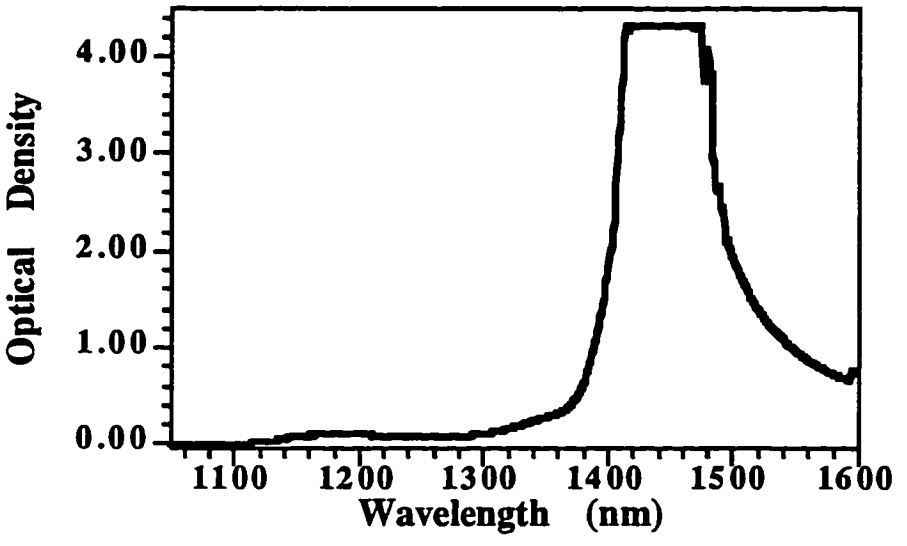

Figure 6.1. Absorption of water in the near infrared as recorded by a Cary 2400 spectrophotometer (Varian). Two millimeter path length.

Experimental studies of cold denaturation are complicated by the fact that most proteins cold denature appreciably only well below 0°C. One way to observe cold denaturation and to keep the protein solution from freezing is to use a water-oil emulsion so that the aqueous solution is dispersed and the freezing of one droplet does not lead to ice formation in the entire solution(Hatley and Franks 1989a). Alternatively, a cryosolvent such as methanol may be added to the protein solution in order to decrease the freezing point. In this case the cold denaturation temperature, T_g^c, will be dependent on the cryosolvent concentration(Hatley and Franks 1989b) since T_g^c is affected by interactions between the cryosolvent and the protein (Privalov et al. 1986). A third method is to subject

Reproduced with permission of the copyright owner. Further reproduction prohibited without permission.

the protein to mildly denaturing conditions, slightly acidic pHs and/or low concentration of urea or guanidinium hydrochloride, which decrease the enthalpy difference between the denatured and native state (Privalov 1992) and thus increase T_g^c. Even under such conditions T_g^c is often less than 0°C so that experiments must be conducted using dust free aqueous solutions which may be cooled to -15°C without freezing (Privalov et al. 1986).

Selection of proteins is critical for temperature jump experiments. For the experiments discussed here, there must be a relatively large change in an optical signal such as absorption or fluorescence over the range of the temperature jump. In practice, this criterion means that the narrower the temperature region over which the protein folds or unfolds, the more suited it is for temperature jump experiments. Given a narrow temperature range for protein denaturation, a protein can be jumped from one side of the transition to the other yielding the largest possible signal.

Selection of proteins for cold denaturation experiments is further complicated by the lack of relevant data for most proteins. Also, much of the available cold denaturation data relates to oligomeric proteins where this denaturation often corresponds to dissociation rather than to loss of tertiary and secondary structure (Privalov 1990).

For heat denaturation experiments, proteins should preferably not aggregate upon unfolding. Although, given the short time scale and low protein concentrations used in laser temperature jump experiments, protein-protein interactions may not be a problem even for proteins prone to aggregation.

Cold and Heat Denaturation

Protein unfolding is often considered a 2 state transition from a native, compact, state, N, to a denatured, noncompact state or set of states, D. If this transition is in fact thermodynamically 2 state then, the change in enthalpy upon cooperative protein folding or unfolding, $\Delta_N^D H$, will be the same whether determined by calorimetry or by the van't Hoff equation (Privalov 1992). Calorimetrically, $\Delta_N^D H^{cal}$ can be determined by integrating the

Reproduced with permission of the copyright owner. Further reproduction prohibited without permission.

area under the heat capacity peak across the thermal transition. The van't Hoff change in enthalpy may be calculated from any observable parameter, Y, which changes upon denaturation (Privalov 1992):

$$K = \frac{Y_X - Y_N}{Y_D - Y_N} \tag{6.1}$$

$$\frac{\partial \ln K}{\partial\left(\frac{1}{T}\right)} = \frac{-\Delta H_N^{D\,van't\,Hoff}}{R} \tag{6.2}$$

where K is the equilibrium constant, Y_X is the value of the observable at any arbitrary temperature T and R is the gas constant. $\Delta H_N^{D\,van't\,Hoff}$ should be calculated at the midpoint of the thermal denaturation in order to make the comparison to $\Delta_N^D H^{cal}$.

For small (≤20 kDa), compact globular proteins the ratio $\frac{\Delta H_N^{D\,van't\,Hoff}}{\Delta H_N^{D\,cal}}$ is within 5% of unity (Privalov 1992) and the thermal transition may be considered thermodynamically 2 state. Assuming that $\Delta_N^D C_p$, the change in heat capacity between the denatured and native states, is independent of temperature, the change in Gibbs free energy, $\Delta_N^D G$, of such a two state transition may be described by the equation (Privalov et al. 1986):

$$\begin{aligned}\Delta_N^D G &= G_D - G_N = \Delta_N^D H - T\Delta_N^D S \\ &= \Delta_N^D H_g + \Delta_N^D C_p (T - T_g) - T\Delta_N^D S_g - \Delta_N^D C_p \left(T \ln\left[\frac{T}{T_g}\right]\right) \\ &= \Delta_N^D H_g \left(\frac{T_g - T}{T_g}\right) + \Delta_N^D C_p (T - T_g) - \Delta_N^D C_p \left(T \ln\left[\frac{T}{T_g}\right]\right)\end{aligned} \tag{6.3}$$

All temperatures are in Kelvin. The subscript g refers the temperature, T_g, at which $\Delta_N^D G = 0$. $\Delta_N^D H_g$ and $\Delta_N^D S_g$ are the change in enthalpy and entropy at T_g respectively, and $\Delta_N^D H_g = T_g \Delta_N^D S_g$. Equation 6.3 equals zero at T_g, the melting temperature of the protein and at a second, lower temperature T_g^c which corresponds to cold denaturation. When $\Delta_N^D G$ is maximized, the native protein is maximally stable.

According to equation 6.3, the only term which can contribute to the cold denaturation is $\Delta_N^D C_p (T - T_g)$ since all the other terms stabilize the native conformation ($\Delta_N^D H_g = T_g \Delta_N^D S_g > 0$ and $T_g^c < T_g$). This destabilizing term comes from the expression for

Reproduced with permission of the copyright owner. Further reproduction prohibited without permission.

enthalpy making cold denaturation an enthalpically driven process. To a first approximation T_g^c may be expressed as (Privalov et al. 1986)

$$T_g^c = \frac{T_g^2}{\left(\frac{2\Delta_N^D H_g}{\Delta_N^D C_p} + T_g\right)} \qquad (6.4)$$

(for a higher order approximation see Agashe & Udgaonkar (1995)). T_g^c is well below 0°C for most proteins .

In order for T_g^c to be experimentally accessible, $\Delta_N^D H_g$ must be small and $\Delta_N^D C_p$ must be large. As mentioned above, $\Delta_N^D H_g$ may be lowered by denaturants. However, even low denaturant concentrations may change the rates of protein folding/unfolding. Additionally, the kinetics of processes such as denaturant dissociation might be rate limiting and the kinetic data would not then be a measure of the kinetics of protein conformational changes.

To study protein folding in as mild conditions as possible an effort should be made to pick proteins which have a small value of $\frac{\Delta_N^D H_g}{\Delta_N^D C_p}$ (Privalov et al. 1986). Myoglobin is one such protein (Privalov et al. 1986) and it has been shown to cold denature under acidic conditions in both its holo and apo forms (Griko and Privalov 1994; Griko et al. 1988; Nishii et al. 1994; Privalov et al. 1986). Another protein which has an unusually high value of $\Delta_N^D C_p$ and an unusually low value of $\Delta_N^D H_g$ is barstar which cold denatures at accessible temperatures in solutions containing guanidine hydrochloride (Agashe and Udgaonkar 1995).

In the case of proteins for which no cold denaturation studies have as yet been conducted, values of $\Delta_N^D H_g$ may be calculated using van't Hoff equations. Values of $\Delta_N^D H$ do not depend on the pH of the protein solution although the melting temperature does (Privalov 1979). Therefore, the thermal denaturation of a protein at various pHs will yield a plot of $\Delta_N^D H$ vs. T the slope of which is $\Delta_N^D C_p$ (Privalov 1979) (see equation 6.3). Thermal denaturation is relatively easy to measure and thus such data is available for a wide

Reproduced with permission of the copyright owner. Further reproduction prohibited without permission.

variety of proteins. Mutant proteins with melting temperatures that are lower than the wild type protein may be of especial interest since such destabilized mutants may have higher cold denaturation temperatures than the wild type. Those proteins which possess small values of $\frac{\Delta_N^D H_g}{\Delta_N^D C_p}$ and which can be described by a two state folding transition may then be investigated to see if they are suitable for studies of early events in folding following cold denaturation.

Myoglobin & Apomyoglobin

Sperm whale myoglobin (Mb) was the first protein whose crystal structure was determined (Kendrew et al. 1958; Kendrew et al. 1960) and is thus one of the best studied proteins . Horse heart Mb has also been crystallized and a high resolution structure is available for this protein (Evans and Brayer 1990). The experiments described below were performed on horse skeletal muscle Mb which has an identical sequence to horse heart Mb as well as to zebra skeletal muscle Mb (Darbre et al. 1975; Romero-Herrera and Lehmann 1974). Horse Mb is 88 percent homologous to sperm whale Mb and has the same overall structure (Evans and Brayer 1990).

Horse Mb is made up of 153 amino acids comprising 8 α helices, labeled A through H, and no β strands (Fig. 6.2). Mb contains no disulfide bonds. The heme is liganded to histidine residues on helices E and F (Takano 1977).

Mb both heat and cold denatures (Cho and Chan 1984; Privalov et al. 1986) , but it is prone to aggregation following heat denaturation. The heme in myoglobin quenches the fluorescence of the myoglobin aromatic residues (Weber and Teale 1959) leading to the appearance of fluorescence only as the molecule unfolds. Additionally, the near UV absorption of Mb changes very little upon denaturation. These complications make it difficult to study the folding and unfolding of Mb with UV or visible optical techniques.

Reproduced with permission of the copyright owner. Further reproduction prohibited without permission.

Apomyoglobin (apoMb), myoglobin without the heme group, is also extremely well studied. The NMR structure of sperm whale apoMb at pH 6.1 was recently published (Eliezer and Wright 1996). Helices A, B, C, D and E are entirely intact. The EF loop, F helix, FG loop and first few residues of the G helix display fluctuating conformations which cannot be resolved by NMR; however they do not display the NMR signal of a random coil. The remainder of the G helix and the first half of the H helix are intact while the C terminal end of the H helix is frayed. Calorimetry studies demonstrate that near neutral pH, apoMb undergoes cooperative transitions upon heat and cold denaturation (Griko et al. 1988).

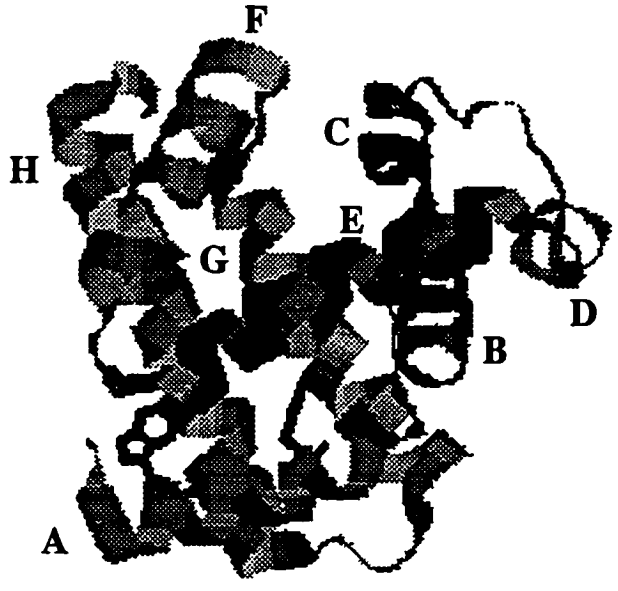

Figure 6.2. Horse heart myoglobin structure, heme not shown, with Trp residues in black (Protein Databank 1myb). The kinetic folding scheme of Jennings & Wright (1993) for sperm whale myoglobin is also shown.

Reproduced with permission of the copyright owner. Further reproduction prohibited without permission.

The two tryptophan (Trp) residues are located in helix A and the two tyrosine (Tyr) residues are in helices G and H in horse apoMb. Since apoMb lacks the heme it shows fluorescence in the native state, and this fluorescence shifts as the protein unfolds (Fig. 6.5 & Fig. 6.6). Analogously to holoMb there is no significant change in absorption upon unfolding.

The folding pathway of apoMb has been extensively studied. In both equilibrium and kinetic experiments using hydrogen exchange methods, folding intermediates of apoMb have been detected (Barrick and Baldwin 1993; Hughson et al. 1990; Jennings and Wright 1993; Loh et al. 1995) (Fig. 6.2). The conformation of apoMb can be changed by modifying the pH and/or salt concentration of the solution. At low salt concentrations (<0.1 ionic strength) apoMb is in the native state above pH 5, between pH 5 and pH 3 apoMb is in the intermediate state (A state) which appears to consist of helices A, G and H (Hughson et al. 1990) while below pH 3 the protein is acid denatured (Goto and Fink 1990). At higher salt concentrations, the protein never makes the transition from the intermediate to the acid denatured state (Goto and Fink 1990). The equilibrium A state found in moderately acidic conditions is also the first intermediate in the kinetic folding pathway (Fig. 6.2) (Jennings and Wright 1993).

Ribonuclease T_1

Aspergillus oryzae Ribonuclease T_1 (RNase T1) is a 104 amino acids protein consisting of a 2 stranded antiparallel β sheet, an α helix and a 5 stranded antiparallel β sheet (Protein Databank entry 2rnt) (Fig. 6.3). RNase T1 has one Trp residue in the 5 stranded β sheet and eleven Tyr residues (Takahashi et al. 1970). It also has two disulfide bonds, two *trans* and two *cis* prolines (Pro) (Protein Databank structure 2rnt).

RNase T1 was chosen for thermal unfolding experiments because it unfolds over a temperature range of approximately 10° C, a range which is easily accessible using a temperature jump, and it has a large signal change for both near UV absorption and

Reproduced with permission of the copyright owner. Further reproduction prohibited without permission.

fluorescence (Thomson et al. 1989). The thermal unfolding of RNase T1 is a reversible process if the time spent in the denatured state is minimized (Oobtake et al. 1979; Plaza del Pino et al. 1992; Thomson et al. 1989). It is unclear why the heat denaturation is partially irreversible on long time scales. The denaturation is not conducted under reducing conditions and all the cystine residues are disulfide bonded so that shuffling of disulfide bonds is unlikely. Proline isomerization is unlikely to be responsible since even after twenty four hours at temperatures well below the melting temperature no additional recovery is seen (data not shown). As judged by eye, the turbidity of the heat denatured solutions does not increase nor are precipitates seen (as in the case of heat denaturation of apomyoglobin) making it unlikely that large scale aggregates are responsible for the irreversibility.

Figure 6.3. Crystal structure of *Aspergillus oryzae* Ribonuclease T_1 (Protein Databank 2rnt). Trp residue is shown in red and the Tyr residues in blue. The folding scheme is two state.

There are no reports of cold denaturation of RNase T1 or its mutants although several of the mutants have reduced stabilities (Fabian et al. 1994; Garrett et al. 1996; Mayr et al. 1993; Pace et al. 1988; Shirley et al. 1992). The reduced form of RNase T1, which

Reproduced with permission of the copyright owner. Further reproduction prohibited without permission.

is still active in molar salt concentrations, also has reduced stability (Pace et al. 1988). The refolding of RNase T1 is complicated by the presence of the two *cis* Pro residues. Refolding of RNase T1 is characterized by three components, one fast (milliseconds), one intermediate (tens of seconds) and one very slow (hundreds of seconds) (Kiefhaber et al. 1990b). The intermediate and slow steps correspond to proline isomerization (Kiefhaber et al. 1990a; Kiefhaber et al. 1990b). Depending on the amount of time spent in the cold denatured state, proline isomerization would be less of a problem in cold denaturation experiments than in other types of denaturation experiments since the rate of *cis-trans* isomerization is temperature dependent.

Materials & Methods

The pH indicator methylthymol blue (MTB) was purchased from Sigma Chemical Co. All other chemicals were obtained from Sigma Chemical Co.

Temperatures for fluorescence and absorption experiments, both equilibrium and kinetic, were regulated using a circulating water bath. Temperatures were monitored by a K type thermocouple immersed in the protein solution. In some cases, to avoid interference in data collection, the temperature of the sample was recorded following data acquisition. The uncertainties in the temperatures are ±1° C.

Steady state fluorescence spectra were recorded by the SPEX fluorimeter described in chapter 5. Circular dichroism (CD) experiments were performed on a temperature controlled Aviv CD spectrophotometer model 62DS.

RNase T1 was purchased from Sigma Chemical. Steady state absorption measurements were conducted with path lengths of 4 mm and 1 mm and protein concentrations of 10 and 75 μM. RNase T1 steady state fluorescence measurements were conducted with 4 mm path lengths and protein concentrations of 5 μM.

Reproduced with permission of the copyright owner. Further reproduction prohibited without permission.

Preparation of ApoMb

Horse skeletal muscle Mb was purchased from Sigma Chemical Co. ApoMb was prepared using the acid-acetone method (Ascoli et al. 1981; Fanelli et al. 1958). Mb was dissolved in water at a concentration of 10 mg/ml using sonication. The sample was filtered through a 0.2 μm syringe filter (Gelman Sciences) to remove any undissolved protein and dialyzed for 48 hours at 4° C against water to remove any residual salts.

The acid-acetone mixture (5 ml of 1 M HCl per liter of acetone) was cooled to at least -15°C by immersion in either a water bath or an ice-salt bath. 1 ml of Mb was added dropwise to 30 ml of the acid-acetone mixture while stirring. This solution was allowed to sit for 10 minutes at -15 to -20° C and was then centrifuged at 5,000 rpm and -20° C for 12 minutes . Suction was used to remove the supernatant which was red colored due to the presence of free heme. The pellet was resuspended in water and examined by eye to see if it looked red. If a reddish tint was still visible, the acid-acetone procedure (excluding the dialysis step) was repeated; otherwise, the resulting apoMb was dialyzed against one liter of 134 mg/l sodium bicarbonate for 24 hours. During this dialysis step, some of the protein precipitated and the precipitate was removed by filtering the sample through a 0.2 μm syringe filter. The apoMb was then dialyzed for 24 hours against 10 mM sodium acetate pH 6.0.

The concentration of apoMb was determined from the optical density at 280 nm (OD_{280}) as measured on a Shimadzu UV-260 UV-visible spectrophotometer using a molar extinction coefficient at 280 nm of 15,900 M^{-1} cm^{-1} (Sanctis et al. 1994). The optical density at 405 nm (OD_{405}) was also recorded since OD_{405}/OD_{280} is approximately equal to 0.1 for one percent residual heme (Ascoli et al. 1981). All of the apoMb samples had less than one percent residual heme.

With the exception of pH 2, all buffers for apoMb were 10 mM sodium acetate at different pHs. In an experiment comparing various buffers Privalov, et al (1986) showed that the denaturation enthalpy of holoMb was minimized in sodium acetate buffer. 10 mM

Reproduced with permission of the copyright owner. Further reproduction prohibited without permission.

hydrochloric acid was used for pH 2 solutions. For cold denaturation experiments, buffers were filtered through 0.22 μm Sterivex filters (Millipore) for at least 30 minutes and apoMb samples were further filtered through 0.2 μm Acrodisc (Gelman Sciences) syringe filters. (In future experiments it might be more efficient to filter apoMb using Centricons (Amicon), which have smaller pore sizes.) ApoMb concentrations, measured following filtrations, of 0.5 to 3 μM (OD_{280} from 0.01 to 0.04) were used for all experiments. One centimeter path lengths were used for both steady state fluorescence and steady state far UV CD experiments.

Temperature Jump Instrumentation

A laser temperature jump experiment is a pump-probe experiment (Fig. 6.4). The pump beam was the near IR beam used to change the temperature of the solution, and, for this experimental apparatus, the probe beam was a near UV beam used for both absorption and fluorescence experiments. The experimental apparatus was constructed as described below (Fig. 6.4).

In order to generate a near IR pulse, the 1064 nm fundamental of a Continuum Surelite Nd-YAG laser with a 5 to 7 nsec pulse width, pulse energy of 2.4 mJ and Gaussian pulse shape was Raman shifted. Originally, the 1064 nm pulses were Raman shifted to 1540 nm through 0.6 m of methane at 400 psi, but this led to problems with Brilliouin scattering and severe damage to the optics. Therefore, the 1064 nm pulses were Raman shifted through deuterium (D_2) at 1150 psi. The first Stokes shift for 1064 nm through D_2 occurs at 1560 nm; Raman shifting generates higher order Stokes shifts as well as anti-Stokes shifts (the Raman shift for D_2 is 2987 cm^{-1}). These other Raman shifted beams were filtered out as was the residual 1064 nm beam.

Much of the 1560 nm beam was backscattered from the Raman shifter. In order to increase Raman shifting efficiency, this backscattered beam was reflected back through the Raman shifter using a zero degree dichroic mirror placed before the Raman shifter which

Reproduced with permission of the copyright owner. Further reproduction prohibited without permission.

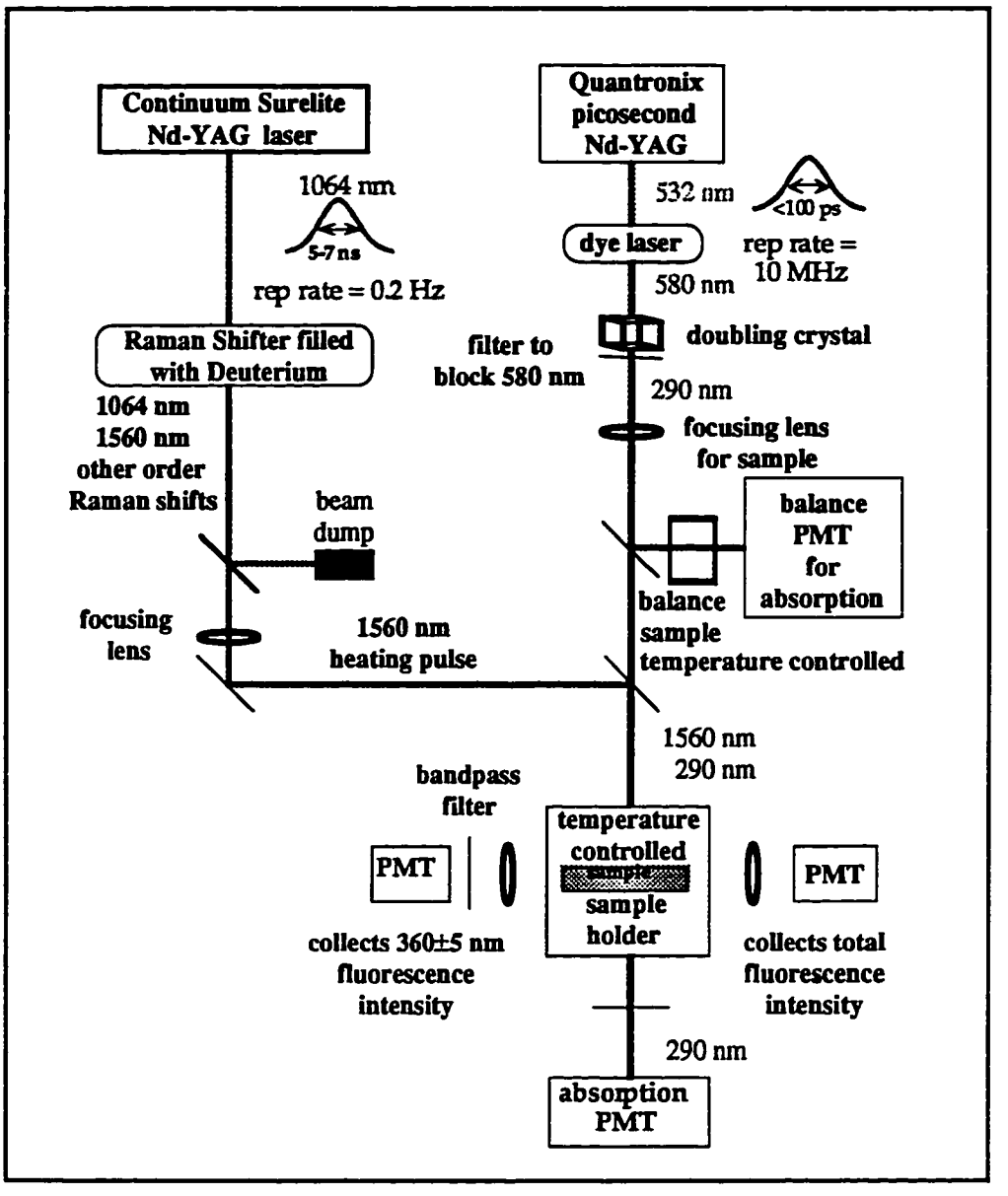

Figure 6.4. Block diagram of the temperature jump apparatus.

transmitted 1064 nm and reflected 1560 nm light. The use of the zero degree dichroic necessitated that the Raman shifter be placed far from the Nd-YAG laser to avoid retroreflection of the 1064 nm beam into the laser cavity resulting in damage. To compensate for beam divergence between the laser and the Raman shifter, a Gallilean telescope was used to reduce the beam size before the 1064 nm beam was focused into the Raman shifter. A 500 mm focal length lens was used to focus the 1064 nm beam in the

Reproduced with permission of the copyright owner. Further reproduction prohibited without permission.

center of the Raman shifter; after the Raman shifter, the 1560 nm beam was recollimated using a 500 mm lens located 1 meter from the first focusing lens.

Raman shifting heated up the D_2 in the Raman shifter which decreased the Raman shifting efficiency and skewed the 1560 nm beam profile. The maximum repetition rate from the Continuum Nd-YAG laser is 10 Hz, but the heating of the Raman cell necessitated the use of a repetition rate of 0.5 Hz or less. To further alleviate this problem 400 psi of helium gas was added to the Raman cell to help dissipate the heat; this addition noticeably improved the 1560 nm beam profile. The Raman cell emitted 40 mJ of 1560 nm near IR light when pumped with 240 mJ 1064 nm pulses.

The 290 nm probe beam was generated by a Quantronix picosecond Nd-YAG laser running at 76 MHz with a pulse width of approximately 100 picoseconds. The 532 nm second harmonic of the Nd-YAG was used to pump a cavity dumped dye laser (Coherent 700 dye laser) containing rhodamine dye which shifted the 532 nm beam to 580 nm at 38 MHz or less. This 580 nm beam was then sent through a doubling crystal to generate 290 nm.

The 1560 nm pump and 290 nm probe were combined by a dichroic mirror which reflected 1560 nm and transmitted 290 nm. Prior to combining the beams were sent through 500 mm focal length lenses so that they focused within centimeters of the sample. The samples used had path lengths of 1 millimeter so that they were heated relatively uniformly. Spot sizes in the sample were calculated to be approximately 0.4 mm (see appendix C).

Numerical calculations of thermal and spatial diffusion from an infinite cylinder (Carslaw and Jaeger 1959; Crank 1956) were used to approximate the maximum time that the temperature and protein population would be constant in the temperature jumped region. For a spot size of 0.4 mm, ignoring thermal diffusion through the ends of the cylinder, a temperature jump of 12° C took 100 msec to drop by 1° C. Spatial diffusion is much slower since proteins are relatively large. Based on the diffusion coefficient of myoglobin,

Reproduced with permission of the copyright owner. Further reproduction prohibited without permission.

9.4×10^{-7} cm^2/sec at 25° C (Riveros-Moreno and Wittenberg 1972), even one second after heating there is no significant spatial diffusion. Of course, the spatial diffusion will be faster at higher temperatures, but not as fast as the thermal diffusion.

Both absorption and fluorescence were detected using two side-on photomultiplier tubes (PMT) (Hamamatsu R950). For absorption measurements, the UV was split 50-50 prior to combination with the near IR probe. The first, balance, beam was detected by a PMT and this signal was used to correct for any intensity changes due to laser fluctuations in the second, sample beam. The two fluorescence PMTs were needed to correct for changes in fluorescence due solely to temperature. As the temperature is decreased, the fluorescence intensity increases independent of changes in protein conformation.

The magnitude of the temperature jump due to the 1560 nm heating pulse was determined using the method of Bremer, et al (1993). The pK_a of Tris buffer decreases 0.031 per degree C (Calbiochem 1975) thus the pH of a Tris solution decreases with temperature (see Appendix C). This change in pH with temperature may be monitored by observing the absorption at 633 nm of the pH indicator MTB if the solution pH is between 6.5 and 8.5. For this experiment, the beam from a Helium-Neon laser (Laboratory for Science) was overlapped with the 1560 nm heating pulse and the transmission of the 632.8 nm beam through the sample was monitored using a silicon photodiode (Thor Labs). The signal from the photodiode was amplified and then recorded by an Analogic Data 6000 Universal Waveform Analyzer (D6000) or a 200 MHz digital oscilloscope (Gould).

Results

To investigate the cold denaturation of apoMb, the steady state fluorescence spectrum (Fig. 6.5) and far UV CD spectrum of apoMb were recorded for pH 2, 3.7, 4.0, 4.7 and 6.0 between 29°C and -8°C. The spectra for pH 6 showed no change with temperature. ApoMb at pH 4.7 showed a significant change in far UV CD with

Reproduced with permission of the copyright owner. Further reproduction prohibited without permission.

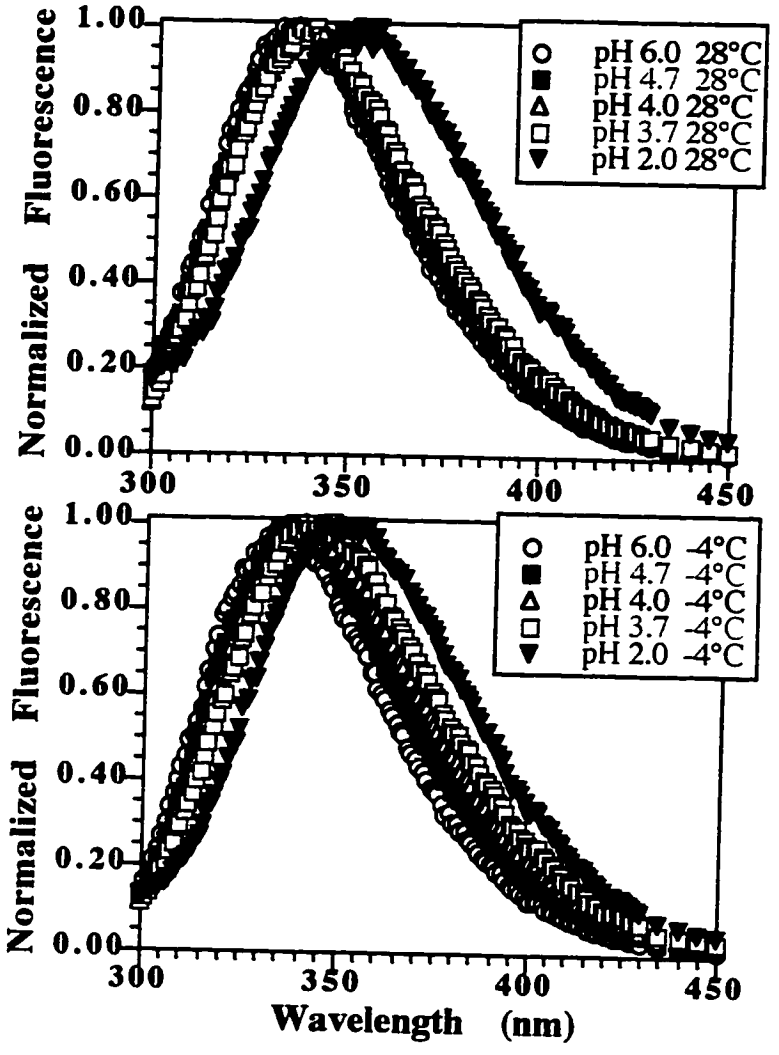

Figure 6.5. Normalized, corrected fluorescence spectra of horse skeletal muscle apomyoglobin. Protein concentrations were 1 to 3 μM.

Reproduced with permission of the copyright owner. Further reproduction prohibited without permission.

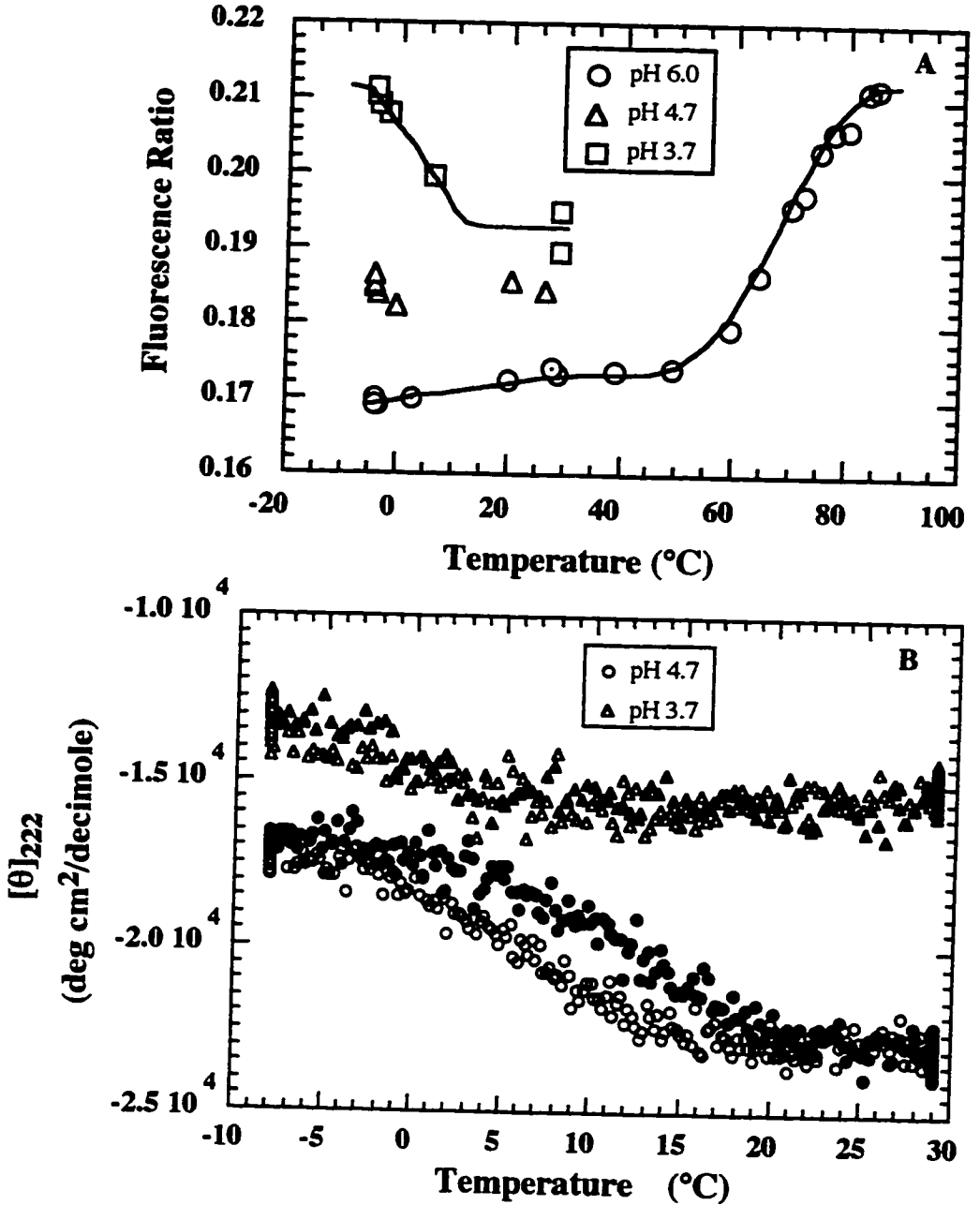

Figure 6.6. Changes in fluorescence (A) and circular dichroism (B) due to cold and heat denaturation of 1 to 3 μM horse apomyoglobin in 10 mM sodium acetate. (A) Fluorescence ratio, fluorescence from 355 to 365 nm divided by the total fluorescence, versus temperature. pH 6 data are the results from two experiments, one heat denaturation and one cold denaturation. Lines are just to guide the eye. (B) CD signal at 222 nm for cold denaturation. Open symbols are data collected when ramping the temperature down and filled symbols were collected when raising the temperature.

Reproduced with permission of the copyright owner. Further reproduction prohibited without permission.

temperature but an almost negligible change in fluorescence with temperature while the pH 4.0 and pH 3.7 samples displayed fluorescence changes with temperature and much smaller changes in far UV CD (Fig. 6.6). All changes in spectra were reversible upon raising the temperature although it should be noted that far UV CD data in which the temperature was ramped down and then up displayed hysteresis, indicating that the conformational changes were faster as the protein was heated than when it was cooled (Fig. 6.6B).

The values of the molar ellipticity, [θ], displayed in figure 6.6 are at least twice as high as the published values for horse or sperm whale apoMb (Ballew et al. 1996; Griko and Privalov 1994; Nishii et al. 1995). The calibration of the ellipticity, θ, from the CD machine was checked using +-10-camphor sulfonic acid and no correction was necessary. The only other quantities in the calculation of [θ] are the path length which is known and the protein concentration (see ch. I). The apomyoglobin samples were filtered prior to far UV CD experiments in order to allow the samples to be cooled below zero. This filtering resulted in optical densities at 280 nm between 0.035 and 0.015 (between 93 and 97 percent transmission) and is possible that the signal to noise of the spectrophotometer is low in this range. Thus, the uncertainty in the concentrations calculated from the absorbances is large although measurements of the protein concentration by other methods, Bradford assay and BCA assay, yielded concentrations that were only ten percent smaller. Fortunately, the uncertainty in the value of [θ] does not affect the shape of the curve in figure 6.6, it only represents an offset of the data.

The fluorescence change of apoMb upon heat denaturation was also investigated using apoMb in 10 mM sodium acetate at pH 6 (Fig. 6.6). Experiments were not conducted at lower pHs since apoMb is more likely to aggregate at lower pHs. Even at pH 6, apoMb precipitated following heat denaturation.

The steady state UV absorption of RNase T1 upon raising the temperature from 24° C to 65° C was investigated (Fig. 6.7). In 10 mM sodium acetate pH 6 RNase T1 heat

Reproduced with permission of the copyright owner. Further reproduction prohibited without permission.

denatured between 40°C and 50°C with a 2.5 percent change in transmission. The absorption did not fully recover upon cooling, presumably due to the large amount of time (20 minutes or more) spent in the heat denatured state and the low salt concentration since RNase T1 is stabilized by interactions with anions and cations (Pace and Grimsley 1988).

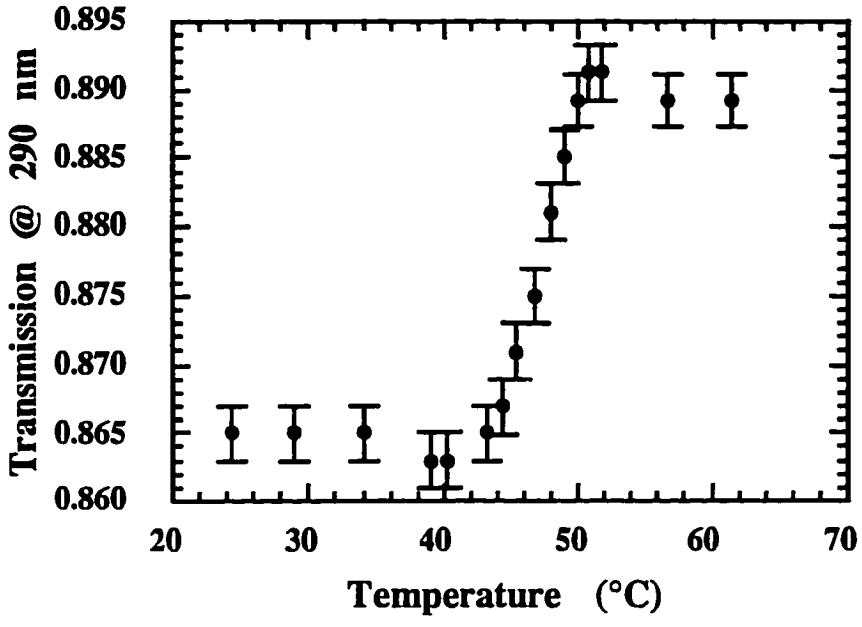

Figure 6.7. The data shown are the transmission at 290 nm of 54 μM ribonuclease T1 in 10 mM sodium acetate pH 6.0 with a path length of 1 mm. The change in transmission is due to the heat denaturation of ribonuclease T1.

The magnitude of the temperature jump was measured using MTB. Even in the absence of MTB, a signal was seen due to the movement of the 633 nm beam on the photodiode caused by thermal lensing. This thermal lensing signal was subtracted from the MTB data in order to determine the magnitude of the temperature jump. The experiment was originally conducted using electronics with a resolution of microseconds (Fig. 6.8, inset) and was later repeated following changes to the Raman shifting setup and the electronics (Fig. 6.8). For 0.5 mM MTB in 25 mM Tris pH 7.3 (pH at room temperature) a temperature jump of at least 20° C in a path length of 0.1 cm was measured (Fig 6.8, inset).

Reproduced with permission of the copyright owner. Further reproduction prohibited without permission.

For preliminary temperature jump experiments involving proteins, attempts were made to exactly balance the signals from the two absorbance PMTs in the absence of a heating pulse. The signals from the PMTs were pulses with widths of nanoseconds. In order to integrate these pulses, the outputs from the PMTs were sent into RC circuits with time constants of microseconds and then these signals, which were constant rather than pulsed, were recorded by an oscilloscope. The offset on the oscilloscope was used to help balance the signals. The signal from one of the PMTs was inverted and the difference between the two signals was displayed. This was the least complicated method of collecting temperature jump data, but it was, unfortunately, not successful. Thus, more sophisticated electronics were necessary and the design of these electronics is discussed in the next section.

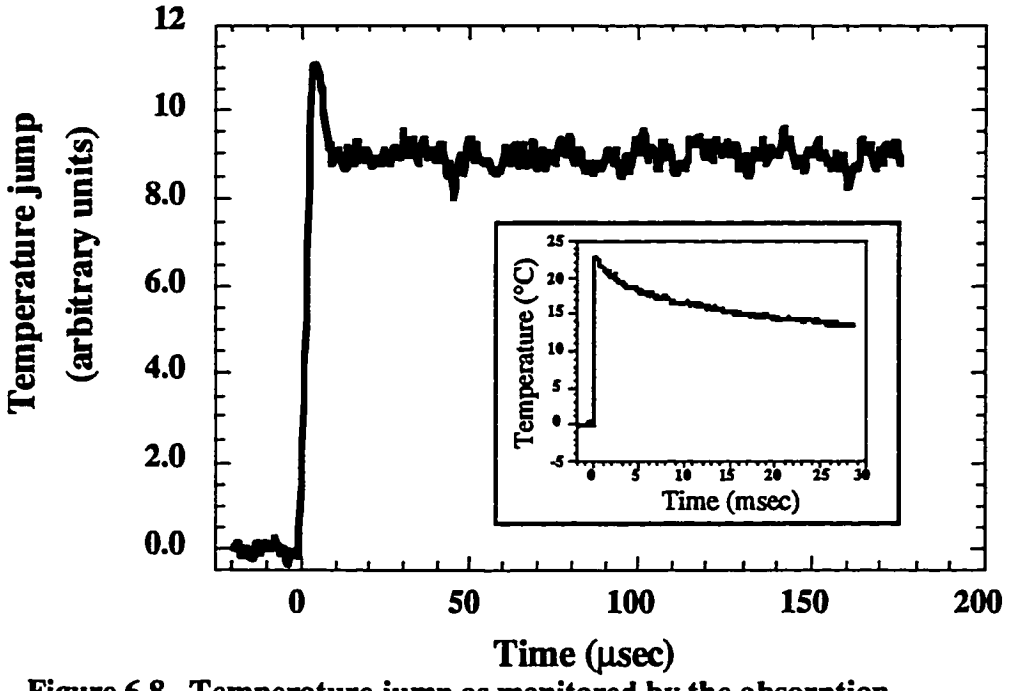

Figure 6.8. Temperature jump as monitored by the absorption at 632.8 nm of the pH indicator methylthymol blue.

Reproduced with permission of the copyright owner. Further reproduction prohibited without permission.

Discussion, Improvements & Conclusions

The discrepancy between the unfolding pattern reported by steady state far UV CD and fluorescence data for apoMb at pHs 4.7, 4.0 and 3.7 is a reflection of the loss or softening of different parts of the apoMb structure under different conditions. Far UV CD measures global structure and cold denaturation leads to a general loss of helicity. However, the fluorescence excited at 290 nm measures the local environment of the Trp residues which for horse apoMb are both in the A helix, a relatively stable helix since it is part of the A state folding intermediate,

At pH 4.7, apoMb is in the transition region between the native state and the A state (Goto and Fink 1990) so that cold denaturation leads to a structure which is more like that of the A state. Thus, a larger change is seen in the far UV CD than in fluorescence as helical structure is lost in helices other than A. At pHs 3.7 and 4.0, apoMb is in the transition region between the A state and the denatured state. Upon cooling, there is little loss of secondary structure indicating that the A, G, H α helices which form the A state (Fig. 6.2) are still relatively intact. The shift in fluorescence, however, indicates that although the overall structure may still be intact at sub-zero temperatures, the local environment of the Trp residues is perturbed. Note that cooling, at least at the temperatures used, does not result in as much loss of secondary structure as do other perturbations such as acid or heat.

The temperature jump induced by our laser pulse, as measured using MTB in Tris, is more than adequate for protein folding/unfolding experiments, and the temperature is stable over microseconds. However, the overlap of the 633 nm beam with the 1560 nm beam may be different than the overlap of the 290 nm beam with the 1560 nm beam since exact alignment of two laser beams is quite difficult. Thus, the temperature region measured in an MTB experiment might be slightly different than that probed in an actual protein experiment. To eliminate this discrepancy it is necessary to use the 290 nm beam itself to measure the temperature change. One approach to this problem (Thompson 1996)

Reproduced with permission of the copyright owner. Further reproduction prohibited without permission.

is to use the fluorescence intensity of free Trp or N-acetyltryptophanamide (NATA), which changes with temperature, as a temperature probe. This temperature measurement technique will be used in future experiments.

The electronics for recording protein fluorescence and absorption are currently being perfected and will serve to provide kinetic data for apoMb or RNase T1. The collection of such data is complicated by the pulsed nature of the UV probe beam, the pulse-to-pulse as well as limited long term stability of the probe beam and the timing between the temperature jump and probe beams. The solutions to all of these data collection problems are being pursued by Dr. Joseph Schauerte and Chris Fischer.

The new, improved data acquisition system consists of the following elements. In order to maximize the information derived from the data, the signals from the PMTs are sent into a dual sum and invert which inverts one of the signals and then adds the two signals for each UV laser pulse. This summed signal is then read by a 1.25 MHz data acquisition card (National Instruments). This method is easier than integrating each pulse digitially and then dividing or subtracting off the balance as was previously attempted.

The timing between the pulse and probe beam is complicated because the picosecond laser used to generate the UV is running at 76 MHz on its own internal clock. The laser used to generate the temperature jump is running on its internal clock and Q-switching at 10 Hz (for a discussion of Q-switching see Siegman (1986)). The picosecond laser could be used as an external trigger for the other Nd-YAG, but this would not synchronize the two lasers because the 10 Hz laser would not emit a pulse immediately after reading the external trigger, it would just emit the next pulse in its 10 Hz train inducing a delay between the pump and the probe which would vary from probe pulse to probe pulse making it difficult to average or sum different experiments. To solve this problem, the temperature jump pulse triggers an external clock which is connected to the data collection card so that the computer records the time between the temperature jump pulse and UV probe pulses.

Reproduced with permission of the copyright owner. Further reproduction prohibited without permission.

One possible problem which remains to be solved, revolves around thermal lensing. Heating of the sample leads to a gradient in the index of refraction of the solution and this results in movement of the probe beam across the PMT's photocathode. Since, the photocathodes of side-on PMTs are not spatially uniform, changes in beam position result in signal alterations. These spurious changes must be subtracted off any protein data. It would be advantageous to replace the side-on PMTs used for absorption measurements with head-on PMTs which have spatially uniform photocathodes.

A temperature jump experiment involving the fluorescence of cold denatured horse apoMb has been conducted by a Ballew, et al (1996). Their experimental apparatus consisted of a 1540 nm heating pulse and a 280 nm probe beam from a tripled titanium:sapphire laser. For apoMb in 10 mM sodium acetate at pH 5.9 they report a kinetic phase with a lifetime of 7 ± 5 μsec, and for apoMb at pH 5.2 a kinetic phase of 5 ± 1 μsec was reported. They also report steady-state far UV CD data showing cold denaturation below 0° C at pH 5.9 and correlate this to far UV CD data from Nishii and coworkers (1995) which was collected at pH 5.5 and also showed cold denaturation.

The data at pH 5.9 contradicts our steady state finding of little or no fluorescence shift upon cooling apoMb below 0° C in 10 mM sodium acetate pH 6.0. Both Ballew, et al (1996) and Nishii, et al (1995) used the 2-butanone (Ascoli et al. 1981) procedure for heme abstraction rather than the acid-acetone procedure. Both techniques are accepted, well used methods for heme extraction so it seems unlikely that this is the source of the discrepancy especially since the apoMb prepared by the acid-acetone method and used in our experiments was capable of reincorporating heme indicating that the protein structure was relatively intact (data not shown).

At least for the laser temperature jump experiments, Ballew, et al (1996) used apoMb concentrations of hundreds of micromolar. These concentrations are significantly higher than those used in the experiments described here. Considering only our steady state fluorescence data (Fig. 6.5), the discrepancy in cold denaturation behavior could be

Reproduced with permission of the copyright owner. Further reproduction prohibited without permission.

caused by a lower signal to noise ratio at low concentrations. It is difficult at 28° C to see a difference in fluorescence between pH 6.0 and pH 4.0 (Fig. 6.5) despite the difference in structure at the two pHs and it is expected that any fluorescence change due to cooling at pH 5.9 would be of the same order of magnitude. However, for steady state far UV CD experiments, Ballew and coworkers see an ellipticity change of approximately ten percent at low temperatures which should be within the resolution of our far UV CD experiments.

The most likely source for the discrepancy is the amount of time the apoMb spends at low temperature. Ballew, et al (1996) allowed the apoMb to equilibrate for at least one hour at the lowest temperature. The equilibration times for the data shown here were much shorter, for far UV CD experiments the temperature was ramped at a rate of -0.13°C per second. Steady state fluorescence experiments were conducted on only slightly longer time scales. This difference in equilibration time could be crucial for cold denaturation experiments where the lower temperature used increases the time necessary for conformational changes.

The work of Ballew and coworkers (1996) represents a first step in using temperature jump experiments to study the folding of horse apoMb, but several key questions remain unanswered For example, they did not address the question of whether the kinetics of fluorescence changes are altered by changing the pH and thus the conformation of apoMb. The affects of mutations on the kinetics also have yet to be studied. Of particular interest, would be mutations which result in cold denaturation above 0° C. So far, no such mutants have been identified, but the behavior of apoMb mutants at low temperatures is not well studied.

Additionally, it would be interesting to determine how the kinetics of early events in protein folding vary among myoglobins from different species. Trp 14 is a conserved residue (Viswanadhan and Sundaram 1983) so that all apomyoglobins should display some Trp fluorescence. Myoglobin is a highly conserved protein with few differences among mammalian species (Romero-Herrera et al. 1973); comparisons of apomyoglobins from

Reproduced with permission of the copyright owner. Further reproduction prohibited without permission.

different mammals could show whether small (20-30 amino acids) differences in sequences lead to changes in the kinetics of early events. To investigate larger structural and amino acid sequence alterations it would also be of interest to study tuna myoglobin, the fluorescence of which is well characterized (Bismuto et al. 1993; Irace et al. 1981; Ragone et al. 1987), and which is missing the D helix (Birnbaum et al. 1994).

Similarly to apomyoglobin, there are a number of mutants of RNase T1 available, some of which lack disulfide bonds and/or one of the *cis* Pro residues. It would be intriguing to investigate the thermal unfolding behavior of these mutants. Since RNase T1 is largely β sheet it would also be of interest to compare the time scale of RNase T1 unfolding to α helical proteins.

There are a number of microbial (fungal and bacterial) ribonucleases which have the same structural motif as RNase T1, an antiparallel β sheet packed against an α helix, and which share varying amounts of sequence homology (Sevcik et al. 1990). Again, as in the apoMb case, it would be interesting to compare the folding behavior of these related proteins. One complication in comparisons of ribonucleases is that several ribonucleases lack Trp residues so that the signals from the more numerous Tyr residues would have to be monitored instead, unless mutants with Trp residues are available or can be easily produced.

One assumption made in all of the proposed studies is that the measured rates are temperature independent. This assumption needs to be tested by performing temperature jumps of different magnitudes. It is possible that some of the properties of the systems, such as the interconversion rates of the conformational states of the protein under study, will depend on the magnitude of the temperature jump.

Phillips, et al (1995) have published the results of laser temperature jump studies on ribonuclease A (RNase A), a pancreatic rather than microbial ribonuclease. There is no sequence homology between RNase A and RNase T1 (Hill et al. 1983) , RNase A has no Trp residues and three α helices (Protein Databank 1rtb) as opposed to one for RNase T1.

Reproduced with permission of the copyright owner. Further reproduction prohibited without permission.

However both are α–β proteins. Phillips and coworkers observed a change in the IR spectrum between 1600 and 1700 cm^{-1}, the amide I region corresponding to the C=O stretch, upon jumping the temperature from 59°C to 62.5°C. The time scale for the change was 3.5 nsec and it was attributed to conformational changes within the β sheet of RNase A. Despite the differences in structure, comparisons between RNase A and RNase T1 could be illuminating as might comparisons between a global probe such as IR absorption and local probes such as UV absorption and fluorescence.

Laser temperature jump studies have also been conducted on a 21 residue, alanine based α helical polypeptide (Williams et al. 1996). This peptide is α helical at temperatures near 0° C and it loses its helicity over a temperature range of tens of degrees indicating that the transition is not two state (Williams et al. 1996). Williams and coworkers (1996) investigated amide I IR absorption at several wavelengths following a temperature jump. They found that for the peptide starting in an α helical conformation, an 18°C temperature jump yielded an unfolding time of 160 μsec. From the kinetic as well as the steady state data, they calculated a refolding rate of $6X10^7$ s^{-1}.

It is obvious that the study of early events in protein folding using laser temperature jumps is just beginning. The instrumentation is still being perfected and the choice of which proteins to study is not entirely clear. At a minimum, proteins should be monomeric, so that changes in structure will not be confused with oligomerization, and very well studied by conventional methods. In addition, it would be useful if a crystal structure is available. As shown by Williams, et al (1996) it is possible to calculate the refolding rate from the combination of unfolding rate and steady state data making measurements of heat denaturation kinetics even more versatile. Laser temperature jump protein folding/unfolding experiments should lead to insights into the early events in protein folding and the mechanisms of protein collapse.

Reproduced with permission of the copyright owner. Further reproduction prohibited without permission.

References

Agashe, V. R., and Udgaonkar, J. B. (1995). "Thermodynamics of Denaturation of Barstar: Evidence for Cold Denaturation and Evaluation of the Interaction with Guanidine Hydrochloride." *Biochemistry*, 34, 3286-3299.

Anfinrud, P. A., Han, C., and Hochstrasser, R. M. (1989). "Direct Observations of Ligand Dynamics in Hemoglobin by subpicosecond Infrared Spectroscopy." *Proceedings of the National Academy of Sciences, U.S.A.*, 86, 8387-8391.

Ascoli, F., Fanelli, M. R. R., and Antonini, E. (1981). "Preparation and Properties of Apohemoglobin and Reconstituted Hemoglobins." *Methods in Enzymology*, 76, 72-87.

Ballew, R. M., Sabelko, J., and Gruebele, M. (1996). "Direct Observation of Fast Protein Folding: The Initial Collapse of Apomyoglobin." *Proceedings of the National Academy of Sciences, USA*, 93, 5759-5764.

Barrick, D., and Baldwin, R. L. (1993). "Three-State Analysis of Sperm Whale Apomyoglobin Folding." *Biochemistry*, 32, 3790-3796.

Birnbaum, G. I., Evans, S. V., Przybylska, M., and Rose, D. R. (1994). "1.70 Å Resolution Structure of Myoglobin from Yellowfin Tuna. An Example of a Myoglobin Lacking the D Helix." *Acta Crystallographica Section D*, 50, 283-289.

Bismuto, E., Gratton, E., Sirangelo, I., and Irace, G. (1993). "Structure and Dynamics of the Acidic Compact State of Apomyoglobin by Frequency-Domain Fluorometry." *European Journal of Biochemistry*, 218, 213-219.

Bremer, C., Bergbauer, R., Ruf, H., Banister, J. J., and Grell, E. (1993). "A Laser Temperature Jump Apparatus Based on Commercial Parts Equipped with Highly Sensitive Spectrophotometric Detection." *Measurement Science and Technology*, 4, 1385-1393.

Calbiochem. (1975). *Buffers: A guide for the preparation and use of buffers in biological systems*, .

Carslaw, H. S., and Jaeger, J. C. (1959). *Conduction of Heat in Solids*, Oxford University Press, London.

Cho, K. C., and Chan, K. K. (1984). "Kinetics of cold-induced denaturation of metmyoglobin." *Biochimica et Biophysica Acta*, 786, 103-108.

Crank, J. (1956). *The Mathematics of Diffusion*, Oxford University Press, London.

Creighton, T. E. (1993). *Proteins: Structures and Molecular Properties*, W. H. Freeman and Company, New York.

Darbre, P. D., Romero-Herrera, A. E., and Lehmann, H. (1975). "Comparison of the Myoglobin of the Zebra (*Equus burchelli*) with that of the Horse (*Equus caballus*)." *Biochimica et Biophysica Acta*, 393, 201-204.

Reproduced with permission of the copyright owner. Further reproduction prohibited without permission.

Eliezer, D., and Wright, P. E. (1996). "Is Apomyoglobin a Molten Globule? Structural Characterization by NMR." *Journal of Molecular Biology*, 263, 531-538.

Evans, S. V., and Brayer, G. D. (1990). "High-resolution Study of the Threee-dimensional Structure of Horse Heart Myoglobin." *Journal of Molecular Biology*, 213, 885-897.

Fabian, H., Schultz, C., Backmann, J., Hahn, U., Saenger, W., Mantsch, H. H., and Naumann, D. (1994). "Impact of Point Mutations on the Structure and Thermal Stability of Ribonuclease T1 in Aqueous Solution Probed by Fourier Transform Infrared Spectroscopy." *Biochemistry*, 33, 10725-10730.

Fanelli, A. R., Antonini, E., and Caputo, A. (1958). "Studies on the Structure of Hemoglobin I. Physicochemical Properties of Human Globin." *Biochimica et Biophysica Acta*, 30, 608-615.

Garrett, J. B., Mullins, L. S., and Raushel, F. M. (1996). "Are Turns Required for the Folding of Ribonuclease T1." *Protein Science*, 5, 204-211.

Genberg, L., Heisel, F., McLendon, G., and Miller, R. J. D. (1987). "Vibrational Energy Relaxation Processes in Heme Proteins: Model Systems of Vibrational Energy Dispersion in Disordered Systems." *Journal of Physical Chemistry*, 91, 5521-5524.

Goto, Y., and Fink, A. L. (1990). "Phase diagram for acidic conformational states of apomyoglobin." *Journal of Molecular Biology*, 214, 803-805.

Griko, Y. V., and Privalov, P. L. (1994). "Thermodynamic puzzle of apomyoglobin unfolding." *Journal of Molecular Biology*, 235(1318-1325).

Griko, Y. V., Privalov, P. L., Venyaminov, S. Y., and Kutyshenko, V. P. (1988). "Thermodynamic study of the apomyoglobin structure." *Journal of Molecular Biology*, 202, 127-138.

Hatley, R. H. M., and Franks, F. (1989a). "The cold-induced denaturation of lactate dehydrogenase at sub-zero temperatures in the absence of perturbants." *FEBS Letters*, 257(1), 171-173.

Hatley, R. H. M., and Franks, F. (1989b). "The effect of aqueous methanol cryosolvents on the heat- and cold- induced denaturation of lactate dehydrogenase." *European Journal of Biochemistry*, 184, 237-240.

Hill, C., Dodson, G., Heinemann, U., Saenger, W., Mitsui, Y., Nakamura, K., Borisov, S., Tischenko, G., Polyakov, K., and Pavlovsky, S. (1983). "The Structural and Sequence Homology of a Family of Microbial Ribonucleases." *Trends in Biochemical Sciences*, 8, 364-369.

Hughson, F. M., Wright, P. E., and Baldwin, R. L. (1990). "Structural characterization of a partly folded apomyoglobin intermediate." *Science*, 249, 1544-1548.

Irace, G., Balestrieri, C., Parlato, G., Servillo, L., and Colonna, G. (1981). "Tryptophanyl Fluorescence Heterogeneity of Apomyoglobins. Correlation with the Presence of Two Distinct Structural Domains." *Biochemistry*, 20, 792-799.

Reproduced with permission of the copyright owner. Further reproduction prohibited without permission.

Jennings, P. A., and Wright, P. E. (1993). "Formation of a molten globule intermediate early in the kinetic folding pathway of apomyoglobin." *Science*, 262, 892-896.

Kendrew, J. C., Bodo, G., Dintzis, H. M., Parrish, R. G., Wycoff, H., and Phillips, D. C. (1958). "A three-dimensional model of the myoglobin molecule obtained by x-ray analysis." *Nature*, 181, 662-666.

Kendrew, J. C., Dickerson, R. E., Strandbery, B. E., Hart, R. G., Davies, D. R., Phillips, D. C., and Shore, V. C. (1960). "Structure of myoglobin." *Nature*, 185, 422-427.

Kiefhaber, T., Grunert, H.-P., Hahn, U., and Schmid, F. X. (1990a). "Replacement of a Cis Proline Simplifies the Mechanism of Ribonuclease T1 Folding." *Biochemistry*, 29, 6475-6480.

Kiefhaber, T., Quaas, R., Hahn, U., and Schmid, F. X. (1990b). "Folding of Ribonuclease T1. 2. Kinetic Models of Folding and Unfolding Reactions." *Biochemistry*, 29, 3061-3070.

Lian, T., Locke, B., Kholodenko, Y., and Hochstrasser, R. M. (1994). "Energy Flow from Solute to Solvent Probed by Femtosecond IR Spectroscopy: Malachite Green and Heme Protein Solutions." *Journal of Physical Chemistry*, 98, 11648-11656.

Loh, S. N., Kay, M. S., and Baldwin, R. L. (1995). "Structure and Stability of a Second Molten Globule Intermediate in the Apomyoglobin Folding Pathway." *Proceedings of the National Academy of Sciences, U.S.A.*, 92, 5446-5450.

Mayr, L. M., Landt, O., Hahn, U., and Schmid, F. X. (1993). "Stability and Folding Kinetics of Ribonuclease T1 are Strongly Altered by the Replacement of *Cis* -Proline 39 with Alanine." *Journal of Molecular Biology*, 231, 897-912.

Nishii, I., Kataoka, M., and Goto, Y. (1995). "Thermodynamic Stability of the Molten Globule States of Apomyoglobin." *Journal of Molecular Biology*, 250, 223-238.

Nishii, I., Kataoka, M., Tokunaga, F., and Goto, Y. (1994). "Cold denaturation of the molten globule states of apomyoglobin and a profile of protein folding." *Biochemistry*, 33, 4903-4909.

Oobtake, M., Takahashi, S., and Ooi, T. (1979). "Conformational Stability of Ribonuclease T1 I. Thermal Denaturation and Effects of Salts." *Journal of Biochemistry*, 86, 55-63.

Pace, C. N., and Grimsley, G. R. (1988). "Ribonuclease T1 is Stabilized by Cation and Anion Binding." *Biochemistry*, 27, 3242-3246.

Pace, C. N., Grimsley, G. R., Thomson, J. A., and Barrett, B. J. (1988). "Conformational Stability and Activity of Ribonuclease T1 with Zero, One, and Two Intact Disulfide Bonds." *Journal of Biological Chemistry*, 263(24), 11820-11825.

Phillips, C. M., Mizutani, Y., and Hochstrasser, R. M. (1995). "Ultrafast Thermally Induced Unfolding of RNase A." *Proceedings of the National Academy of Sciences, USA*, 92, 7292-7296.

Reproduced with permission of the copyright owner. Further reproduction prohibited without permission.

Plaza del Pino, I. M., Pace, C. N., and Friere, E. (1992). "Temperature and Guanidine Hydrochloride Dependence of the Structural Stability of Ribonuclease T1." *Biochemistry*, 31, 11196-11202.

Privalov, P. L. (1979). "Stability of Proteins: Small Globular Proteins." *Advances in Protein Chemistry*, 33, 167-241.

Privalov, P. L. (1990). "Cold Denaturation of Proteins." *Critical Reviews in Biochemistry and Molecular Biology*, 25(4), 281-303.

Privalov, P. L. (1992). "Physical Basis of the Stability of the Folded Conformations of Proteins." Protein Folding, T. E. Creighton, ed., W. H. Freeman and Company, New York, 83-126.

Privalov, P. L., Griko, Y. V., Venyaminov, S. Y., and Kutyshenko, V. P. (1986). "Cold Denaturation of Myoglobin." *Journal of Molecular Biology*, 190, 487-498.

Ragone, R., Colonna, G., Bismuto, E., and Irace, G. (1987). "Unfolding Pathway of Myoglobin: Effects of Denaturants on Solvent Accessibility to Tyrosyl Residues Detected by Second-Derivative Spectroscopy." *Biochemistry*, 26, 2130-2134.

Riveros-Moreno, V., and Wittenberg, J. B. (1972). "The Self-Diffusion Coefficients of Myoglobin and Hemoglobin in Concentrated Solutions." *Journal of Biological Chemistry*, 247, 895-901.

Romero-Herrera, A. E., and Lehmann, H. (1974). "Residue 122 of Sperm Whale and Horse Myoglobin." *Biochimica et Biophysica Acta*, 336, 318-323.

Romero-Herrera, A. E., Lehmann, H., Joysey, K. A., and Friday, A. E. (1973). "Molecular Evolution of Myoglobin and the Fossil Record: A Phylogeneitc Synthesis." *Nature*, 246, 389-395.

Sanctis, G. D., Ascoli, F., and Brunori, M. (1994). "Folding of Apominimyoglobin." *Proceedings of the National Academy of Sciences*, 91, 11507-11511.

Sevcik, J., Sanishvili, R. G., Pavlovsky, A. G., and Palyakov, K. M. (1990). "Comparison of Active Sites of some Microbial Ribonucleases: Structural Basis for Guanylic Specificity." *Trends in Biochemical Sciences*, 15, 158-162.

Shirley, B. A., Stanssens, P., Hahn, U., and Pace, C. N. (1992). "Contribution of Hydrogen Bonding to the Conformational Stability of Ribonuclease T1." *Biochemistry*, 31, 725-732.

Siegman, A. E. (1986). *Lasers*, University Science Books, Mill Valley, California.

Takahashi, K., Uchida, T., and Egami, F. (1970). "Ribonuclease T1: Structure and Function." *Advances in Biophysics*, 1, 53-98.

Takano, T. (1977). "Structure of Myoglobin Refined at 2.0 Å Resolution I. Crystallographic Refinement of Metmyoglobin from Sperm Whale." *Journal of Molecular Biology*, 110, 537-568.

Thompson, P. (1996). personal communication.

Reproduced with permission of the copyright owner. Further reproduction prohibited without permission.

Thomson, J. A., Shirley, B. A., Grimsley, G. A., and Pace, C. N. (1989). "Conformational Stability and Mechanism of Folding of Ribonuclease T1." *Journal of Biological Chemistry*, 264(20), 11614-11620.

Viswanadhan, V. N., and Sundaram, K. (1983). "Structural Conservation in Globular Proteins." *International Journal of Peptide and Protein Research*, 21, 190-195.

Weber, G., and Teale, F. J. W. (1959). "Electronic Energy Transfer in Haem Proteins." *Discussions of the Faraday Society*, 27, 134-141.

Williams, S., Causgrove, T. P., Gilmanshin, R., Fang, K. S., Callender, R. H., Woodruff, W. H., and Dyer, R. B. (1996). "Fast Events in Protein Folding: Helix Melting and Formation in a Small Peptide." *Biochemistry*, 35, 691-697.

Reproduced with permission of the copyright owner. Further reproduction prohibited without permission.

CHAPTER VII

CONCLUSION OR THE IMPORTANCE OF LASER PUMP-PROBE SPECTROSCOPY

Protein folding is the process by which a one dimensional chain of amino acids becomes a three dimensional functional protein. Laser pump-probe spectroscopy can monitor this process in real time on time scales from nanoseconds to seconds. This spectroscopy may be used to either excite molecules and probe their excited states, transient absorption for example, or to change solution characteristics such as pH and temperature, thereby triggering protein conformational changes. The laser pump-probe technique has the advantage of allowing the use of small volumes which can be important in cases where large quantities of a protein are not readily available. In addition, low (micromolar) protein concentrations may be used; this is particularly important in refolding experiments where protein aggregation can be a problem. In the case of transient absorption, pump-probe spectroscopy also allows the detection of states such as short lived tryptophan (Trp) triplet states and Trp cation and neutral radicals which are difficult or impossible to detect using luminescence techniques.

The changes in protein absorption or emission in all of these pump-probe experiments are very small, often one percent or less . These low signal strengths mean that care must be taken to reduce noise by using techniques such as balanced detection. Balanced detection virtually eliminates noise arising from instabilities in the probe beam. Laser pump-probe experiments can be further complicated by the requirement that two laser beams be well aligned so that the region being probed is the same as the region being excited. This alignment necessitates the ability to make very fine changes in laser beam

Reproduced with permission of the copyright owner. Further reproduction prohibited without permission.

pointing. Additionally, for experiments that take seconds or longer diffusion of molecules out of the region being probed can become a problem.

In luminescence experiments, signals are only seen from the excited singlet or triplet states. The difference in time scales (nanoseconds versus milliseconds) makes the differentiation of these two signals quite simple. In transient absorption experiments, however, a plethora of species may absorb at any given wavelength. The differing absorption spectra and oxygen sensitivity serve to identify the chemical species and the signals from these additional species can provide valuable information on Trp photochemistry.

Transient absorption and phosphorescence experiments were conducted on *Escherichia coli* alkaline phosphatase (AP) and rabbit phosphoglycerate kinase (PGK). AP has a triplet state lifetime of ca. 2 seconds as measured by phosphorescence and the long lifetime seen in transient absorption experiments was identified as the Trp triplet state due to its oxygen dependence and larger signal strength at 457.9 nm versus 514.5 nm. However, the lifetime of the long component as measured by phosphorescence and by transient absorption did not agree, indicating the possible presence of a long lived non-luminescent species. PGK displays negligible phosphorescence, but it did show transient absorption with a lifetime of hundreds of milliseconds. This long lived component arises from one of the tryptophan radical species. PGK transient absorption data also contain a short-lived (millisecond) oxygen sensitive component which could arise from the Trp triplet state, but this assignment is tentative since the low time resolution of the transient absorption experiments did not allow measurement of the spectral dependence of this component.

For transient absorption experiments aimed at monitoring protein conformational changes, the fact that the excited state lifetimes as measured by absorption and those measured by luminescence, particularly phosphorescence, do not always agree is not necessarily a concern. As long as the lifetimes measured by transient absorption differ

Reproduced with permission of the copyright owner. Further reproduction prohibited without permission.

among protein conformations, such experiments may be used to study conformational changes. Transient absorption measurements of protein conformation may also yield more insight into the local environment surrounding Trp residues since the lifetimes and signals from the Trp triplet state and Trp radical states differ in their dependence on the proximity of the solvent and of other amino acids.

Experiments on early events in protein folding or unfolding allow direct measurements of the time scales and mechanisms of collapse from the random coil or breakdown of the native structure respectively. In such experiments, a laser pulse is used to change the pH or temperature of the protein solution. pH jumping experiments currently only allow measurements of protein unfolding while temperature jump experiments may be used to study early events in unfolding following thermal denaturation or in refolding from cold denatured states.

In such experiments, care must be taken to insure that the signal arises from the protein and not from experimental artifacts such as thermal lensing. Additionally, the emission and absorption characteristics of proteins can change with temperature or pH independent of changes in protein conformation. Such complications as well as the sophisticated data acquisition systems necessary to distinguish small changes in optical signals make pH jump and temperature jump experiments quite difficult.

pH jump experiments are further complicated by the fact that the dyes used to change the pH usually absorb heavily in the ultra-violet obscuring intrinsic protein fluorescence and absorption. Therefore, peptides or proteins used for such experiments must be labeled with extrinsic probes. These probes must be able to reveal protein conformational changes without interfering in the protein folding process itself. Additionally, as was shown by the experiments using acridine orange as an extrinsic probe of conformational changes of poly-glutamic acid, the probes must not interact with the pH jumping dyes.

Reproduced with permission of the copyright owner. Further reproduction prohibited without permission.

The criteria for protein selection for temperature jump experiments are not nearly as exacting. The selected protein should be monomeric, so that changes in structure will not be confused with oligomerization, have well characterized protein folding and, if at all possible, an x-ray structure should be available. The steepness of the folding transition with temperature should also be considered since it is advantageous to be able to jump the temperature so that the maximal change in protein conformation, and thus in monitored signal (such as absorption or fluorescence), is achieved. An additional useful criterion for UV absorption and fluorescence experiments is the presence of one or more tryptophan residues. Preliminary steady state studies of horse apomyoglobin and ribonuclease T1 demonstrate the suitability of these proteins for temperature jump experiments involving refolding from cold denatured states and heat denaturation respectively.

Cold denatured proteins, apomyoglobin for example, exhibit much more secondary structure as probed by far UV circular dichroism (CD) than do proteins denatured by heat, acid or chaotropic agents. The presence of secondary structure means that any kinetics measured for protein folding following temperature jumps will not be the same as the kinetic parameters associated with folding from a random coil state. If the contacts in the cold denatured state are the same as in the native protein, the folding kinetics measured in temperature jump experiments are likely to be faster than the kinetics of folding from the random coil. However, if the cold denatured state has some nonnative contacts, these contacts could slow down protein folding due to steric hindrance. Folding rates may also be calculated from the rate of unfolding due to heat denaturation and steady state data (Williams et al. 1996). Differences in rates may allow studies of early events in folding from cold denatured states to distinguish between hierarchical models of folding, in which folding intermediates have only native contacts, and nonhierarchical models, in which folding intermediates may have non-native contacts so, for example, a β sheet protein may have an α helical intermediate.

Reproduced with permission of the copyright owner. Further reproduction prohibited without permission.

Despite the complications and difficulties, laser temperature jump experiments, and potentially pH jump experiments as well, should yield insight into early events in protein folding and unfolding. Comparisons between data gained from temperature jump experiments using local probes, such as fluorescence and near UV absorption, and global probes, such as infrared absorption and possibly far UV circular dichroism, should lead to a better understanding of what happens early in protein folding and how proteins restrict the number of available conformations.

Reproduced with permission of the copyright owner. Further reproduction prohibited without permission.

References

Williams, S., Causgrove, T. P., Gilmanshin, R., Fang, K. S., Callender, R. H., Woodruff, W. H., and Dyer, R. B. (1996). "Fast Events in Protein Folding: Helix Melting and Formation in a Small Peptide." *Biochemistry*, 35, 691-697.

Reproduced with permission of the copyright owner. Further reproduction prohibited without permission.

APPENDICES

Reproduced with permission of the copyright owner. Further reproduction prohibited without permission.

APPENDIX A

ABBREVIATIONS & VARIABLES

AO	Acridine Orange
AP	Alkaline Phosphatase
ApoMb	Apomyoglobin
BG	Bromcresol Green
BrDMC	4-(bromomethyl)-6,7-dimethoxycoumarin
CD	Circular Dichroism
CO	Carbon Monoxide
Cys	Cystine
Cyt c	Cytochrome c
D	Diffusion Coefficient
DETAPAC	Diethylenetriamine Pentaacetic Acid
Gdn-HCl	Guanidine Hydrochloride
HCl	Hydrochloric acid
HIn	Protonated pH Indicator
His	Histidine
HPTS	8-hydroxypyrene-1,3,6-trisulfonic acid
In^-	Deprotonated pH Indicator (alkaline form)
IR	Infra red
lis	Laser intensity stabilizer
M	Molar (moles/liter)
Mb	Myoglobin
n	index of refraction
NaCl	Sodium Chloride
NaOH	Sodium Hydroxide

Reproduced with permission of the copyright owner. Further reproduction prohibited without permission.

Nd-YAG	Neodymium Yttrium Aluminum Garnet
NMR	Nuclear Magnetic Resonance
OD	Optical Density
ORD	Optical Rotatory Dispersion
P/D	Polymer Residue to Dye Molar Ratio
PGA	Poly-L-glutamic Acid
PGK	Phosphoglycerate Kinase
PMT	Photomultiplier Tube
Pro	Proline
RTP	Room Temperature Phosphorescence
Si Diode	Silicon Photodiode
t	Time
T	Transmision or Temperature
TA	Transient Absorption
TNBS	Picrylsulfonic or Trinitro-benzene-sulfonic Acid
T jump	Temperature Jump
Trp	Tryptophan
T-T	Triplet-Triplet
Tyr	Tyrosine
UV	Ultraviolet
ε	Extinction Coefficient
[]	Concentration

Reproduced with permission of the copyright owner. Further reproduction prohibited without permission.

APPENDIX B

CHEMICAL STRUCTURES

Structures for chapter V:

Acridine Orange (AO)

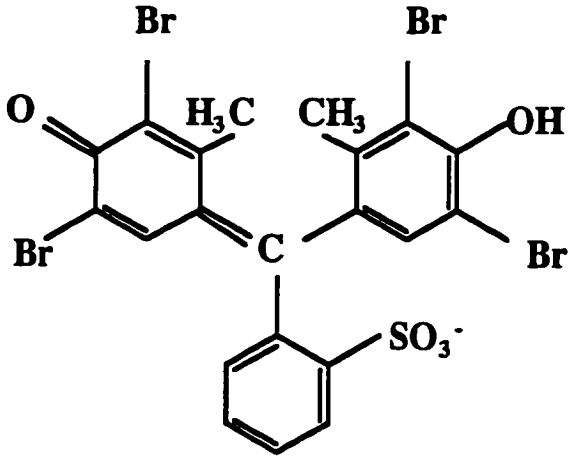

Bromcresol Green (BG)

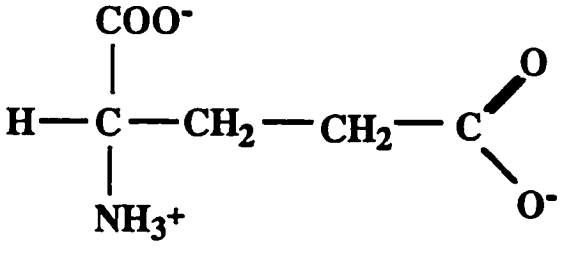

Glutamic Acid

Reproduced with permission of the copyright owner. Further reproduction prohibited without permission.

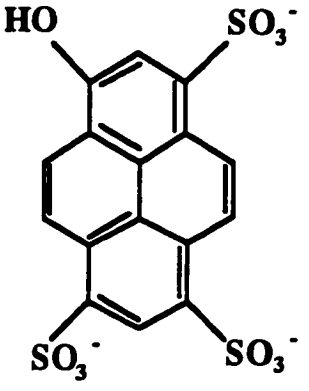

8-hydroxypyrene-1,3,6-trisulfonic acid
(HPTS)

Reproduced with permission of the copyright owner. Further reproduction prohibited without permission.

APPENDIX C

SOME USEFUL EQUATIONS

1. Beer-Lambert Law (Cantor and Schimmel 1980):

The amount of light transmitted through an absorbing sample, I:

$$I = I_o 10^{-\varepsilon C \ell} \qquad (C.1)$$

where I_0 is the intensity of the incident light, ε is the molar extinction coefficient in liter/(mole cm) which is dependent on the incident wavelength, C is the concentration of absorbing molecules in moles/liter and ℓ is the path length of the light. The exponent, $\varepsilon C \ell$, is referred to as the absorbance or the optical density (OD).

In physics, Beer's law is normally expressed as (Möller 1988):

$$I = I_o e^{-\alpha \ell} \qquad (C.2)$$

where α is the wavelength dependent absorption coefficient in cm^{-1}. Thus,

$$\alpha = (\ln 10)\varepsilon C \qquad (C.3)$$

2. Laser spot sizes:

According to Siegman (1986), when a Gaussian laser beam of wavelength λ is focused by a lens of focal length f the effective beam diameter, d_0, at the focal length is given by:

$$d_o = \frac{2f\lambda}{\pi w(f)} \qquad (C.4)$$

where w(f) is the beam diameter at the lens, i.e. the Gaussian spot size. This equation was used to calculate approximate laser spot sizes following focusing. However, for the UV beam obtained by doubling the output of a dye laser this equation is a rather crude estimate. The angle of acceptance of the doubling crystal is quite small and while the dye laser beam has a Gaussian profile, the UV output from the doubling crystal looks more like a line than a dot.

Reproduced with permission of the copyright owner. Further reproduction prohibited without permission.

3. Acids & Bases (Stryer 1988):

$$HA \rightleftharpoons H^+ + A^- \qquad \text{(C.5)}$$

where H is hydrogen, HA is a weak acid and A^- is the conjugate base. The pH is defined in terms of the hydrogen ion concentration ($[H^+]$) as:

$$pH = -\log_{10}[H^+] \qquad \text{(C.6)}$$

Alternatively, the pH may be defined in terms of the pK of an acid:

$$K = \frac{[H^+][A^-]}{[HA]} \qquad \text{(C.7)}$$

$$pK = -\log_{10} K \qquad \text{(C.8)}$$

$$pH = pK + \log_{10}\frac{[A^-]}{[HA]} \qquad \text{(C.9)}$$

K is the apparent equilibrium constant and equation C.9 is the Henderson-Hasselbalch equation. From Henderson-Hasselbalch it is easy to see that if pH>pK then the acid is mainly in the deprotonated state and if pH<pK the acid is mainly protonated.

References

Cantor, C. R., and Schimmel, P. R. (1980). *Biophysical Chemistry Part II: Techniques for the Study of Biological Structure and Function*, W. H. Freeman and Company, New York.

Möller, K. D. (1988). *Optics*, University Science Books, Mill Valley, CA.

Siegman, A. E. (1986). *Lasers*, University Science Books, Mill Valley, California.

Stryer, L. (1988). *Biochemistry*, W. H. Freeman and Company, New York.

Reproduced with permission of the copyright owner. Further reproduction prohibited without permission.